POLITECNICO DI MILANO

Scuola di Ingegneria Civile, Ambientale e Territoriale

Master of Science in Civil Engineering for Risk Mitigation

FATIGUE BEHAVIOUR OF THE HISTORICAL WROUGHT IRON TIE-RODS IN THE DUOMO DI MILANO

Supervisor: Prof. Roberto Felicetti

Co-supervisor: PhD Mira Vasic

Mater thesis by Ilina Georgieva Stefanova

Id number: 797012

ACADEMIC YEAR 2013 – 2014

Acknowledgments

I would like to express my acknowledgements to my supervisor Prof. Roberto Felicetti and cosupervisor Mira Vasic for their guidance and advisement, for being so supportive and making this work very productive and pleasant.

The research was supported by the Veneranda Fabbrica del Duomo, which is gratefully acknowledged for the documents provided. Furthermore, the author would like to especially thank Eng. B. Mörling and Mr. F. Aquilano for the cooperation throughout this research project. Execution of on-site experimental tests by Mr. M. Cucchi and Arch. C. Tiraboschi from Politecnico di Milano is particularly acknowledged. The author is grateful to Prof. Giussani and Prof. Cigada from Politecnico di Milano for provided monitoring data and to Prof. Coronelli for scientific contribution to the research. The author would like to acknowledge the tests made by Department of Mechanical Engineering at Politecnico di Milano and Prof. Carboni in particular.

Moreover I would like to give my gratitude to all the people who were involved in the experiments and who make this whole process possible.

Furthermore I want to thank to all of my friends and colleagues who were always there for me during this time. Who believed in me and encouraged me to not give up no matter how hard it is. But I am especially grateful to one particular person – my roommate Mariya. Thanks for convincing me to come here in a first place and also for these two amazing years.

And last but not least, I would like to thank my family and especially my brother for all the support and love they gave me and without whom I won't be the person I am today. So mom, dad, bro, thanks for letting me follow my dreams and being always behind my back no matter what.

Abstract

When dealing with historical buildings it is very important to understand their structural behavior and present state in order to be able to predict their future performance and residual life. The assessment of this kind of buildings consists of many aspects such as historical investigation of the original design, evolution of construction and damage in time, monitoring, numerical models etc. The Cathedral of Milan (further in the text indicated as Duomo di Milano) was chosen as a case study for the present thesis for which the fatigue behavior of its iron ties due to the temperature change was assessed. Tie-rods in Duomo di Milano are active in bearing the lateral thrust from the vault and the arch above. Their performance is relevant for the overall stability of the structure, which makes their assessment of great importance. Since the ties are made of wrought iron, for which little information on the material properties is available in the literature, series of experiments were conducted on specimens, taken from the original tie – visual inspection, tensile test, magnetic particle examination, and toughness test. The data from previous studies, monitoring and investigations of the structure were used in order to create a simplified numerical model for assessing the influence of the daily and seasonal temperature variations on the elements. The aim of the thesis is to provide instructions for estimation of the residual fatigue life of the tie-rods once a defect in them has been detected, using the results from the numerical model along with the principles of Linear Elastic Fracture Mechanics (LEFM). Some remarks on further improvements of the models are given in the present work in order to improve the obtained results.

Estratto

Lo stato attuale e la “risposta” strutturale degli edifici storici sono parametri fondamentali da comprendere se si vuole capire le loro “risposte” future e le loro vite residue. La valutazione di questi particolari edifici può essere effetuata considerando diversi aspetti come: la ricerca di documenti storici quali progetto originario,evoluzione delle fasi costruttive e dei eventuali danni nel tempo, il monitoraggio, analisi numeriche ed etc. Il caso studiato in questa tesi riguarda il Duomo di Milano, più nello specifico la risposta a fatica delle sue catene a diverse temperature. Le catene sono soggette ad una forza di trazione dovuta dalla spinta laterale delle volte e degli archi sopra di esse. La loro stabilità è essenziale al fine di garantire una buona risposta strutturale, per questo motivo la loro verifica è molto importante. Le catene sono in ferro battuto, a causa delle scarse informazioni dell’analisi storica riguardanti le loro proprietà (fisiche,chimiche e meccaniche), si è provveduto ad eseguire alcuni test su pezzi di esse come: ispezione visiva, prova a trazione, analisi con particelle magnetiche e prova di durezza. Il modello numerico usato per definire l’influenza del cambiamento di temperatura stagionale e giornaliero si basa su dati provenienti da studi effetuati in passato oltre che a quelli delle prove qui condotte. Lo scopo di questa tesi è quello di fornire informazioni sulla stima della resistenza residua a fatica delle catene con la presenza di un difetto individuate in esse usando un modello numerico basato sulla meccanica lineare elastica delle fratture. Nel presente lavoro vi sono anche alcuni suggerimenti per future approfondimenti, in maniera tale da migliorare l’analisi.

Content

List of figures

List of tables

List of equations

1. Introduction

Many mechanical failures of metallic structures are due to fatigue. This phenomenon is complex and not yet fully understood. The fatigue failure is often a brittle failure, very sudden, with no obvious warnings, which makes it highly dangerous. Often it may lead to unexpected failure of parts or even of the whole structure. Throughout the years many examples of failure of metallic elements and structures due to fatigue were evidenced. One of them is the Dee Bridge (located in Chester, England). It was designed using cast iron girders reinforced with wrought iron struts. The bridge collapsed on 24 May 1847 and it was the subject of one of the first formal inquiries into a structural failure. The inquiry showed that the design of the structure was fundamentally flawed, as the wrought iron did not reinforce the cast iron at all, and due to repeated flexing it suffered a brittle failure due to fatigue (Godfraind S. et al. 2012).Another example is the Ashtabula River Railroad (Ashtabula/Edgewood, Ohio, USA), which collapsed on 29 December 1876 due to the fatigue of the cast iron lug pieces, which were used to anchor the wrought iron bars. One of the recent failures of metallic structure due to fatigue is the partial collapse of the Sgt Aubrey Cosens VC Memorial Bridge (Latchford, Ontario, USA), which happened on 14 January 2003. The cause for this failure is fatigue fracture on the three steel hanger rods. These examples show the importance of the fatigue behavior of the metals and the necessity of its consideration in the design of new structures and the assessment of the existing ones.

In this thesis the Duomo di Milano was chosen as a study case. This Cathedral is one of the most remarkable historical buildings from religious, artistic and architectural aspect. Its overall performance should be very well understood in order to be able to preserve the structure in the future. Duomo di Milano has a unique structural system with respect to the other representatives of Gothic cathedrals, which consists in the presence of metallic ties under the arches. In many other cathedrals these elements were also present but only as temporary parts, used during the construction and removed later on (Fitchen 1961). Recent studies (Coronelli et al. 2014 and Vasic et al. 2015) showed that the iron ties in Duomo di Milano are active members in resisting the lateral thrust coming from the arches and the vaults, so their structural behavior and current state should be investigated within the health monitoring strategy.

Fatigue is one of the possible deterioration phenomena; relevant for the performance of the ties in Duomo di Milano, which the present thesis work aims to analyze.

In Figure 1 the general process of assessment of an historical structures is summarized.

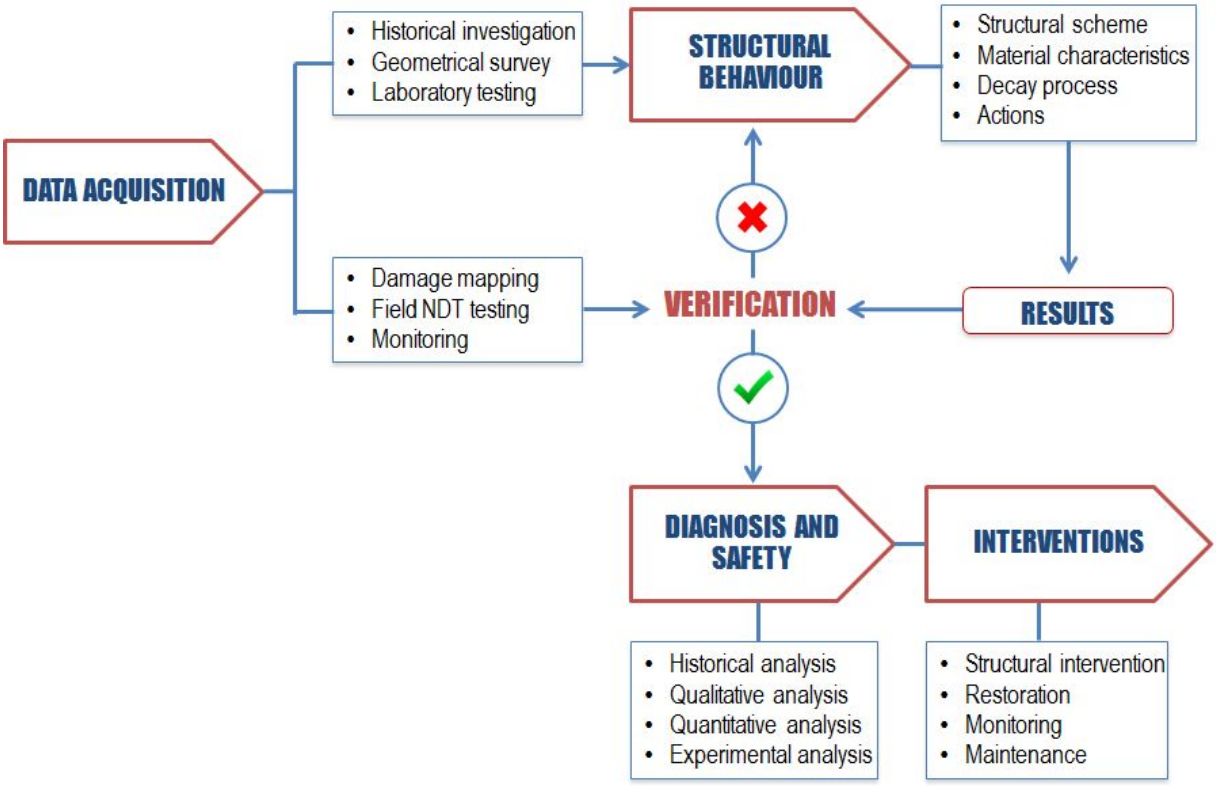

Figure 1: Map of activities

As a first step of the analysis, a historical investigation of the design of the Duomo di Milano, construction and damage evolution in time was done from the relevant literature (Ferrari da Passano 1998 and 2005, Coronelli et al. 2014a, Coronelli et al. 2014b,, Vasic et al. 2015). Further data from previous monitoring (Cigada et al.2011, Giussani and Roncoroni 2009-2014) and experimental campaigns (Guidobaldi et al. 2014) were collected as well as the information about numerical models already developed (Vasic 2014, Coronelli et al. 2014b). Results from the dynamic testing of the ties, records for temperature measurements in the indoor and outdoor environment, vertical and horizontal movements of the pillars in the Cathedral were taken from the previous studies (Giussani and Roncoroni 2009-2014, Guidobaldi et al. 2014, Vasic et al. 2015).

In the assessment of fatigue resistance very important is the knowledge of material properties and it is one of the first-stage tasks. Literature review was done in order to better understand the behavior of the wrought iron. However, very limited information on material properties of this material is available in nowadays literature. During this research it was found that the characteristics of the wrought iron considerably differ depending on the iron ore it was produced from and on the method and quality of production. Since it is difficult to find consistency in both of these factors, it is also difficult to find consistency in the material properties. Therefore, the properties of different elements may differ from each other even if they are made from the same type of material. Keeping in mind this and taking into account that the placement of the iron ties in Duomo di Milano was done in a time span of 200 years (Vasic et al. 2015), one can understand how difficult the material characterization of such elements is. Moreover, since the wrought iron is a man-made material, its production process implies the material entirely structurally non-homogeneous in its nature, with very high possibility of inclusions and voids in

it. These imperfections may have a significant influence on the behavior of the elements and their performance will vary considerably.

In order to determine the properties and behavior of the historical wrought iron a review of the previous studies was done as well as testing on samples, taken from the original tie-rod that was replaced within a maintenance of the Cathedral. The experimental campaign consisted in visual inspection of the pieces, tensile tests on three different series of samples, magnetic particle examination and toughness test. Their results confirmed high variability of mechanical properties, already found during the literature review.

This thesis considers the daily and seasonal variations in temperature as a possible cause for the fatigue in the ties of Duomo di Milano. A simplified numerical model of one of the representative Gothic arches in the lateral nave of the Cathedral together with the tie-rod was developed in commercial FEM program (SAP2000). The obtained results were used together with the daily and yearly records of the temperature in the indoor and outdoor environment of Duomo di Milano in order to assess its influence on the stresses in the tie-rods. However, this representation is very rough and could be used only as a first approximation of the problem. Further improvements of the model should be done in order to be able to obtain better results, closer to the real situation. However, more sophisticated numerical representation is demanding and requires a great amount of material characteristics that should be measured.

Since the main aim of this thesis is to describe the fatigue behavior of the ties of Duomo di Milano, the results from the numerical analysis in terms of stress variation due to temperature change and the one measured on-site were used together with the principles of Linear Elastic Fracture Mechanics. Different approaches for determination of the main fatigue properties (taken from the literature, analytically or experimentally obtained) and methods for describing the fatigue behavior were introduced. A procedure for the assessment of the future performance in terms of critical length of the crack and residual fatigue life of the tie is synthetized in the present work. Procedure describes steps to be followed once a discontinuity is detected in the tie-rod, as well as was created. All needed parameters and different methods to obtain them. Few examples of application of this methodology using the material properties found in the literature or experimentally obtained and the stresses that result from the measurements and numerical analysis are also given.

2. Duomo di Milano

Duomo di Milano is a Gothic cathedral with imposing dimensions and very complex structural system. Because of its size, it is one of the largest churches ever built (Figure 2). It consists of five naves where in each one of them columns are connected by means of iron ties under the arches in both transversal and longitudinal direction. This makes the structure unique in comparison with the other cathedrals from the same period. As described in the study by Coronelli et al. 2014a, initially all the piers were supposed to have the same dimensions of the cross section (2.55m diameter), but later by advice of Matteo da Campione the four columns under the *tiburio* were built with slightly larger cross-section – 2.95m diameter. The foundations of the piers are at 7m below the ground level with brick spread foundations realized under the internal ones and stonewalls along the perimeter.

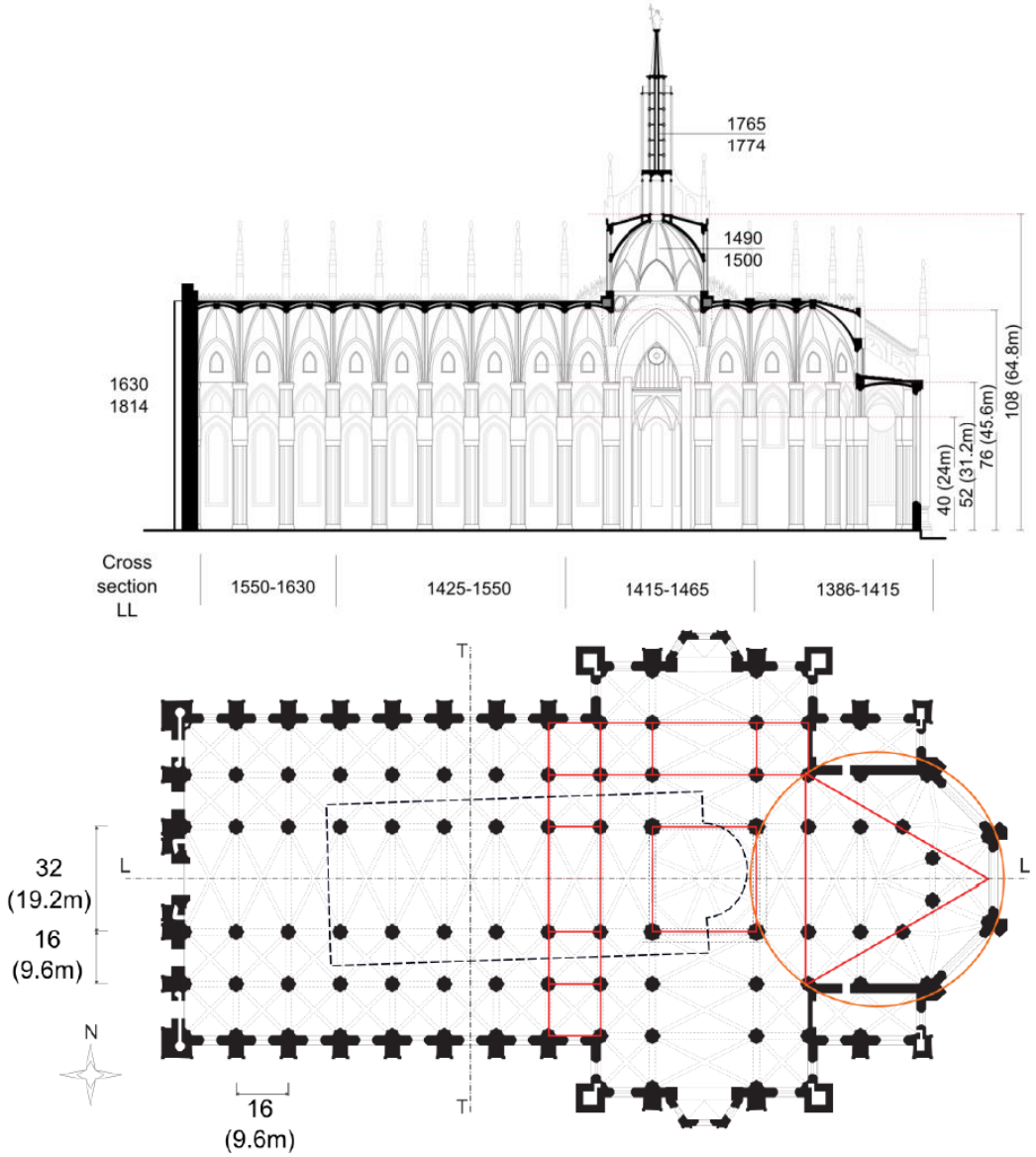

Figure 2: Geometry and history of the construction (Coronelli et al., 2014a)

The layout of the Cathedral and the main phases of the construction are given in Figure 2. The construction of Duomo di Milano started in 1386 from the West to the East. First the apse and chapels next to it were built in 14th century. Then the construction proceeded to the East, finalizing the five naves in 16th century and the façade in 18th (Vasic at al. 2015). The main spire was built in the late 18th century, followed by the construction of the four towers at the corners of the base of the *tiburio*. Because of the big load due to these new elements, a cracking started in the piers supporting them that led to the closure of the Cathedral for repairs at the end of 19th century. These repairs consisted in substitution of the damaged blocks, binding the new parts to the old ones by means of iron tie rods (Coronelli et al. 2014).

One major event in the history of Duomo di Milano is the excessive water draining by industrial companies from the soil during 1960s (Niccolai 1967). This caused a global lowering of the water table by 20m with respect to the level in 19th century, leading to differential settlement under the piers of the Cathedral. As a result high stress concentration in the *voussoirs* that accelerated the long-term damage in the piers under the *tiburio* present at that time was observed. A structural intervention was done in the last decades of the 20th century. The main piers were encased in reinforced concrete along with 16 others strengthen with steel cages and after that the damaged parts were replaced with new ones. No further damage was observed in these piers ever since (Coronelli et al. 2014a).

In a recent research (Coronelli et al. 2014a) the differential settlement of the soil under Duomo di Milano was modeled by 3D finite element analysis, comparing the results obtained thorough it with the ones of the monitoring campaign that started in 1950s. These models could be used as a base for more refined nonlinear analyses and prediction of future settlements, which is extremely important for the overall stability of the structure.

Another factor that may influence the structural behavior of Duomo di Milano is the temperature change – daily and yearly. These thermal variations may lead to fatigue in the iron ties and since they are active members the effect of these temperature alternations must be assessed. In this thesis an attempt to do that was made by means of simplified models and series of experiments.

Although Milano is not a seismic region, the underground train that runs under Duomo di Milano since 1964 could have dynamic effects on the Cathedral, but till now there are no researches on that topic (Vasic et al. 2015). A modern numerical tool may give an answer about the vibration effects of this on the Cathedral.

2.1. Structural system of Duomo di Milano

As mentioned earlier the structural system of Duomo di Milano is very complex, consisting of columns, connected by iron ties under the arches in transversal and longitudinal direction in each five naves. Some pictures of the internal of the Cathedral are shown in Figure 3.

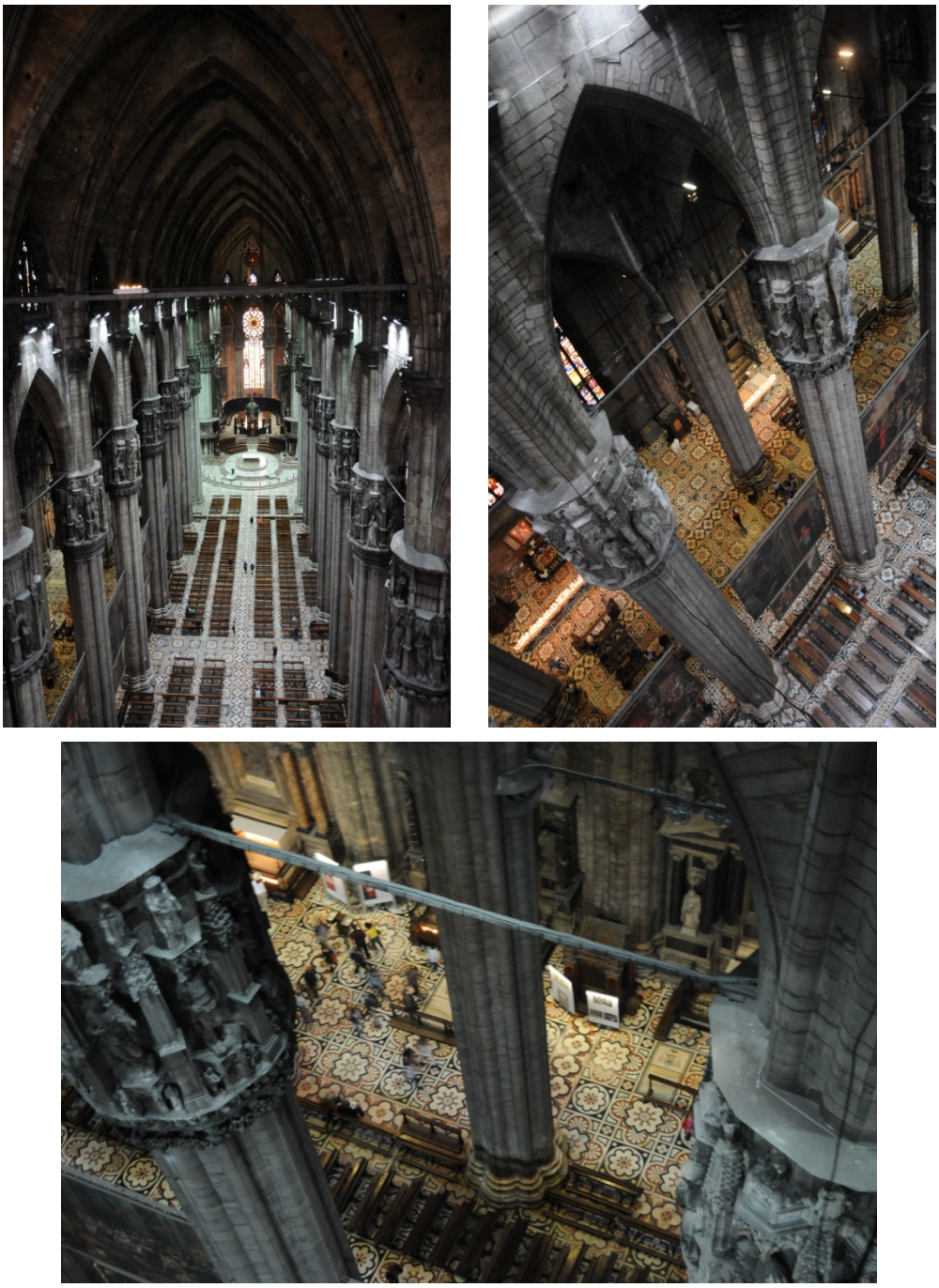

Figure 3: Internal of Duomo di Milano

Recent study (Vasic et al. 2015) showed that the ties of the Cathedral are active elements, which contribute in resisting the lateral thrust coming from the vault and arches. Another characteristic feature of the system is a double vaulting system present in all five naves of the Cathedral. In Figure 4 the structural system of the Cathedral's naves can be seen consisting of iron, lateral walls and buttressing system above the arches, together resisting the lateral thrust from the vaults. Therefore, it is of great importance to understand what part of the lateral thrust coming from the vault and arches is resisted by

the tie-rods take and what part by the lateral masonry structure. Structural analysis of the Cathedral can give an answer to this question and help to better understand the behavior of the structure.

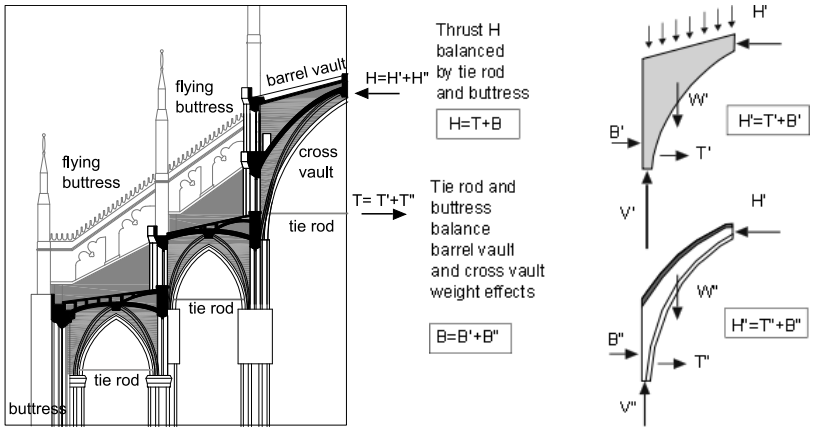

Figure 4: Structural system of Duomo di Milano (Vasic et al. 2013)

Different approaches can be used in the structural behavior analysis when dealing with historical buildings. Simplified methods based on the equilibrium can provide a good interpretation of the structural system and therefore can be chosen as a first approach; while using more sophisticated numerical model might better represent the reality. This can be done with Finite Element Method (FEM) taking into consideration the complexity of the structural system, the long-term effects, the soil settlements, the structural response to seismic loads, the construction process etc. However, this kind of analysis requires a large amount of parameters as an input data, which in the case of historical buildings are usually unknown.

Structural behavior of the arch can be examined with the principles of the structural theory of masonry using the following three simplifying assumptions, although they are not strictly true (Heyman 1995):

- Masonry has no tensile strength;
- Stresses are so low that the masonry has effectively an unlimited compressive strength;
- Sliding failures does not occur.

With these three assumptions the basic theorems of the plasticity it is possible to give a general statement about the behavior of the large masonry structure. In the case of a single-span *voussoir* arch, which is statically determinate, the minimum and maximum thrust can be calculated. Although the principles are presented with reference to a very simple arch, the conclusions apply to any, much more complex form of masonry, such as a complete Gothic cathedral (Heyman 1995).

In order an arch to be stable all possible position of the line of thrust must lie between the minimum and maximum one (Figure 5).

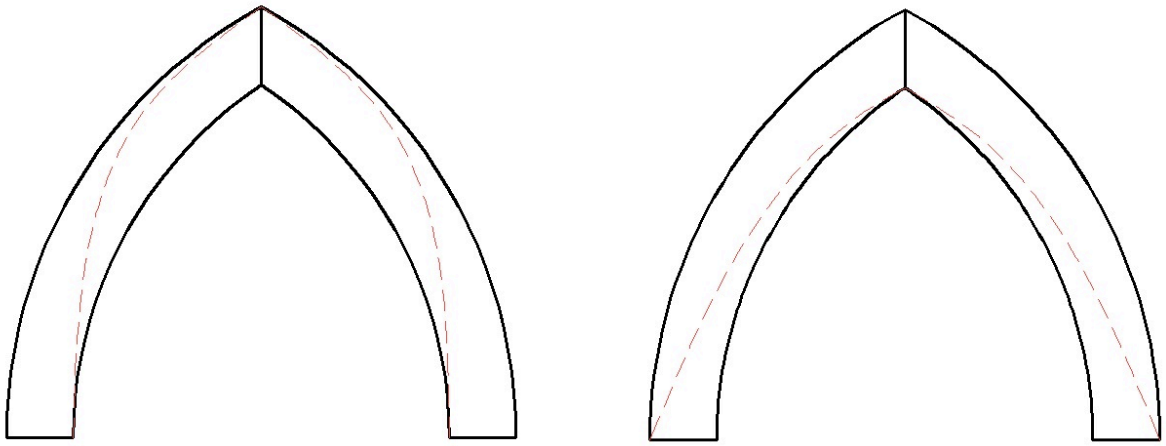

(a) (b)

Figure 5: Minimum (a) and maximum (b) thrust in an arch

2.2. Iron ties of Duomo di Milano

These elements are made from hand-made wrought iron and have rectangular cross section. Because of the large period of construction of the Cathedral, more than 200 years, differences in the tie geometry, properties and the way of clamping with the masonry can be observed.

2.2.1. Wrought iron

Metals have been used since very early ages. Even if it is not possible to know exactly which metal was the first extracted and worked, neither where or when this took place, the use of metals as structural and non-structural elements can be traced back to 2500 BC. Iron was used for the first time structurally in a small manner by the Romans, followed by larger scale application in medieval time. Finally, in 18th century iron became a common building material (Figure 6).

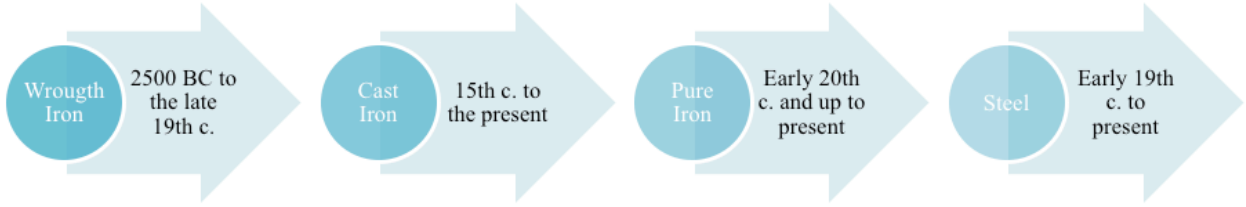

Figure 6: Commonly used ferrous metals

Being one of the first types of metal used examples of wrought iron metalwork can be traced back to 2500 BC.

In ancient times, due to its high cost, it was used for elements that need high strength such as weapons and tools, as architectural elements as nails and cramps, and also to strengthen or repair other building materials. Wrought iron was commonly used for locks, keys, chains, window bars, handles and hinges.

Later, after the Roman invasion of Britain, the wrought iron became a material used for structural purposes of considerable size. Romans made beams from it to support the tanks of water in their bathhouses. It began to be used to cover doors and windows of buildings to protect against attacks. An example of that kind of application is the one from 300AD, found at Hinton St Mary in Dorset (Godfraind S. et al. 2012).

Figure 7: Window grille found at Hinton St Mary in Dorset

In the 13th century wrought iron was used mainly for decorative purposes. Some of these works can still be seen today in famous European landmarks. In Figure 8 some examples of application of wrought iron as a decoration of doors are shown.

Figure 8: From left to right: West portal of Notre Dame de Paris; Split-curl hinges at St John the Baptist, Burford, Oxfordshire; The entrance to the gatehouse at Upnor Castle in Kent

In general metals can be divided in two groups – ferrous and non-ferrous. Ferrous metals are the one that contain iron, and therefore they have magnetic properties. Because of the iron content these types of metals are prone to corrosion, but by far are the most commonly used. In this group all the materials, which has iron as a main constituent belong such as wrought iron, cast iron, mild steel, iron alloys and stainless steel. Their great strength makes them suitable for structural members. On the other hand, non-ferrous do not contain iron and from here origins one of their important advantages – high corrosion resistance. Non-ferrous metals are much lighter than the ferrous and have non-magnetic properties. Because of their corrosion resistance non-ferrous metals have always been a popular choice for roof elements, rainwater goods and plumbing. They are also used as an anti-corrosion coating for ferrous

materials. Non-ferrous materials have excellent electric conductivity, which makes them suitable for lightning rods and electrical wiring. The group of non-ferrous materials consists of lead, copper, copper alloys (bronze, brass), tin, gold, silver, zinc, nickel, aluminum and chromium. They are weaker then iron and steel but in the meanwhile possess great malleability.

Wrought iron is ferrous material and one of the earliest types of metal used. Before inventing the furnaces that were hot enough to melt the metal, iron was produced by hand -repeating process of heating and hammering (Figure 9). Hammering the hot metal on an anvil was the main way to shape the iron.

Figure 9: Hammering of wrought iron

The definition of wrought iron according to the American Society for Testing Materials is:

"A ferrous material aggregated from a solidifying mass of pasty particles of highly refined metallic iron, with which, without subsequent fusion, is incorporated in a minutely and uniformly distributed quantity of slag." Wrought iron consists of two main components: high-purity iron and iron silicate. This iron silicate, which is commonly known as a slag, is a glasslike substance that is mechanically intermingled with the iron. Slag is added to the iron during the process of manufacturing as well as some impurities. Early wrought iron was an expensive material and because of that it was used mostly for coins, decorative ornaments and jewelry. Later the Romans started using it as a structural element like beams and ties (Godfraind S. et al. 2012).

- ❖ Properties of wrought iron

Different types of ferrous materials were used for structural elements during the past, and their origins or characteristics might not be well documented, especially in case of old heritage structures. Since the knowledge of the used metal is of great importance when assessing existing historical buildings, one should employ different techniques for the recognition of the examined material. For example, considering date of the structure, observing its cut section (if available), one can get an idea of the used metal by comparing this data with properties of commonly used ones (Table 1). When possible, direct mechanical test, metallographic and chemical analysis can be used to confirm assumptions or give precise data on properties of examined material. In case when dealing with heritage structures, usually the Non-Destructive Techniques (NDT) are the only permitted tool to be used together with visual inspection or historical research.

Material	Characteristics	Appearance (cut section)	Oxidised colour	Corrosion resistance	Architectural applications	In common use
Wrought iron	Manufactured by smithing, giving a characteristic layered and fibrous appearance	 Fibrous Grey	Reddish-brown	Low Needs coatings	Fastenings Small fittings such as locks, chains, and hinges Railings and gates Beams and tie bars	2500 BC to late 19th century Large components from 18th century onwards
Cast iron: common or grey	Contains flakes of graphite: broken surfaces appear grayish, and form planes of weakness.	 Granular Grey	Reddish-brown	Much more resistant than steel	Fireplaces, railings Load-bearing structures (panels, columns, beams)	15th century to present
Steel: carbon steel	Contains carbon, manganese and silicon, and possibly other elements. Strong, malleable, easy to weld, excellent rigidity. Can be cast, machined and extruded	 Granular Shiny grey	Reddish-brown	Poor Needs coatings	Used extensively for structural applications.	1880 to present

Table 1: Properties of the most commonly used ferrous materials

The structure of the metals not only makes distinction of metals possible, but strongly affects the mechanical properties of the material (Table 2). Because of the production technology the wrought iron has fibrous structure, very similar to the wood grain, which is due to the elongated inclusions of slag in it. It is therefore easily distinguished from cast iron or mild steel, which due to their production technique have granular structure. Even more important, it has good tensile strength along its fibers and mainly was used for tension members, opposite to cast iron which good compression properties were commonly exploited for columns and arches. Generally, the strength of the material depends upon the grains and slag relation and on the possibility of deformation. The slag inclusions entrapped in the structure, if distributed correctly, confer appreciable strength on pure, soft iron. Although it is vulnerable to splitting, the low content of carbon makes wrought iron more ductile in comparison with the cast iron for example.

Wrought iron is a strong material with high elasticity and tensile strength, which makes it very suitable for structural applications. Moreover its malleability allows to be shaped in different forms, leading to its usage as a decoration. Wrought iron is also easy to weld because of its low carbon content. It can be heated and reheated and this process makes it become even stronger.

Another very important property of the wrought iron is its high fatigue resistance due to the high toughness it possess. It will deform considerably, within its elastic limit, without failure. In the meanwhile it is prone to corrosion, which might be improved by means of coatings. The presence of slag inclusions makes the corrosion more uniform and prevent from pitting corrosion, but in the same time they can be considered as pathways to corrosion.

The elastic and plastic properties of wrought iron depend on the variety of its microstructure. The phenomenon of static fracture is of an intermediate character between plastic and brittle process of specimens due to heterogeneity of wrought iron.

Collected results for the properties of the wrought iron are given in Appendix A.

The slag inclusions prevent longitudinal and transverse strains and decrease elastic ones.

Material	Wrought iron	Cast iron	Carbon steel
Specific weight [kg/m^3]	7700	7500	7800
Yield strength [MPa]	220÷310	/	240÷280
Tensile strength [MPa]	280÷400	90÷135(265)	370÷450
Compression strength [MPa]	200	700	370÷450
Elongation [%]	5÷20	0	15÷20
Temperature of melting [°C]	~1500	~1200	~1000

Table 2: Mechanical properties of commonly used metals

Because the cast iron was easy to be produced at the beginning it was the preferred material for structural components, while the wrought iron was mainly used for decorative work. But the cast iron is brittle material, and after the failure of several structures made by it in the early 19th century, the wrought iron that has good tension and compression strength, was increasingly used for load-bearing applications.

Cast iron continued to be popular for structural elements under compressive loads, as well as for non-structural and decorative applications such as fences, mileage-markers and plaques, roof crests, street furniture, rainwater goods, piping, stoves and fire backs, and for smaller fittings such as latches, bell-pulls and boot scrapers. Cast and wrought iron were often used together, so the compressive and decorative advantages of cast iron could be used to complement the tensile capabilities of wrought iron. Gradually cast iron was replaced by steel.

2.2.2. Experimental campaign for material characterization

Several tests were conducted on samples taken out from the available original Duomo's tie (Figure 10) - sample for chemical analysis from part 2-3, various samples for density measurements from part 6-7, while series "n", "c" and "r" were used for tensile test.

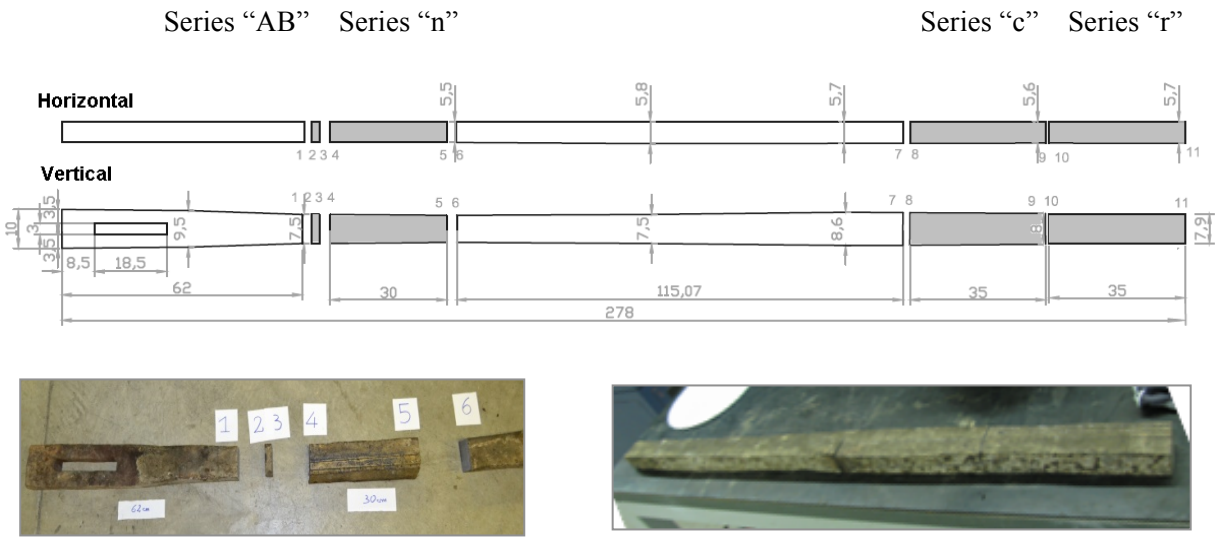

Figure 10: Test samples

- Visual inspection

The surface of the tie under consideration is covered by a thin reddish-brown oxidized layer (Figure 12) while its inner structure has fibrous appearance (Figure 11). This structure is typical for the wrought iron and it not only helps in the identification of the material but also affects its material properties. Because of its fibrous structure wrought iron is easily distinguished from the cast iron or the mild steel for example, which due to their production technique have granular structure.

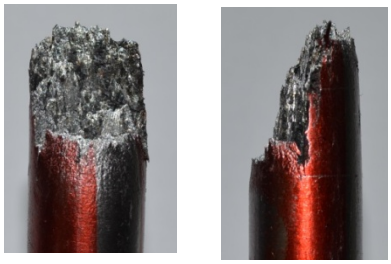

Figure 11: Cut section of Duomo tie

During the visual inspection of the cut samples taken from the original tie of Duomo various voids, inclusions, cracks and discontinuities from few millimeters up to few centimeters were identified (Figure 12). Their amount throughout the volume of the element and origin result in different influence on the mechanical behavior of the tie. It also can contribute the failure and therefore they have to be taken into consideration in the interpretation of the results of material characterization and failure analysis. Most of the observed damage is probably due to inherent problems, related with the working temperature and therefore the production process.

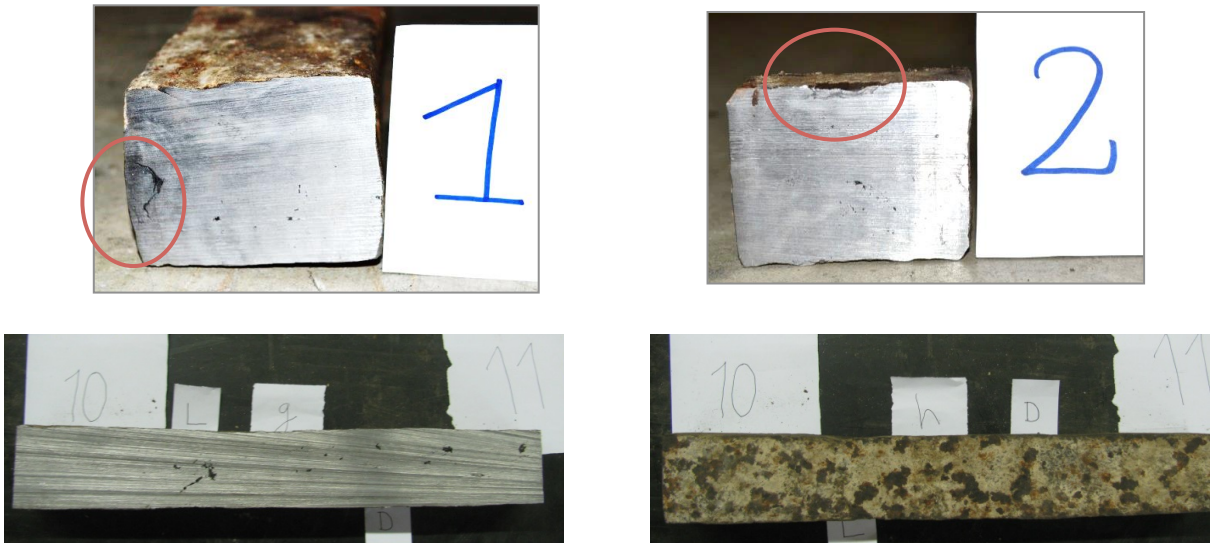

Figure 12: Surface appearance of the ties

- Tensile test

Tensile test has been performed according to European standard EN ISO 6892-1 on 3 series of samples. Series "n" included 2 unmachined test pieces, taken from part 4-5 from the available tie, with rectangular cross section. Series "c" included 3 machined test pieces, taken from part 8-9 from the tie, with circular cross section (Figure 13). The dimensions of the specimens of the series "n' and "c' are given in Table 3. Series "r" included 3 machined test pieces 35 cm long from part 10-11 of the tie with rectangular cross section having dimensions 5.95mmx20.6mm (Figure 13).

(a) (b)

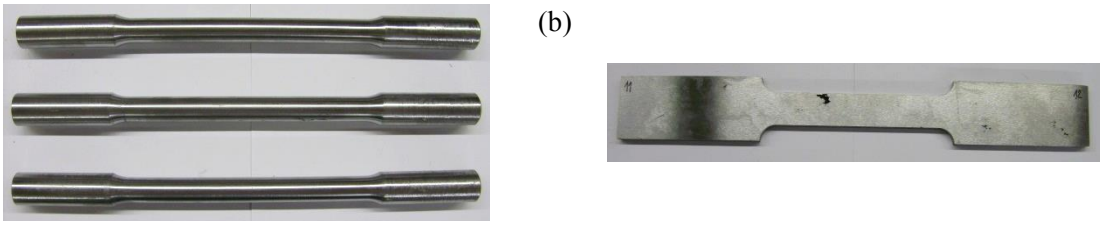

Figure 13: Series "c" (a) and "r" (b)

Sample	Dimensions		
	b (φ) [mm]	h [mm]	l [mm]
n1	18.33	18.66	30
n2	16.63	25.85	30
c1	14.94	/	35
c2	14.95	/	35
c3	14.96	/	35

Table 3: Dimensions of test pieces for series "n" and "c"

The test itself consists in straining a test piece by tensile force to fracture for the determination of the mechanical properties of the material tested. The test is carried out at room temperature between 10°C and 35°C.

The outcome of the tests is the tensile stress-strain diagrams (Figure 14).

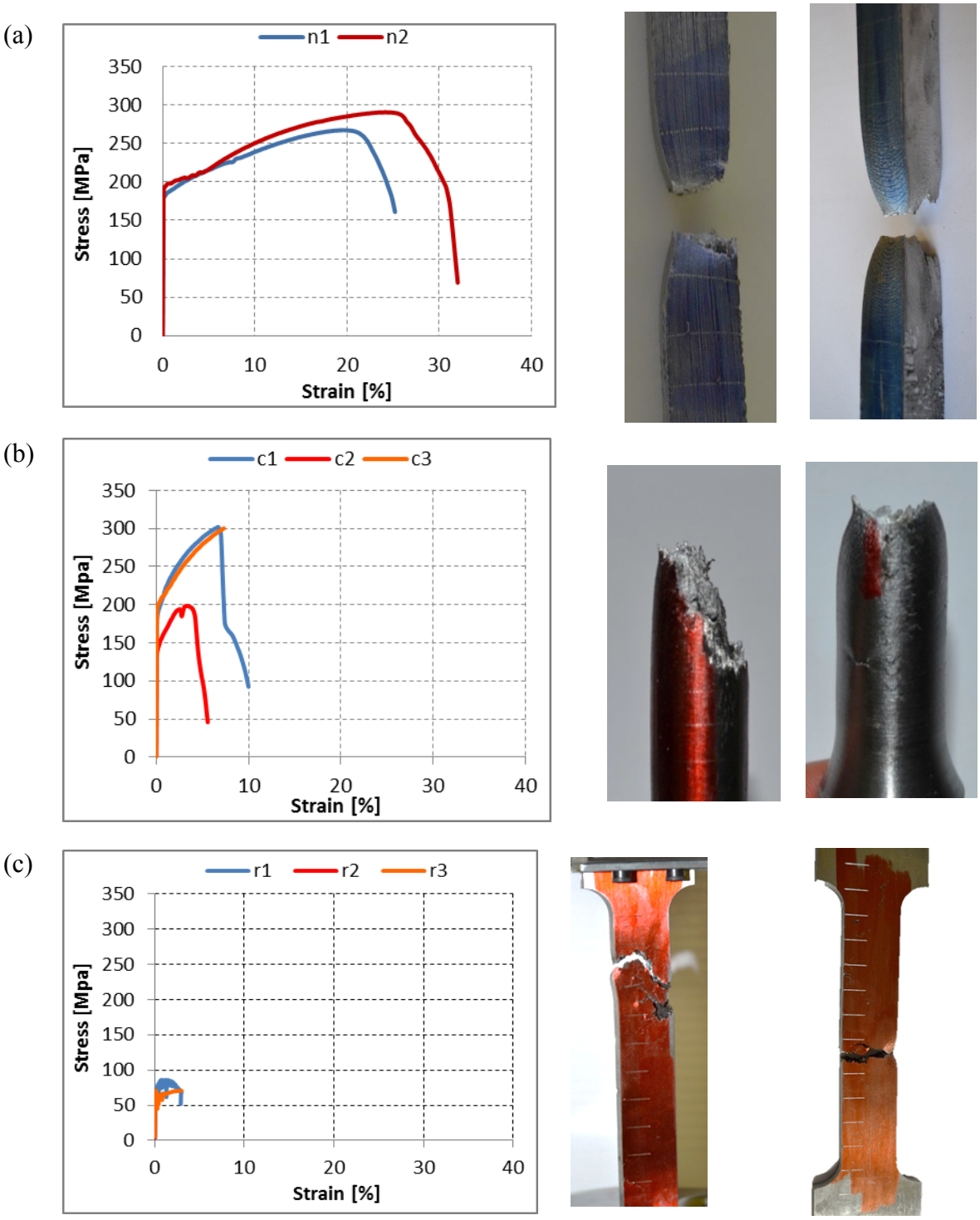

Figure 14: Tensile stress-strain diagrams and sample failures for series "n" (a), "c" (b) and "r" (c)

From these diagrams the upper and lower yield strength (R_{eH} and R_{eL})can be determined. The upper yield strength is equal to the maximum value of stress prior to the first decrease in stress. The lower yield strength is defined as the lowest value of stress during plastic yielding, ignoring any initial transient effect. Some examples for determination of these properties are given in Figure 15.

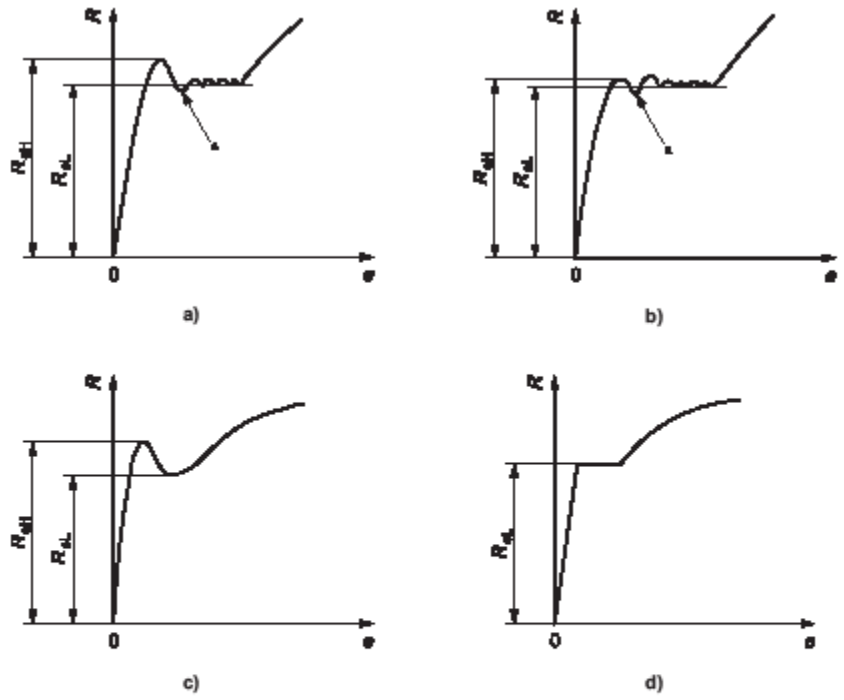

Figure 15: Examples of upper and lower yield strengths for different types of curves

As it can be seen from Figure 14 the observed behavior of the wrought iron is different from the ones shown in Figure 15, which is due to its fibrous microstructure. These differences make the determination of the upper and lower yield strength difficult. Moreover the results from some of the test series differ significantly from the one of the other series, which is the case of series "r". This can be explained with the fact that these samples were taken from the part next to the failed section and most probably they have same damage as micro voids, cracks and inclusions. For this reason the results from test conducted with series "n" and "c" were used in the determination of the mechanical characteristics (Table 4).

Sample	σs	σs	E	RA
	[MPa]	[MPa]	[MPa]	[%]
n1	182	267,3	191,8	-
n2	193	290,45	200,8	-
c1	193,88	302,24	265,51	-
c2	145,63	198,55	237,07	33.33
c3	201,13	318,65	236,45	42.64

Table 4: Mechanical characteristics for series "n" and "c"

2.2.3. Use of the wrought iron in historical constructions

In modern time wrought iron was used not only for decoration. Its properties make it suitable for structural elements as well. In historical masonry structures, particularly in Gothic cathedrals, metallic or wooden ties were extensively used during the construction (Fitchen 1961) or later on during interventions, such as seismic improvement.

One bright example of this kind of application of wrought iron in historical structures is the Salisbury Cathedral in Wiltshire. A wrought iron ring-beam was used there to reinforce the junction between the tower and the spire. Wrought iron ties can be found in the structures of Westminster Abbey, Duomo di Parma and Canterbury Cathedral (Figure 16).

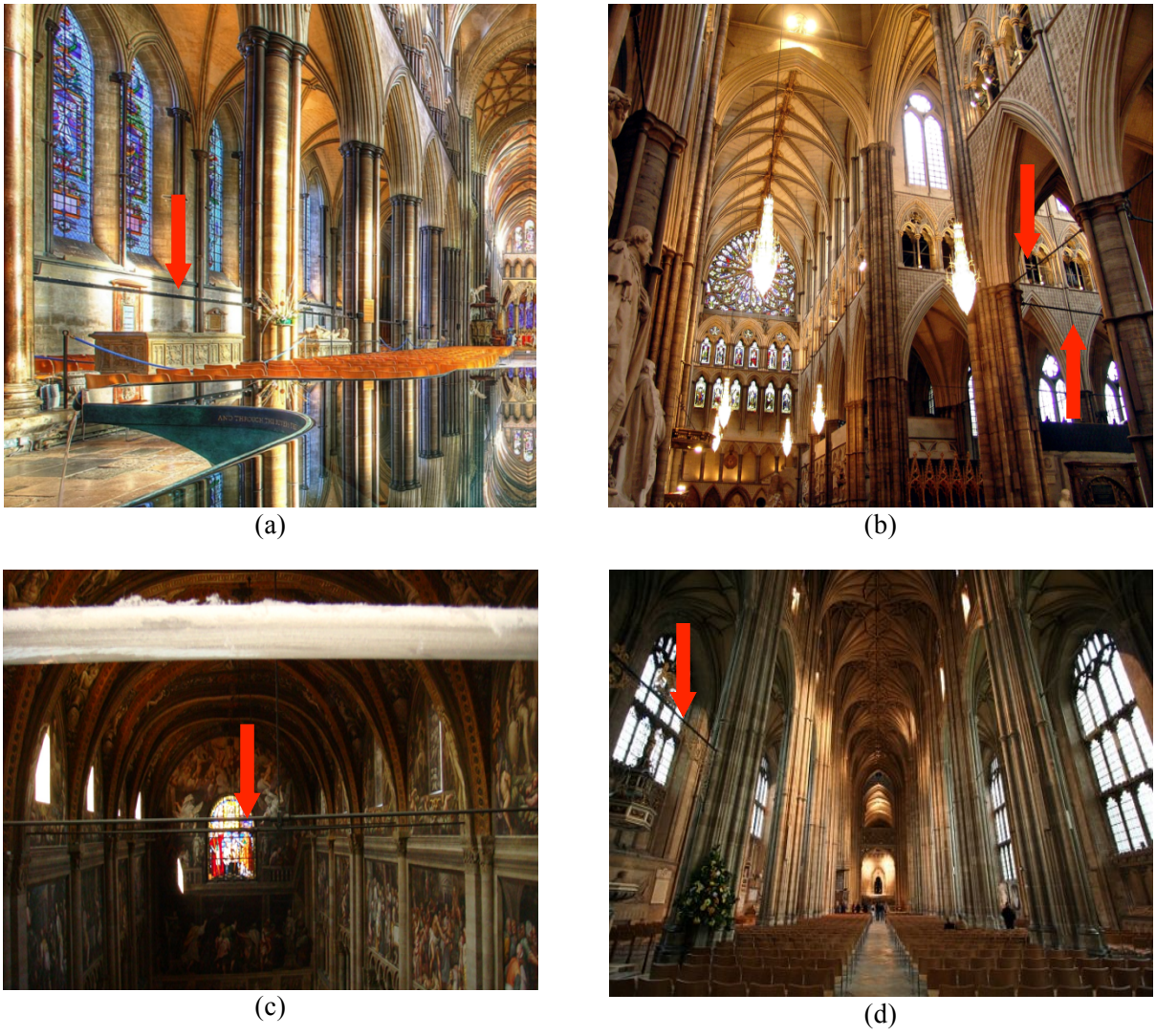

(a) (b) (c) (d)

Figure 16: Salisbury Cathedral (a), Westminster Abbey (b), Duomo di Parma (c) and Canterbury Cathedral (d)

Wrought iron was also extensively used for bridge structures, such as Thomas Telford's suspension bridge over the Menai Straits between Anglesey and Wales, built between 1819 and 1826. Also Weichsel Bridge - the first large wrought iron girder railway bridge built in Germany in 1857 and

Gustav Eiffel's Garabit Viaduct built in France in 1884 in the structure of which for the first time a wrought iron truss arch was used. Another example of the use of the wrought iron as a structural element for bridges can be found in Australia, the Menangle Viaduct in New South Wales built in 1863.

Another application of the wrought iron with structural purpose is the current case study – the ties in Duomo di Milano. The ones in the main nave have about a 92x62 mm cross section, while ones of the inner lateral north and inner lateral south nave have smaller dimensions, but still slightly different in the two naves (74x51 mm and 77x44 mm respectively).

Because of the production technique of wrought iron that was changing in time, most probably the material properties of the different elements vary.

Another difference that can be observed in the ties is the way of clamping into the masonry. Three different types of them can be distinguished

Figure 17: Clamping of the ties in the columns

2.2.4. Present state of the stress in the ties

The present state of stress in the structural elements is one of the most relevant tasks when assessing an existing structure. For example, during the experimental campaign in Duomo di Parma the results showed that the working tensile stress in the metallic ties (which replaced the original ones in 1950's after the failure of one of them) is near the material's yield stress (Garziera and Collini 2010). When the structural system is complex and the thrust is resisted by a combined action between several parts, or in cases when a structural intervention included insertion of elements which influences the original structural system the estimation of the current state of stress is a challenging process. Structural analysis by means of limit analysis and numerical analysis can give one of the infinite numbers of equilibrium solutions, which according to the Safe Theorem (Heyman 1995) should mean that the structure is safe and stable, while only the experimental measurements of stresses in the structure can indicate the actual amount of the thrust resisted by each element (Vasic et al. 2015).

As indicated by recent preliminary dynamic testing (Vasic et al. 2015) and static analysis (Coronelli et al. 2014b), the ties in Duomo di Milano are active elements that balance the lateral thrust and are present in all five naves of the Cathedral. Therefore their origin, material properties, structural role and present condition are of great importance for the remaining life of the structure and should be assessed.

The axial force in metallic ties can be assessed by means of dynamic methods (Lagomarsino and Calderini 2005, Tullini and Laudiero 2008, Amabili et al. 2010, Tullini et al. 2012, Gentilini et al. 2013, Rebecchi et al. 2013). The dynamic characteristics such as natural frequencies, corresponding mode shapes and damping ratios can be derived through different techniques – Experimental Modal Analysis (EMA) (Ewins 2001, Harris and Piersol 2002) or Operational Modal Analysis (OMA) (van Overschee 1996, Brincker et al. 2000, Peeters 2000). EMA techniques identify modal components as a ratio between measured input and structural response, while OMA techniques are output-only and the excitations are the operational conditions of the structure.

A simple method for vibrating string confirmed the existence of axial force (Vasic et al. 2015) in the tie-rods of Duomo di Milano. More refined method (Tullini and Laudiero 2008) was employed and allowed the axial force and the spring stiffness coefficient to be estimated using one flexural mode shape (Guidobaldi et al. 2014)

After a geometric characterization phase, dynamic testing was carried out on the tie-rods by means of classic hammer tests (Harris and Piersol 2002). Each element was equipped with 3 piezoelectric accelerometers (with nominal sensitivity equal to 500 mV/G), installed at 1/4, 1/2 and 3/4 of the total length. The excitation was provided by hitting each of the instrumented cross sections for 5 times as shown in Figure 18.

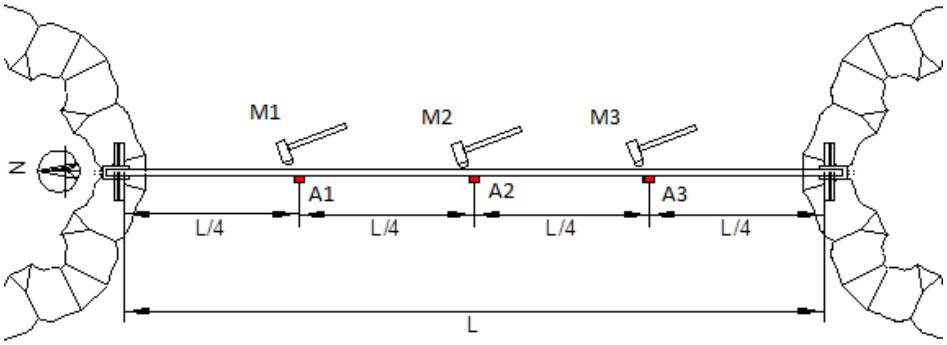

Figure 18: Dynamic testing scheme

The main dynamic characteristics of the tested tie-rods (natural frequencies and corresponding mode shapes) were derived from Frequency Response Functions (FRF) estimated from the time histories recorded during the hammer tests (Harris and Piersol, 2002).

The element was modeled as a beam on elastically restrained supports (Figure 19). Elastic springs in the two extremities of the element can be introduced since the actual boundary conditions of the metallic tie-rod inside the masonry do not correspond exactly to the classic cases of pinned-pinned, clamped-clamped or pinned-clamped beam. The case of pinned-pinned boundary conditions results when the rigidity of these elastic springs is nearly zero, while clamped-clamped is the case of infinite one. The intermediate values represent different degrees of restrain in the springs.

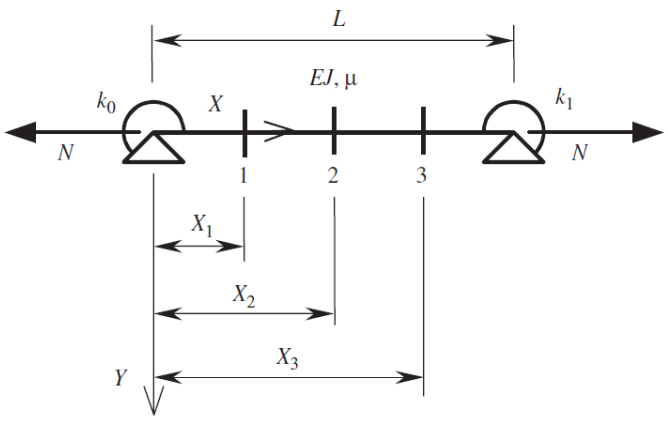

Figure 19: Beam with end flexural constraints and location of the instrumented sections

The elastic spring affects only the boundary conditions and therefore the governing equation is the same as for the small-amplitude, harmonic, transverse vibration of a beam (Virgin 2007):

$$\frac{d^4v(x)}{dx^4} - n\frac{d^2v(x)}{dx^2} + \lambda^4 v(x) = 0 \qquad \textit{Equation 1}$$

$$n = \frac{Nl}{EI} \qquad \textit{Equation 2}$$

$$\lambda^4 = \omega^4 \frac{\mu L^4}{EI} \qquad \textit{Equation 3}$$

Where:

N is the axial force in the vibrating beam;
L is the length of the beam;
E is the modulus of elasticity;
I is the second moment of inertia;
ω is the first circular frequency.

The general solution of the differential equation is:

$$v(x) = C_1 \cos q_1 x + C_2 \sin q_2 x + C_3 \cosh q_3 x + C_4 \sinh q_4 x \qquad \textit{Equation 4}$$

$$q_1 = \frac{1}{2}\left(\sqrt{n^2 + 4\lambda^4} - n\right) \quad \text{and} \quad q_2 = \frac{1}{2}\left(\sqrt{n^2 + 4\lambda^4} + n\right) = q_1 + n \qquad \textit{Equation 5}$$

For control points assumed at sections having non-dimensional coordinates $x_1 = \frac{1}{4}$, $x_2 = \frac{1}{2}$ and $x_3 = \frac{3}{4}$ the solution takes the form:

$$\frac{v_1 + v_3}{v_2} = \frac{1 + 2\cos\left(\frac{q_1}{4}\right)\cosh\left(\frac{q_1}{4}\right)}{\cos\left(\frac{q_1}{4}\right) + \cosh\left(\frac{q_1}{4}\right)}$$ ***Equation 6***

Where:
v_1, v_2 and v_3 are the modal components at control points x_1, x_2 and x_3, respectively.

Finally the axial force in tie-rod was estimated following the procedure:

1. Natural frequencies and corresponding mode shapes were derived from FRFs recorded during hammer test
2. Value of q_1 was calculated from Eq. 6
3. Value of n was calculated from Eq. 5
4. Value of N (axial force) was calculated from Eq. 4

The results in terms of stresses are shown in Figure 20.

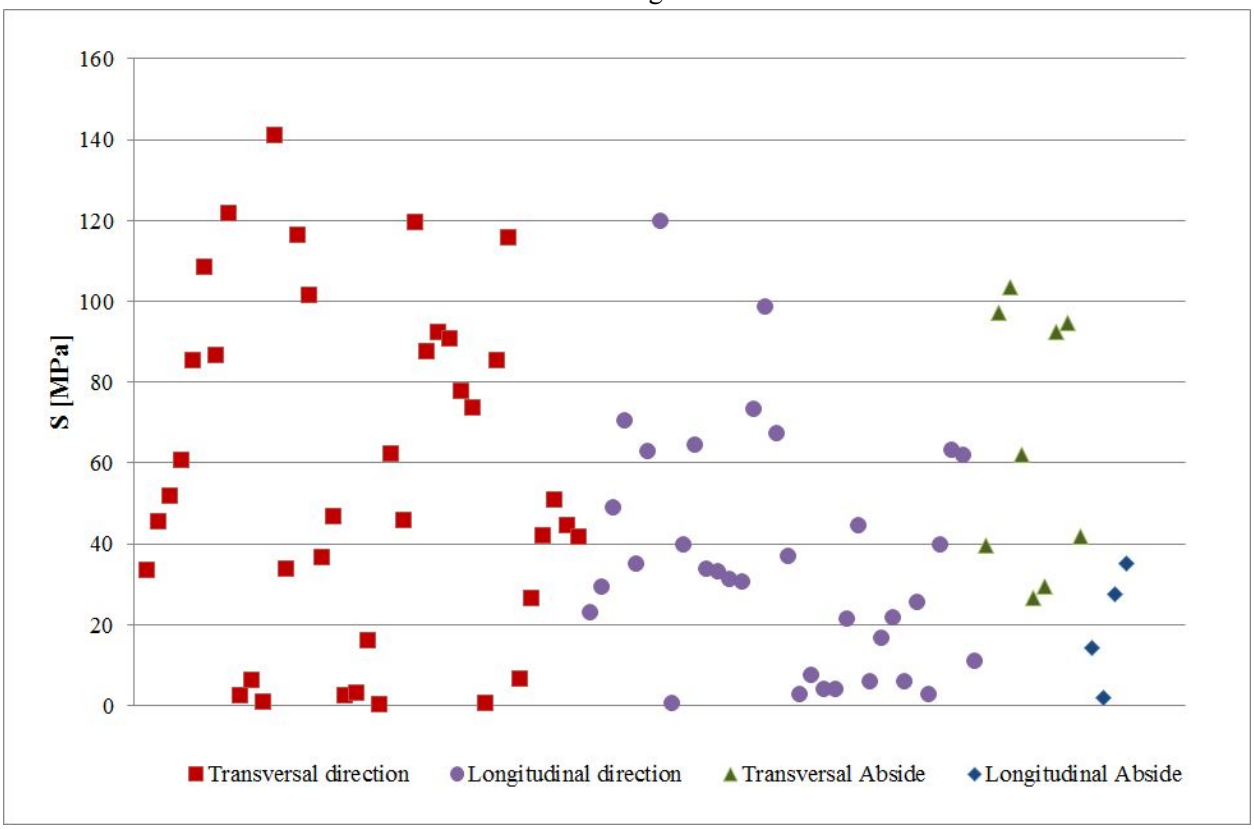

Figure 20: Stress in the ties of Duomo di Milano

Making use of adopted experimental procedure (Tullini and Laudiero 2008), it was possible to estimate state of the stress in one of the tie-rods during a period of a year and during an intervention. In particular, this tie-rod was heated with a thermal blanket which imposed temperature ranging 10°-60°, so the variation of the stress in the tie-rod and the variation in stiffness of the boundary conditions were monitored using the adopted technique. In this way, the effect of the imposed temperature can be observed. After a drop of the stress in the tie-rod when reaching 40°, its level remained almost constant,

while stiffness of boundary conditions kept changing. This demonstrates redundant nature of cathedral's masonry structures and capacity to adapt to newly introduced conditions.

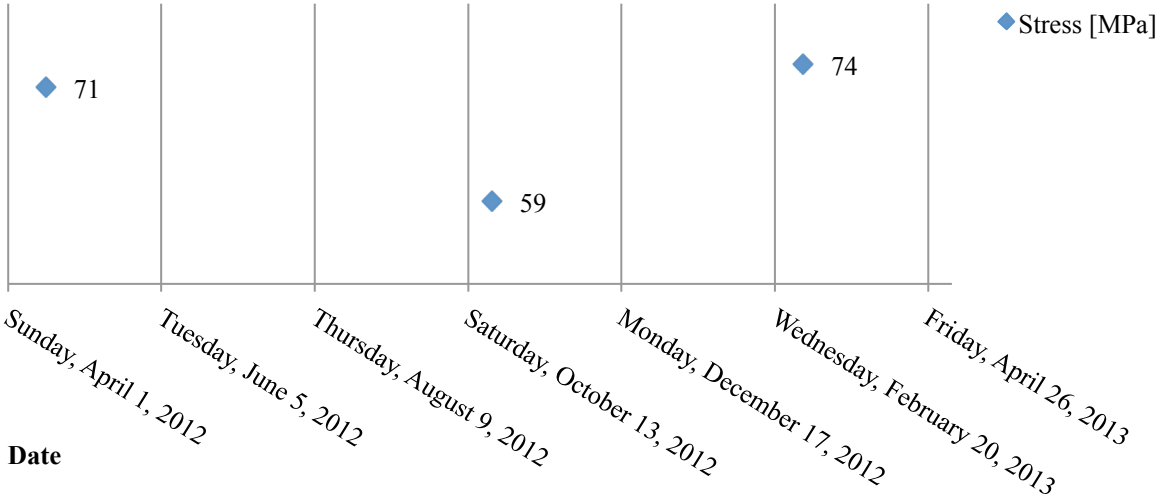

Figure 21: State of the stress in tie 61_91 during a year period

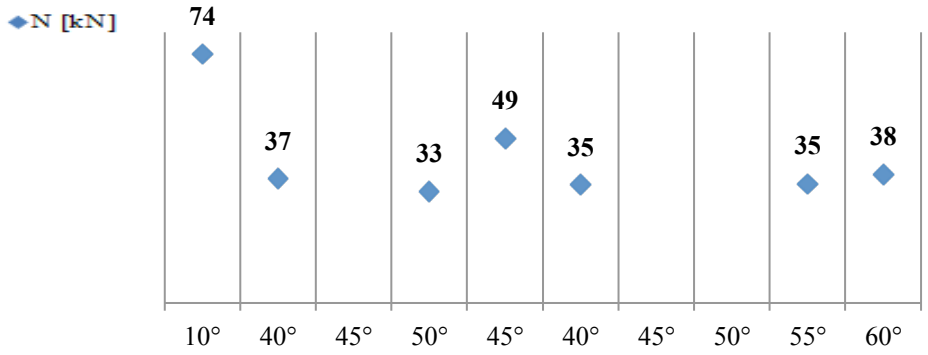

Figure 22: State of stress in tie 61_91 during an intervention

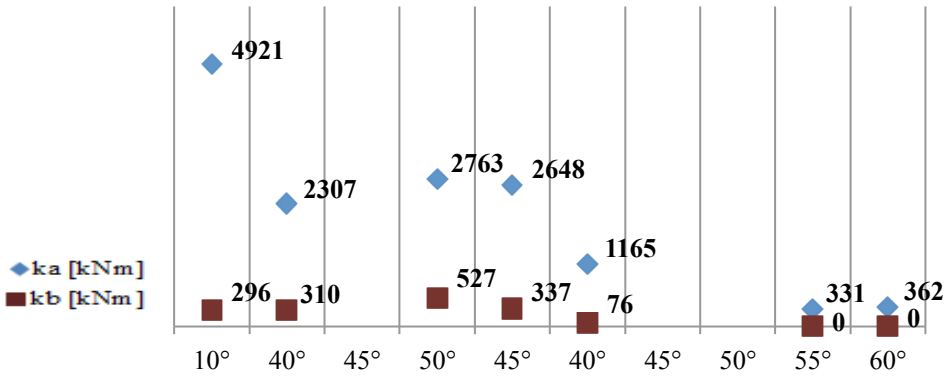

Figure 23: Stiffness of the boundary conditions in tie 61_91 during an intervention

The most relevant causes of damage and deterioration for the case study of Duomo di Milano are the inherent problems, related with defects in the material, as well as the structural problems – fatigue and fracture, and the environmental problems of which temperature is the most important one.

As the main cause for the cyclic loading in the case of the ties in Duomo di Milano it can be pointed out the temperature. In Figure 24 the internal and external temperature variation in one month (March 2014) measured in the lantern of the Cathedral is shown. The internal temperature shows more or less constant behavior in time with a difference in the measurements in the range of 5°C, while the external one has greater variation which reaches a difference of about 20°C. This variation can cause significant alternation in the stresses in the elements and could lead to fatigue phenomenon.

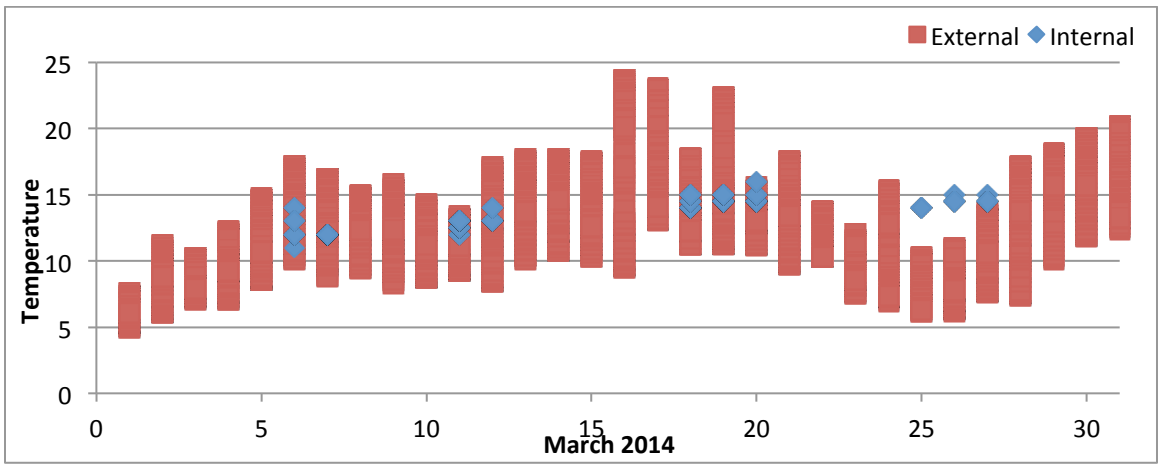

Figure 24: Temperature change in March 2014(private communication from Prof. A. Cigada)

Different kinds of controls were carried out in the zone of the main dome in Duomo di Milano, within the structural health monitoring campaign, required for the recent restoration works on the main spire such as analysis of the vertical and horizontal movements, analysis of slope variations, convergence between the pillars, dome cladding displacements with strain gauges and crack measurements (Cigada et al. 2011).

The deformations in Duomo di Milano are controlled by monitoring system that measures semi-annual variation of piers' verticality and vertical displacements variation of floor points inside and outside of the building. By means of these periodic measurements, a variation of the verticality of pier 88 (Figure 25) was determined partially every 6 months and its relative variation is reported as well as the total one with respect to year 1981 in Figure 26.

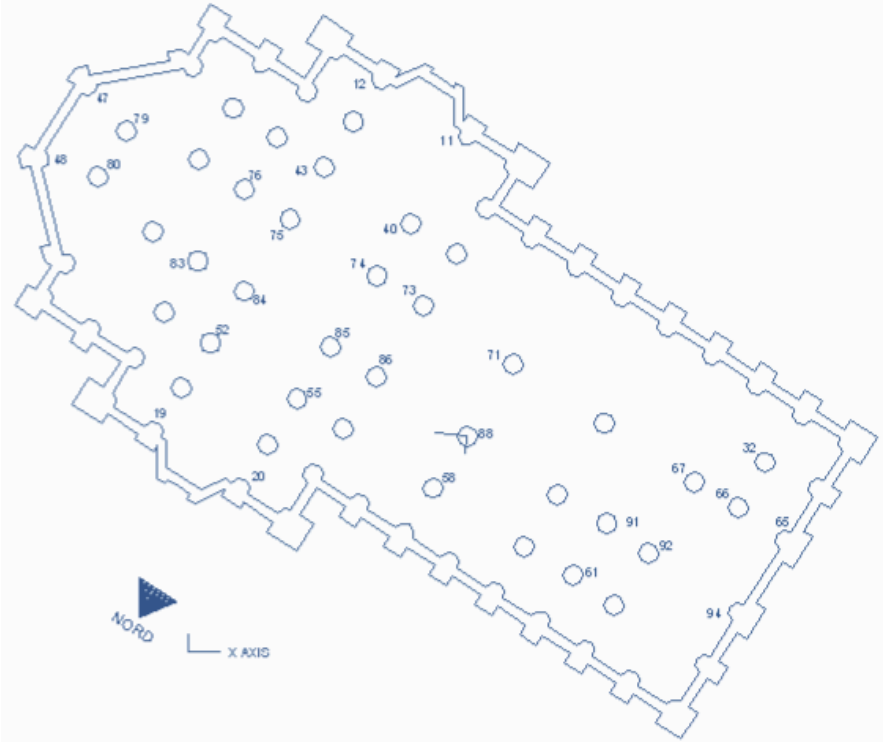

Figure 25: Plan of the first floor of Duomo di Milano (Giussani and Roncoroni 2009-2014)

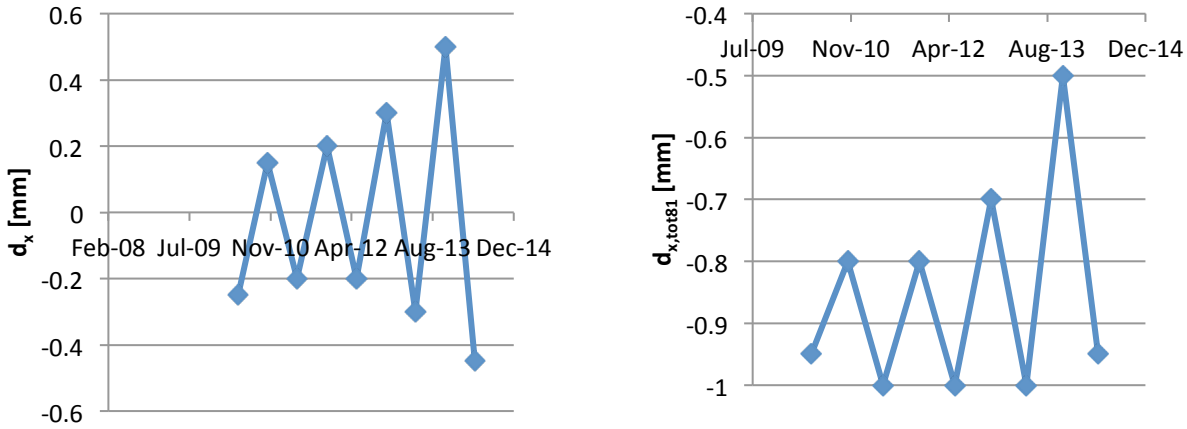

Figure 26: Relative displacements of column 88 in local direction X (Giussani and Roncoroni 2009-2014)

2.3. *Numerical model of a representative arch in Duomo di Milano*

A simplified model of one of the arches with the tie-rod, (Figure 27) was created in this thesis using the software SAP2000 in order to understand the structural behavior of the system. This model was used to assess the influence of the temperature variation (daily and seasonal) on the tie in terms of change in the axial force and the stresses as well.

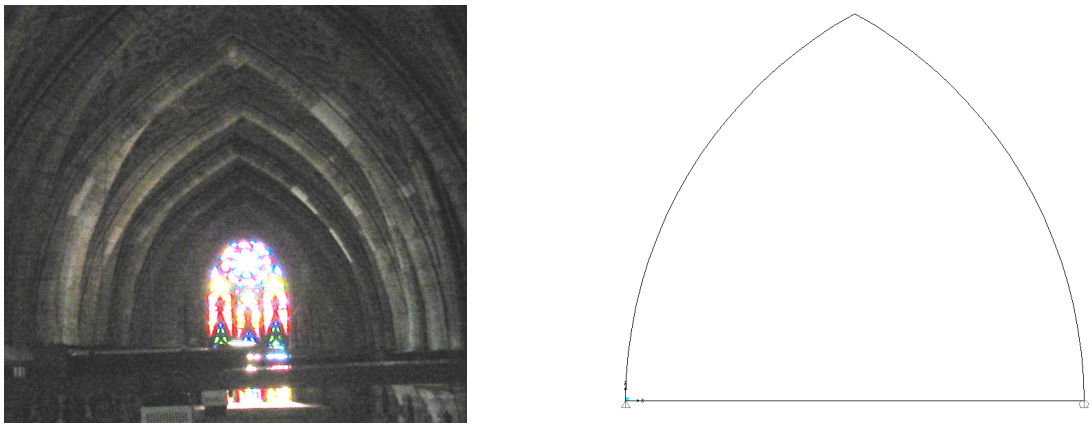

Figure 27: Arch of Duomo di Milano and geometry of the simplified model

The materials for the arch and the tie-rod have characteristics, given in Table 5 and Table 6 respectively.

Weight per unit volume	27.5 kN/m^3
Modulus of elasticity, E	4x10^{9}kN/m^2
Poisson's Ratio	0.2
Specified Compressive Strength	400 kN

Table 5: Material characteristics of the masonry

Since for the case of Duomo di Milano the coefficient of thermal expansion for the stone masonry is not known the value for it is taken from the literature. In Appendix C: Stone and rock properties of the Geological Society, London the coefficient of thermal expansion for marbles is given in the range $2.1 * 10^{-6} \div 5.7 * 10^{-6}\ {}^{1}/_{°C}$. The analysis was done using the two limit values.

Weight per unit volume	78 kN/m^3
Modulus of elasticity, E	2.05x108 kN/m^2
Poisson's Ratio	0.3
Coefficient of thermal expansion	1.17x10^{-5} 1/℃
Minimum Yield stress, F_y	~248200 kN/m^2
Minimum Tensile stress, F_u	~399900 kN/m^2
Effective Yield stress, F_{ye}	~372320 kN/m^2
Effective Tensile stress, F_{ue}	~439900 kN/m^2

Table 6: Material characteristics of the wrought iron

The geometry of the cross sections of the arch and the tie are shown in Table 7.

Element	Width [m]	Depth [m]
Arch	1	0.57
Tie	0.0509	0.0784

Table 7: Geometric characteristics of the cross sections of the elements

During the analysis of the structure with the simplified model it was taken into account the dead load of the structure as well as a constant temperature load and gradient one, acting on the cross-section

of the arch. These loads were assumed to be 1°C and later on the effects of these loads were multiplied by the desired temperature in order to obtain the real axial force and stress in the tie.

The diagram of the axial force due to constant temperature and temperature gradient along the cross-section of the arch are given in Figure 28.

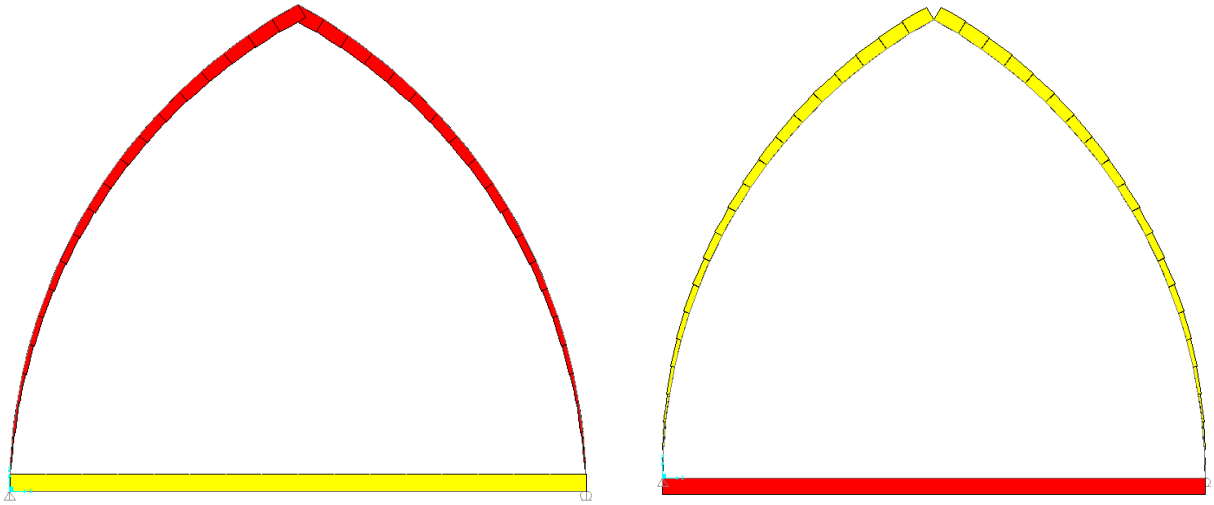

(a) (b)

Figure 28: Axial force in the arch and the tie due to (a) constant temperature and (b) temperature gradient along the cross section of the stone arch

In Table 8 the values of the axial force in the tie due to the constant temperature and temperature gradient along the cross section of the arch are shown for the two cases of coefficient of thermal expansion in the masonry used.

Temperature load	$\alpha = 2.1 * 10^{-6}\ 1/°C$	$\alpha = 5.7 * 10^{-6}\ 1/°C$
Constant temperature 1°C	1.188 kN	3.224 kN
Temperature gradient 1°C	-8.71 kN	-23.641 kN

Table 8: Axial force due to temperature

2.4.1. Daily temperature variation

In order to understand if the daily temperature variation may cause changes in the stresses of the tie big enough to cause fatigue, the data recorded in March 2014 already shown in Figure 24 was used together with the results from the analysis in SAP2000. The maximum thermal gradient during the day is around $10°C$, while in the night it is $-10°C$. The internal temperature in the Cathedral is almost constant and its average in March is taken ($14°C$) and for this reason only the thermal gradient can cause cyclic loading on the tie. The results for the two thermal gradients (during the night and the day) are reported in Table 9.

Temperature load	$\alpha = 2.1 * 10^{-6}\ 1/°C$	$\alpha = 5.7 * 10^{-6}\ 1/°C$
$\pm 10°C$	± 87.1 kN	± 236.4 kN

Table 9: Axial force due to daily thermal gradient

The results for the axial force are quite high and in reality this is not the case. Because of the simplicity of the model several aspects that might lower the value of the axial force are not taken into account.

First of all it should be kept in mind that the model in SAP2000 overestimates the stiffness of the structure. The arch is modeled as a continuous element without any joints, while in reality is composed of number of *voussoirs*. The structure is more deformable than the model in SAP2000 and for that reason the axial force in the tie due to the thermal gradient will be smaller.

A second reason for reducing the effect of the temperature on the tie-rod comes from the static analysis of the arch. If the resultant force is acting in the central 1/3 part the whole section is in compression. On the contrary if the force is outside of that region part of the section will be in compression and the other one in tension (Figure 29).

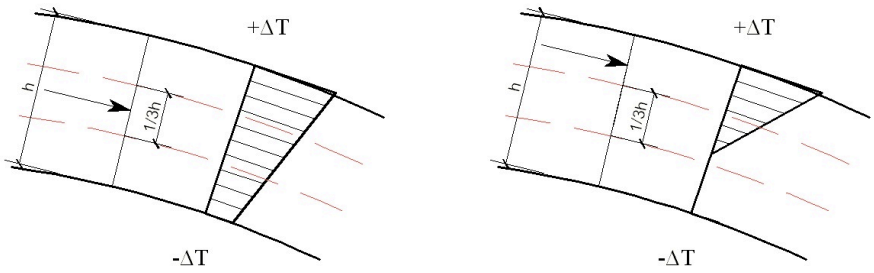

Figure 29

Another aspect that is very important and should be taken into account in the thermal analysis is the thickness of the section of the arch and the vault (Figure 30).

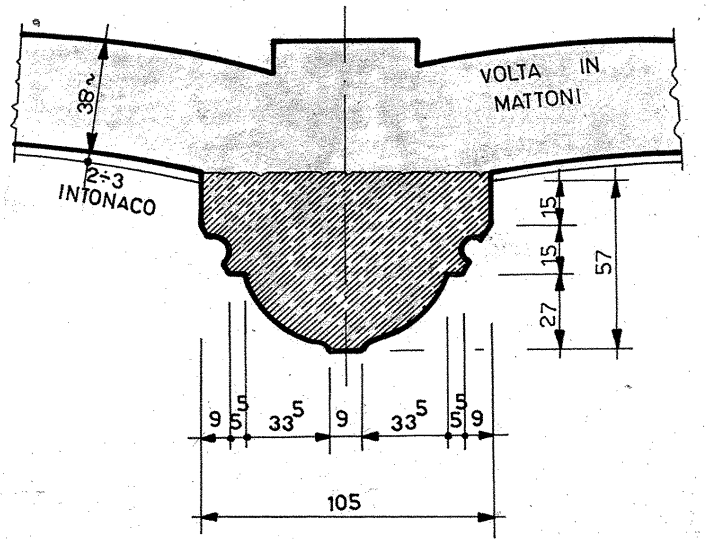

Figure 30: Cross section of the arch and the vault

When an element is subjected to temperature gradient it takes time for the temperature to propagate and stabilize inside the element. The higher the thickness the longer the time needed to reach this steady state. When considering a daily variation in temperature the time of the half cycle (12 hours) is

not enough for the system to reach this stable condition. Since the analysis in SAP2000 is steady state a linear distribution of the temperature gradient, equivalent to the curved real one should be determined.

This equivalent average thermal gradient could be found using the curvature (Figure 31).

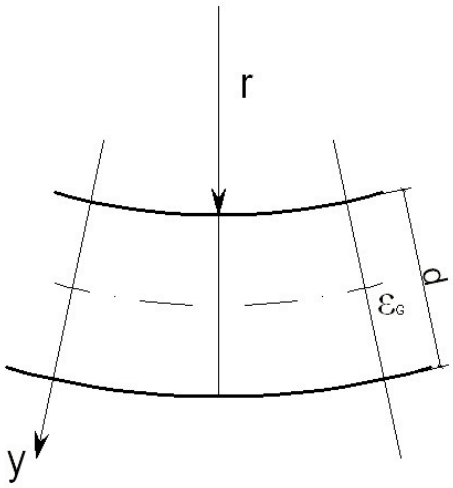

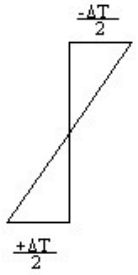

$$\frac{1}{r} = \frac{\Delta T \alpha}{d}$$

Figure 31

$$\varepsilon_{tot} = \varepsilon_G + \frac{y}{r} = \varepsilon_{el} + \varepsilon_{th}$$

$$\sigma = E\varepsilon_{el} = E\left(\varepsilon_G + \frac{y}{r} - \varepsilon_{th}\right)$$

$$N = \int \sigma \, dA = E\int\left(\varepsilon_G + \frac{y}{r} - \varepsilon_{th}\right)dA = 0$$

$$EA\varepsilon_G = E\int \varepsilon_{th} \, dA$$

$$\varepsilon_G = \frac{\int \varepsilon_{th} \, dA}{A}$$

$$M = \int \sigma y \, dA = E\int\left(\varepsilon_G y + \frac{y^2}{r} - \varepsilon_{th} y\right)dA = 0$$

$$\frac{I}{r} = \int \varepsilon_{th} y \, dA$$

$$\frac{1}{r} = \frac{\int \varepsilon_{th} y \, dA}{I}$$

An example of equivalent thermal gradient is given in Figure 32.

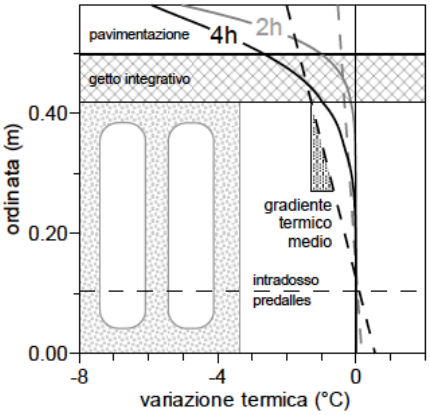

Figure 32: Example of average (effective) thermal gradient

As it can be seen from this example the equivalent ΔT is considerably smaller than the one in the curved temperature profile. Since in SAP2000 the thermal gradient introduced is the real, not the effective one, the axial force in the tie should be further reduced.

Moreover due to convection and radiation the temperature on the surface of the element will be slightly smaller than the ambient one, which also contributes to the reduction of the axial force in the tie.

Taking into account of all these considerations previously done the daily temperature change will not be able to produce an alternation of the stress in the ties big enough to cause a fatigue phenomenon in the elements. Therefore this effect is neglected in the further fatigue life analysis.

2.3.1. Seasonal temperature variation

For the analysis of the seasonal variation in the temperature the results for the stress in the tie obtained through dynamic testing (***Figure 21***) and statistical data for the temperature in region Lombardia for the same period when the testing was performed (Figure 33) were used.

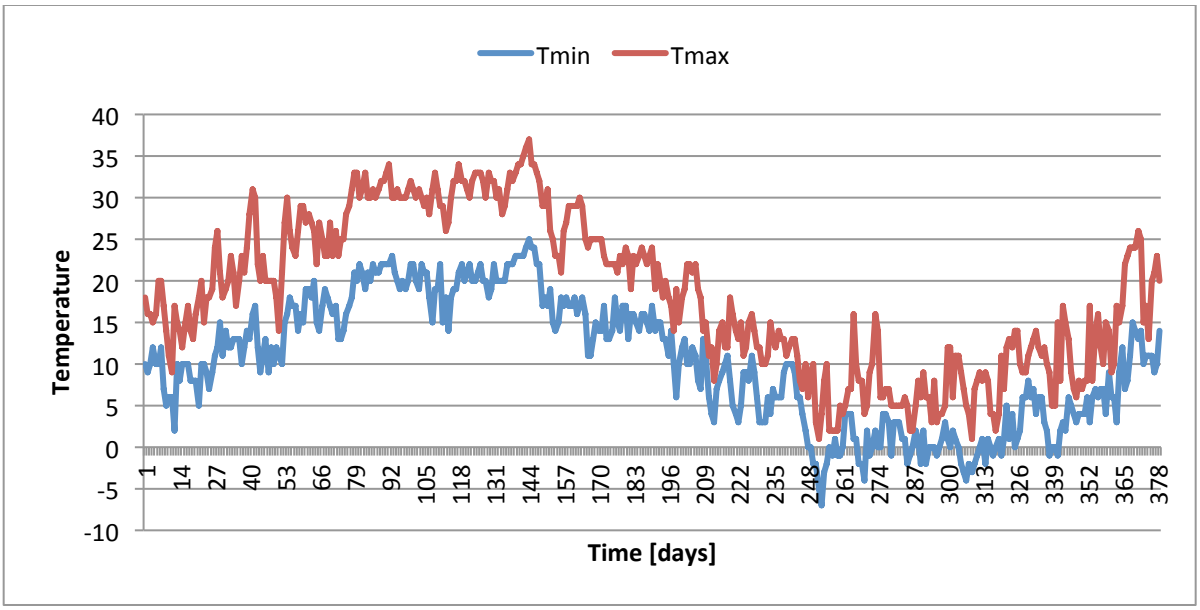

Figure 33: Minimum and maximum temperature in the period 1.04.2012÷26.04.2013

Since the results from the dynamic testing do not give the minimum and maximum expected values, they were fitted with the temperature data in order to determine the desired values (Figure 34).

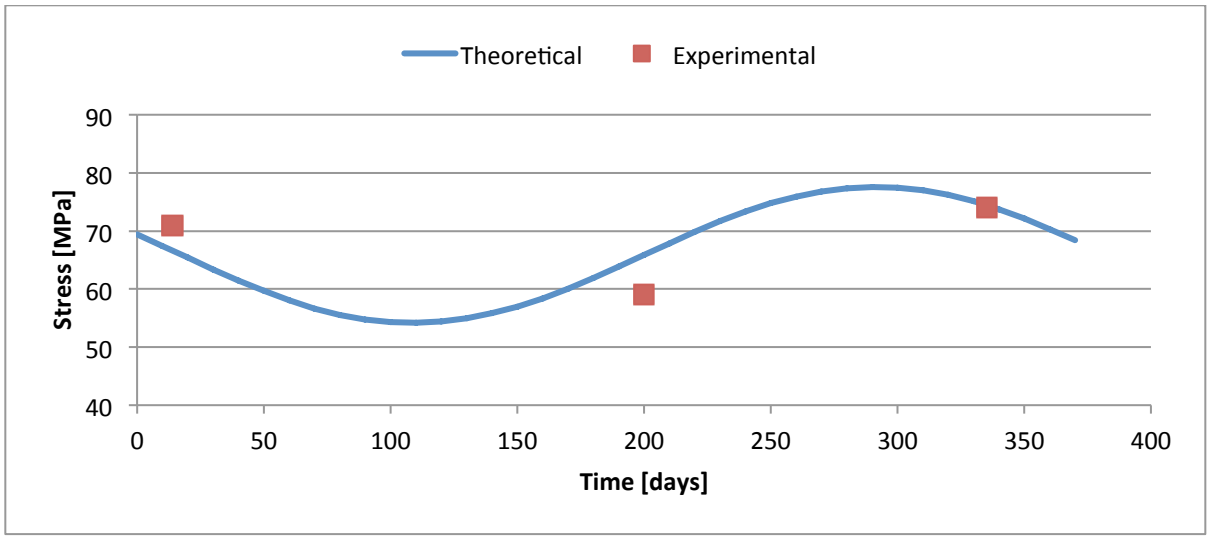

Figure 34: Stress variation in the tie-rod

The minimum expected stress is 54 MPa and the maximum one is 78 MPa. With these results it was possible to estimate the change in the axial force due to the temperature effects, which is around 96 kN.

The obtained value for the variation in the axial force was used together with the numerical model in SAP2000 in order to assess the temperature gradient range that can cause this kind of change. The results are given in Table 10 for the two cases of coefficient of thermal expansion of the masonry.

	$\alpha = 2.1 * 10^{-6}\ 1/℃$	$\alpha = 5.7 * 10^{-6}\ 1/℃$
Temperature gradient	11℃	4.1℃

Table 10: Temperature gradient

The results given in Table 10 are considerably lower than the expected seasonal changes. This difference could be explained again with the limitations of the simplified model in SAP2000, explained previously for the case of daily temperature change.

2.3.2. Further improvements of the model of Duomo di Milano

A sophisticated model, based on the Finite Element Methods, in the case of Duomo di Milano would give an insight on the distribution of the lateral thrust between the wrought iron tie-rods and the lateral walls. Moreover, it could help to explain the present damage in the structure, which is a probably the result of the soil settlements, different constructive phases and long-term damage of the materials (Vasic et al. 2015). The current state observations of the Cathedral, including damage, big deformations and stress level in ties, can be used for verifying the accuracy of the developed numerical model. Therefore, an in-depth knowledge of the geometry, structural features, material's properties and present damage is needed, which requires a multidisciplinary approach. Important aspect of analysis is to take into account different constructive phases of the cathedral, since they might have mayor effect on the results. With the results obtained with the numerical model it is possible to locate vulnerable elements and predict the overall future behavior of the structure.

3. Fatigue in metallic materials

Like all materials, metals cannot last indefinitely. Damage as an alternation of original material and structural performance may rise due to various deterioration processes. The main types of damage in metallic materials are wear and cracking. These may be result of a complex combination of different factors like interaction of the ironwork with other building materials, inherent problems in the material or the design, structural problems, the environment, and other factors like building use, disasters, or poor care and maintenance (Figure 35).

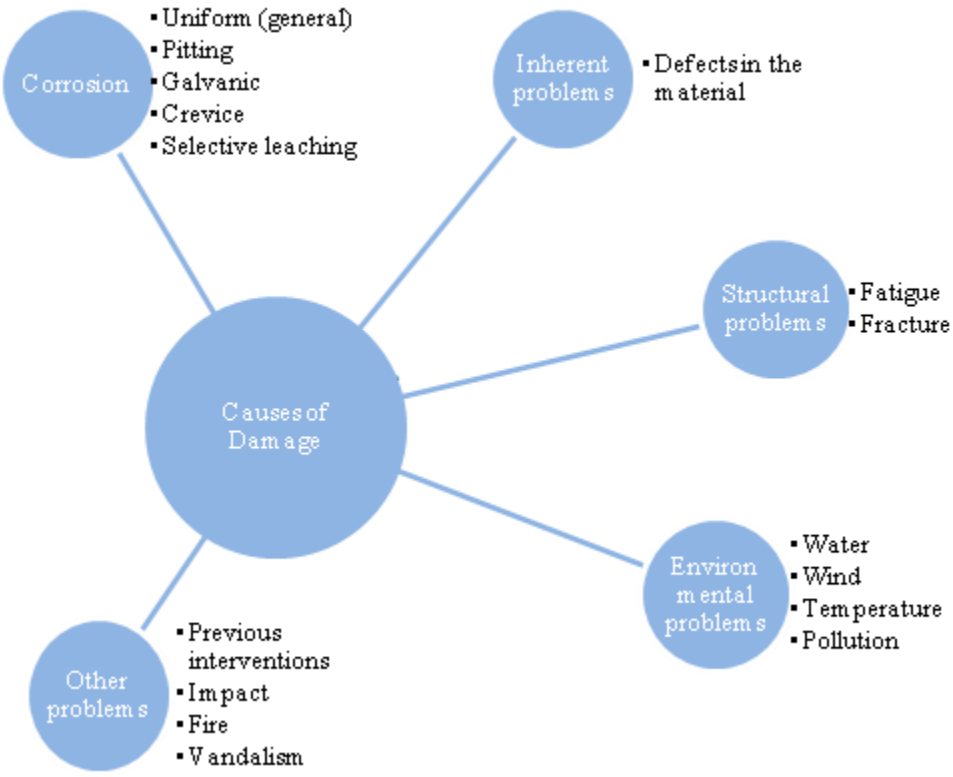

Figure 35: Causes of damage in metals

The inherent problems are related with the working temperature. If the wrought iron was not hot enough during its forging, it may not have fused together properly. This may result in a plane of weakness, called "roke", through which the delamination is more likely to occur. Elongated slag inclusions in the structure of the wrought iron may lead to the same failure. Wrought iron, used for structural applications, is subjected to different loads. These loads may change in time, leading to the collapse of the structure or parts of it. The failure might be accelerated by the presence of some defects in the material. When the structure is subjected to cyclic loading the fatigue may take place. This phenomenon consists in the failure of an element or a structure when it has been repeatedly stressed beyond the elastic limit of the material. Although fatigue can occur well below the elastic limit of a metal, ductile and malleable metals such as wrought iron are often able to deform significantly without failing.

Another structural problem relevant for the study case is the one of the fracture. It is associated with the discontinuities in the element such as different inclusions and voids. Wrought iron as a ductile material distort before fracturing. Therefore, in some cases it may deform completely, dissipating some of the imposed stresses. Overloading, distortion or other damage may cause the fracture. From the environmental deterioration the most crucial one is the temperature. As mentioned earlier it may cause problems with fatigue, as well as changes in the dimensions of the elements, leading to excessive stresses in joints and interfaces.

Definition of fatigue stated by the American Society for Testing and Materials (ASTM):

"The process of progressive localized permanent structural change occurring in a material subjected to conditions that produce fluctuating stresses and strains at some point or points and that may culminate in cracks or complete fracture after a sufficient number of fluctuation."

According to this definition the fatigue phenomenon is a process that occurs over a period of time. Although the failure, caused by this kind of behavior is often very sudden, without any obvious signs for that, the mechanism involved takes time to develop and it may starts even from the beginning of usage of the structure. The fatigue is a phenomenon that can affect the structure in local or global manner. However, it is more likely to occur in localized areas than throughout the entire element. These areas are places that can have high stress and strain due to external load transfer, sudden changes in the geometry, temperature differentials, residual stresses, and material imperfections. Moreover, the fatigue process is irreversible – once there is a change in the structure, it cannot be stopped. This process occurs due to the presence of cyclic stresses and strains, but this condition is not enough for the fatigue to become critical, the magnitude and amplitude of these fluctuating stresses and strains must exceed a certain material threshold. The result of the fatigue process is a sudden fracture – a separation of the element into two or more parts. This is caused by a crack growth to a point at which the remaining cross section of the element is no longer enough to sustain the applied load (Stephens R. I. et al. 2001).

3.1. Fatigue mechanism (Stephens R. I. et al. 2001)

Cyclic applications of inelastic strain to a metal can cause continuous changes until cyclic stability is reached. This means that metal becomes either more or less resistant to the applied strain, i.e., the material either cyclic hardens or cyclic softens. Some materials never stabilize under cyclic applications of inelastic strains, while others are cyclically stable form the onset. The later condition implies that there is no softening or hardening. Of great importance is to understand the reason for this behavior. The answer is related to the density and arrangement of the dislocation structure and substructure of the metal. Therefore, the concept of the dislocations is the most important for understanding the mechanical response of the materials.

There is a relationship between these dislocations and the inelastic deformations, called "slip", which actually are shear deformations of the material. These deformations occur in metals within the grains by dislocations moving along crystallographic planes (Figure 36).

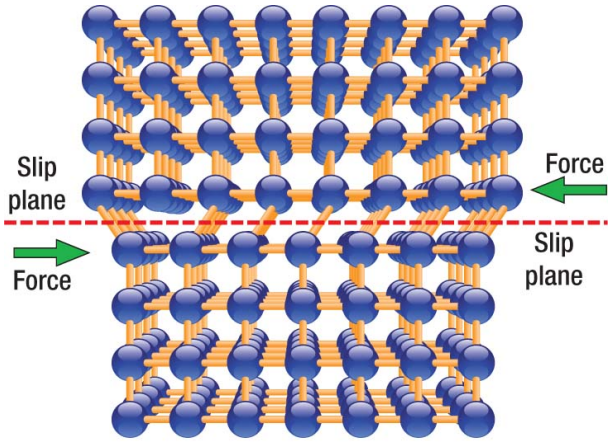

Figure 36: Slip plane between weaker bonds

For initially soft materials the dislocation density is low. With the occurrence of inelastic deformations due to the stress or strain cycling, the density of dislocations increases. This leads to a decrease in dislocation mobility, i.e. the material is said to cyclic harden and the cyclic yield strength becomes greater than the monotonic yield strength. Respectively for materials that are initially hard or have been hardened, inelastic strain cycling causes the existing dislocation structure to rearrange into a configuration such that there is less resistance to deformation. This new configuration tends to promote greater dislocation mobility, overcoming the micro structural barriers such as precipitates and grain boundaries. The material softens and as a result its cyclic yield strength is less than the monotonic one. The hardening and softening of the material can occur in global (net section area) or local scale (at localized regions like in the vicinity of metallurgical discontinuities, notches or cracks).

Metals are crystalline in nature – atoms arranged in ordered manner. They consist in a large number of ordered atoms (grains) each one of them with its own ordering direction, mechanical and directional properties. Some of these grains are ordered in planes of easy slip (dislocation movement), which are in the direction of the maximum applied shear stress. The slip creates one or more planes within a grain, which slide relatively to each other.

The degree of slip is related to the ductility of the material. In brittle materials the dislocations are practically immobile and the extent of slip is very limited while metals that show ductile behavior have very little restriction in the dislocations. For metals with intermediate ductile behavior dislocations are mobile but there is a restriction in the number of slip planes. Therefore, the crack nucleation mechanisms vary, depending on the type of material under the consideration.

The theory of dislocation movements describe the fatigue behavior from microscopic point of view and it is more qualitative and has not so far been developed to a level that permits the quantitative solution of practical engineering problems. From macroscopic point of view the process of initiation and propagation of so-called small cracks is perhaps the most important phenomenon (Murakami Y 2002).

3.2. Crack nucleation and growth

In general fatigue phenomenon consists of three phases – crack nucleation, crack growth and final fracture.

3.2.1. Crack nucleation

In order to understand the fatigue phenomenon, a general situation in which crack nucleation occurs due to slip under fatigue loading conditions may be observed (Figure 37). Figure 37a schematically shows an edge view of coarse slip normally associated with monotonic loading, while Figure 37b shows fine slip due to the cyclic loading. In Figure 37c, where the progressive development of extrusion/intrusion pair is shown, the vertical arrows indicate the loading direction, while the horizontal ones show the progression of slip deformation.

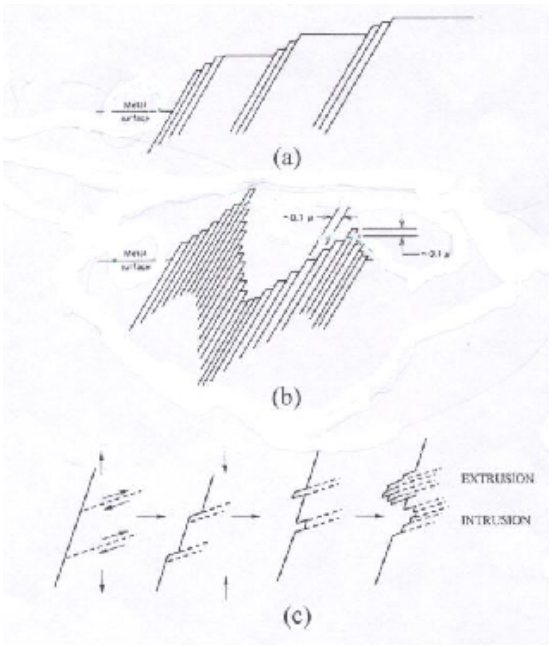

Figure 37: Schematic of slip due to external loads. (a) Static (steady) stress. (b) Cyclic stress. (c) Fatigue progression in the formation of an extrusion/intrusion pair

The early stages of fatigue are mainly surface phenomena. This results in the great importance of the surface and the environment for fatigue life of the structure. Crack nucleation is more likely to occur at the surface of the material or just below it. This is due to the fact that inelastic deformations are easier at the surface and that the slips are able to develop exactly there. Also the stress and strain from an external loading are higher at the surface of the element. But slip bands are not the only reason for the crack nucleation. It may occur because of discontinuities in the material such as inclusions, second-phase particles, corrosion pits, grain boundaries, twin boundaries, pores, and voids.

3.2.2. Crack growth

Initially the cracks that nucleate in local slip grow in the plane of maximum shear stress. This growth is quite small, usually in the order of several grains. It depends on many factors as the slip characteristics of the material, the grain size of the material, the extent of plasticity near the crack tip. When the size of the crack or the plastic deformation near the crack tip is confined within a few grain diameters (typically within 10), fatigue crack growth occurs predominantly by a shear process. This cracking behavior is called “microcrack growth”. Therefore, the physical length that a crack grows due to shear may vary from one material to another, depending on the size of the grains of the material. In the case of high-strength or

brittle materials, where microcracks are often formed at inclusions or voids, the growth is primarily along the planes of maximum tensile stress.

After the nucleation of the microcracks if the cyclic loading continues, these cracks tend to join and grow along the plane of maximum tensile stress. Two stages of the growth can be distinguished – "stage I" also called shear mode and "stage II" – tensile mode.

Fatigue crack growth can be seen on Figure 38 as a microscopic edge view.

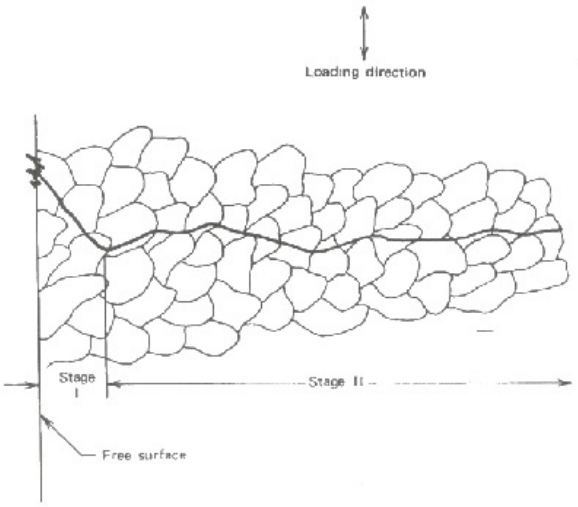

Figure 38: Schematic of stages I (shear mode) and II (tensile mode) transcrystalline microscopic fatigue crack growth (Murakami Y. 2002)

The shown fatigue crack nucleates on the surface and grows across several grains, controlled primarily by shear stresses and strains, and then grows in a zigzag manner, controlled primarily by the maximum tensile range. Most fatigue cracks grow across grain boundaries (transcrystalline) as shown in Figure 39.

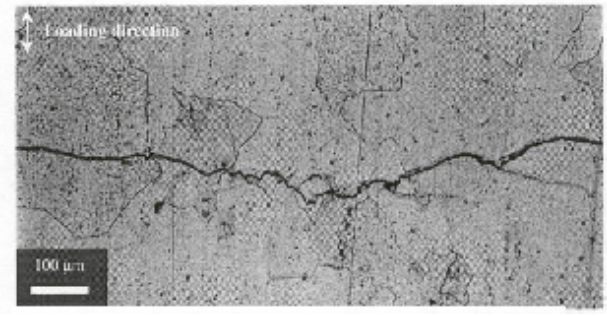

Figure 39: Surface crack profile of transcrystalline fatigue growth

However, in some cases it may grow along grain boundaries (intercrystalline), depending on the material, load, and environmental conditions - Figure 40.

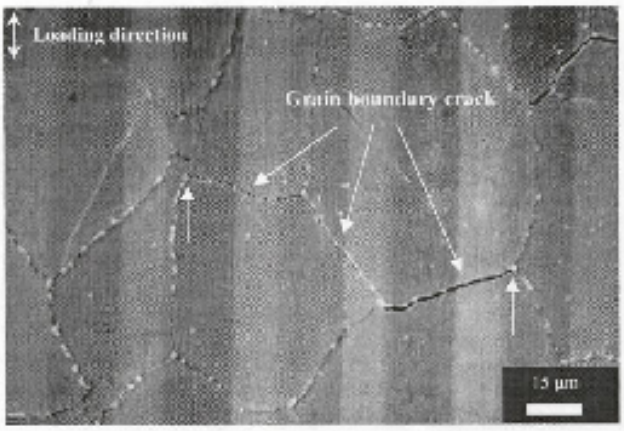

Figure 40: Crack profile of intercrystalline fatigue growth (Murakami Y. 2002)

A wide range of fatigue crack growth mechanism exists. Three of the most common modes are striation formation, microvoid coalescence, and microcleavage, which are shown in Figure 41. Ductile materials often exhibit the first two types of crack growth mechanism.

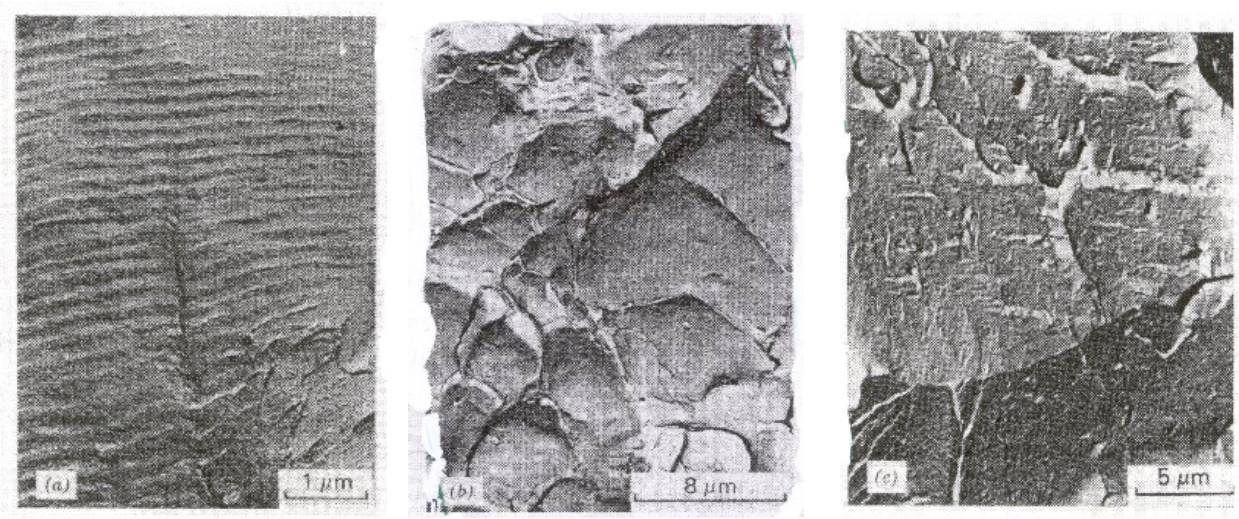

Figure 41: Examples of microscopic fatigue crack growth in 17-4 PH stainless steel - (a)Striation formation. (b) Microvoid coalescence. (c) Microcleavage.

The ripples shown in Figure 41a are called “fatigue striations”. They may be not clearly visible because they are dispersed throughout the fracture surface and it is difficult to find them in high-strength materials. In many studies each striation is represented by one load cycle, the striation forming by a plastic crack tip blunting mechanism during the loading and unloading phases of the fatigue cycle. However, in some other studies, it was shown that there is no such a correspondence. Thus, this fracture mechanism, combined with others, may cause the advancement of the crack front.

Microvoid coalescence is shown in Figure 41b and it is due to nucleation, growth, and coalescence of microvoids during plastic deformations. The formation of these voids, which evolve into “dimples”, is a consequence of the interfacial cracking between precipitate particles or inclusions and the surrounding material matrix. Because of this the size and the density of dimples depends on the size and distribution spacing of the inclusions or precipitants inherent in the metal. This crack growth mechanism

is considered to be high-energy process and it usually occurs at high crack growth rate. The fracture surface is dull and rough or fibrous.

Microcleavage, shown in Figure 41c, is considered to be lower-energy process in comparison with the previous two and therefore it is undesirable one. It is assumed to be characteristic mechanism for brittle materials and the likelihood of it is increased when plastic flow is restricted, like in the cases of low temperatures, high strain rates, or in notched components. Microcleavage involves fracture along specific crystallographic planes and it is transcrystalline in nature. This type of mechanism is more susceptible in metals with body-centered cubic or hexagonal close-packed crystalline structure as opposed to a face-centered cubic crystalline structure. the fracture surface in this case has a bright and shiny appearance.

Microvoid coalescence and cleavage occur under both monotonic and cyclic loading conditions, while striations are characteristic for cyclic loading only.

3.2.3. Final fracture

This last stage of the fatigue phenomenon is irreversible. It consists in the complete separation of the element or the whole structure in two or more parts.

The fatigue mechanism is represented graphically in Figure 42.

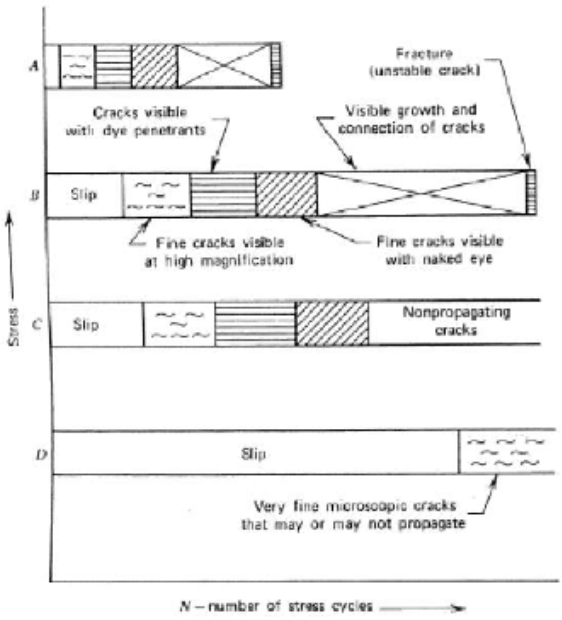

Figure 42: Schematic representation of the fatigue process (Murakami Y. 2002)

As already mentioned before, fatigue process generally consists of crack nucleation, growth, and final fracture. In general the slip occurs first, followed by fine cracks, which continue to grow under cyclic loading and eventually become visible for unaided eye. These cracks tend to combine and only a few major cracks grow. When these cracks reach a critical size a sudden fracture occurs. The process occurs sooner with the increase of the stress magnitude. In some cases where there are compressive residual stress fields the crack growth might be stopped.

At high stress levels, the total fatigue life is associated mainly with microcrack and macrocrack growth, while in low ones s great deal is spent in the nucleation of the crack and the microcrack growth.

Only the nucleation phase of the fatigue process can be absent. Therefore, the way to overcome the fatigue failure is to prevent the nucleation and crack growth.

3.3. Stress based models

3.3.1. Stress cycles

Figure 43 shows the nomenclature for constant amplitude cyclic loading used in fatigue design.

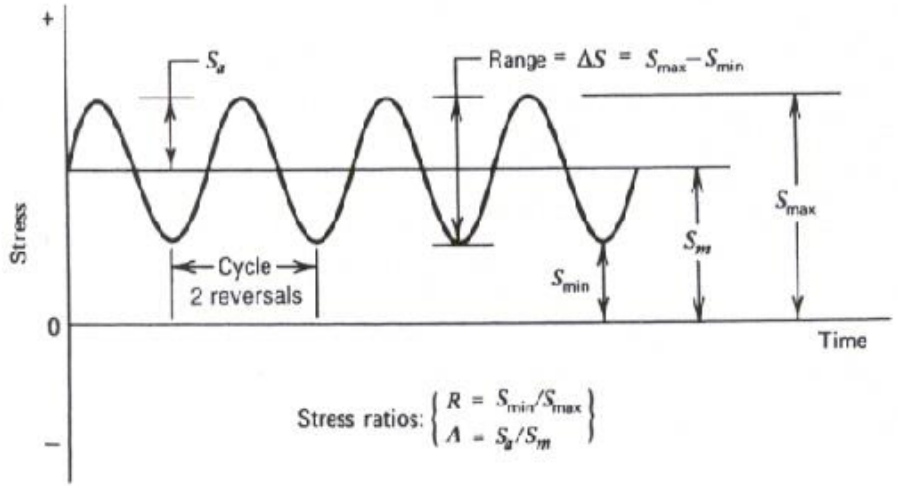

Figure 43: Nomenclature for constant amplitude cyclic loading

The main stress parameters shown in Figure 43 are the maximum stress S_{max}, the minimum stress S_{min}, the stress range (Equation 7), the alternating stress (Equation 8), the mean stress (Equation 9), the stress ratio (Equation 10), and the amplitude ratio (Equation 11).

$$\Delta S \text{ or } S_r = S_{max} - S_{min}$$ ***Equation 7: Stress range***

$$S_a = \frac{\Delta S}{2} = \frac{S_{max} - S_{min}}{2}$$ ***Equation 8: Alternating stress***

$$S_m = \frac{S_{max} + S_{min}}{2}$$ ***Equation 9: Mean stress***

$$R = \frac{S_{min}}{S_{max}}$$ ***Equation 10: Stress ratio***

$$A = \frac{S_a}{S_m} = \frac{1 - R}{1 + R}$$ ***Equation 11: Amplitude ratio***

3.3.2. Stress – life (S – N) curves

Engineering fatigue data is normally represented by means of a plot of stress S against the number of cycles N (S – N curve). The stress used for these curves can be the alternating one (S_a), the maximum (S_{max}), or the minimum (S_{min}).

Typical S – N diagrams are shown in Figure 44.

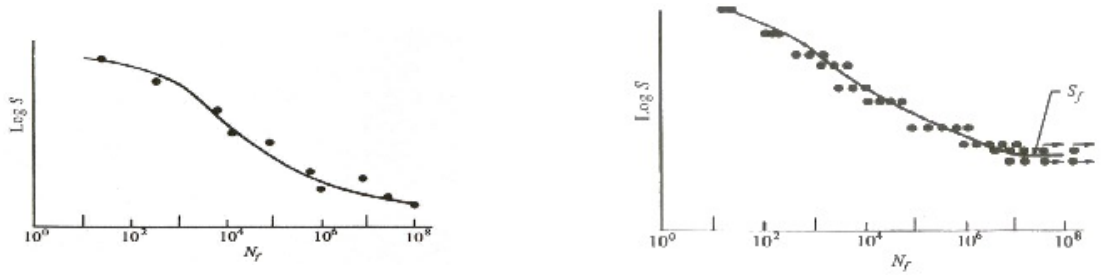

Figure 44: Typical S –N diagrams

Figure 44a shows a continuously sloping curve, while Figure 44b shows discontinuity or so-called "knee" in the S –N curve. The knee is characteristic for low- and medium-strength steels, while the other metals diagrams do not contain it. One of the common terms used with the S – N diagram is the fatigue life, denoted as N_f. It is the number of stress or strain cycles of a specified character that a given specimen sustains before failure occurs. Another important term is the fatigue strength, S_{Nf}, which is a hypothetic value of stress at failure for exactly N_f cycles, as determined from an S – N diagram.

The fatigue limit or also referred, as an endurance limit, S_f, is the limiting value of the median fatigue strength as N_f becomes very large. Under this limit, the material presumably can endure an infinite number of cycles before failure. In the typical S –N diagrams (Figure 44) there is no separation between the crack nucleation and the crack growth. A reasonable crack nucleation life can be assumed for a crack length of 0.25 mm. The number of cycles required for the formation of this crack in smooth, unnotched or notched fatigue specimens can range from a small percentage to almost the entire life. This is represented schematically on Figure 45.

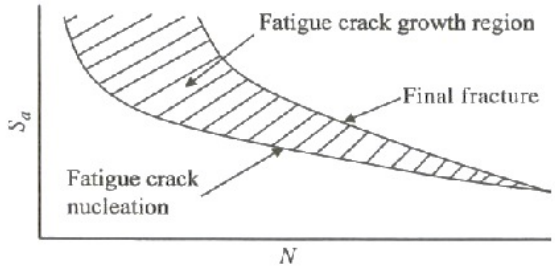

Figure 45: S –N schematic of fatigue crack nucleation, growth, and final fracture

From Figure 45 it can be seen that at higher stress levels a larger fraction for crack growth (the hatched area) occurs, while at lower stress levels a larger fraction for crack nucleation occurs. The size of

the final crack at fracture depends on the fracture toughness of the material and the level of stress. The lower stress levels have larger critical crack sizes, while the higher stress levels have shorter ones.

3.3.3. Fatigue limit

The fatigue limit is considered primarily in long-life fatigue design. It has an enormous range for a given material, depending on the surface finish, specimen or component size, type of loading, temperature, corrosive and other aggressive environments, mean stresses, residual stresses, and stress concentrations. For example the values of fatigue limit based on a nominal alternating stress, S_a, has been ranged from 1 to 70 percent of the ultimate tensile strength, depending on the above-mentioned factors.

The most long-life S – N fatigue data available in the literature consist of fully reversed uniaxial fatigue strengths or fatigue limits of small, highly polished, unnotched specimens based on 10^6 to 5×10^8 cycles to failure in laboratory air environment. A common way to compare different materials for their fatigue resistance is to plot this fatigue limit, S_f, versus the ultimate tensile strength, S_u. The S_f/S_u ratio is called the "fatigue ratio". In Figure 46 the comparison between some metals is shown.

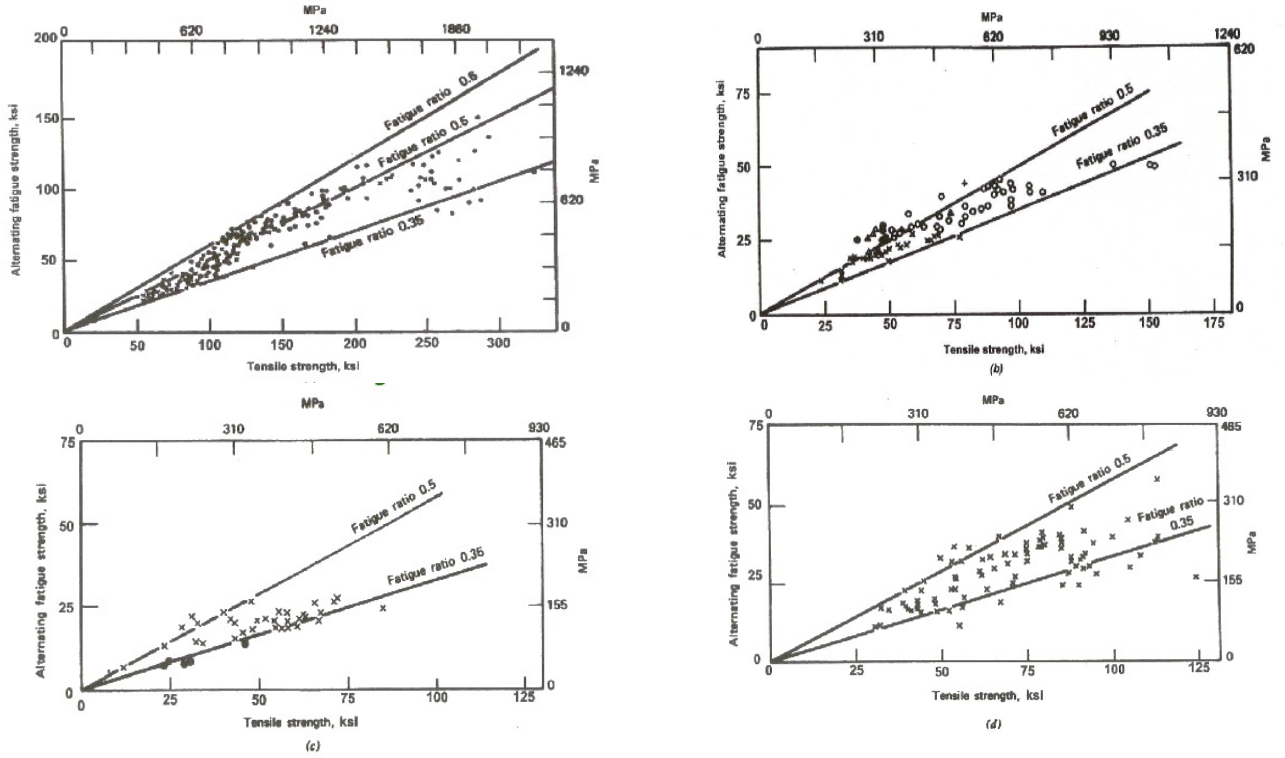

Figure 46: Relation between bending unnotched fatigue strength and ultimate tensile strength. (a) Carbon and alloy steels (10^7 to 10^8 cycles): (●) alloy steels, (x) carbon steels. (b) Wrought and cast irons (10^7 cycles): (x) flake-graphite cast iron, (○) nodular cast iron, (+) malleable cast iron, (Δ) ingot iron, (●) wrought iron. (c) Aluminum alloys (10^8 cycles): (x) wrought iron, (●) cast iron. (d) Wrought copper alloys.

3.3.4. Factors influencing S – N behaviour

The reference fatigue condition for S – N behaviour is usually fully reversed bending or axial loading using small, unnotched specimens. Many factors, main of which are shown in Figure 47, influence the results obtained with the reference conditions.

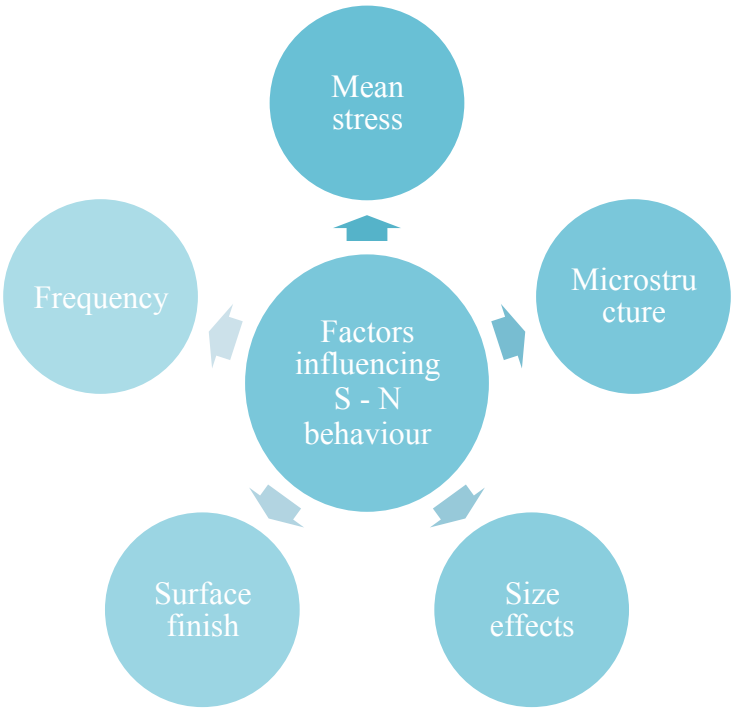

Figure 47: Factors influencing S – N behavior

- Mean stress

The effect on the fatigue behaviour of the mean stress, S_m, is shown in Figure 48.

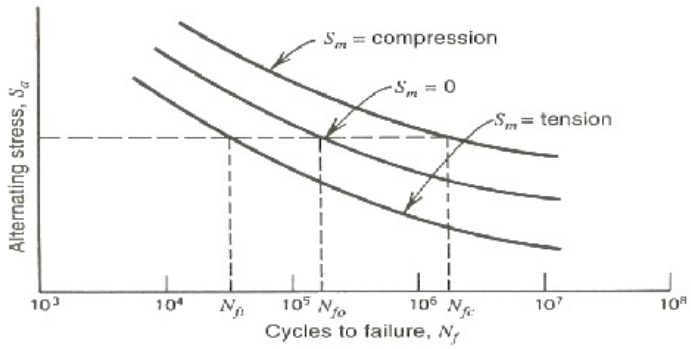

Figure 48: Effect of mean stress on fatigue life

As it can be seen from Figure 48 the tensile mean stresses are detrimental, while the compressive mean stresses are favourable.

In presence of mean stress and at intermediate or high stress levels, substantial cyclic creep (cyclic ratcheting), which increases the mean strain, can occur, as shown by Landgraf in Figure 49. This effect contributes to the detrimental effects of tensile mean stress on fatigue life and leads to additional undesirable deformation.

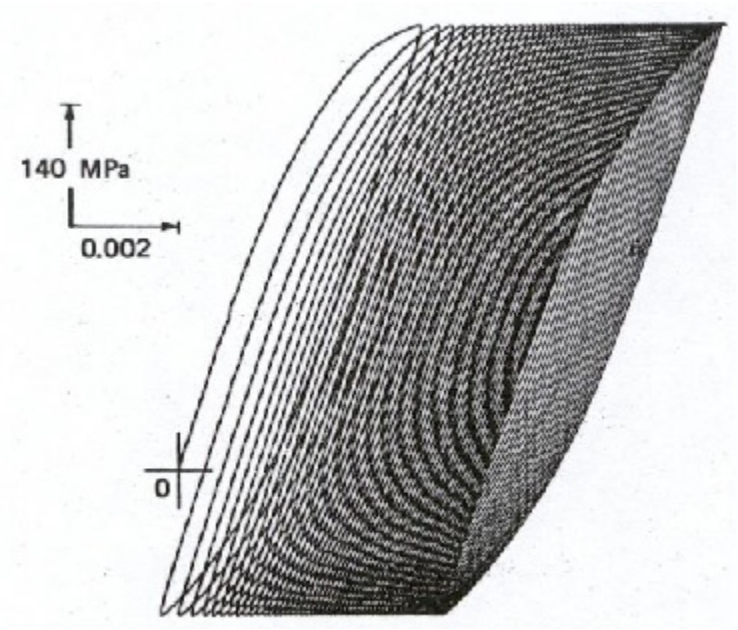

Figure 49: Cyclic creep under load control constant amplitude testing

As a result of further investigations of the tensile mean stress influence on long-life fatigue strength typical dimensionless plots were obtained. On Figure 50 S_a/S_f versus S_m/S_u values for steels are plotted.

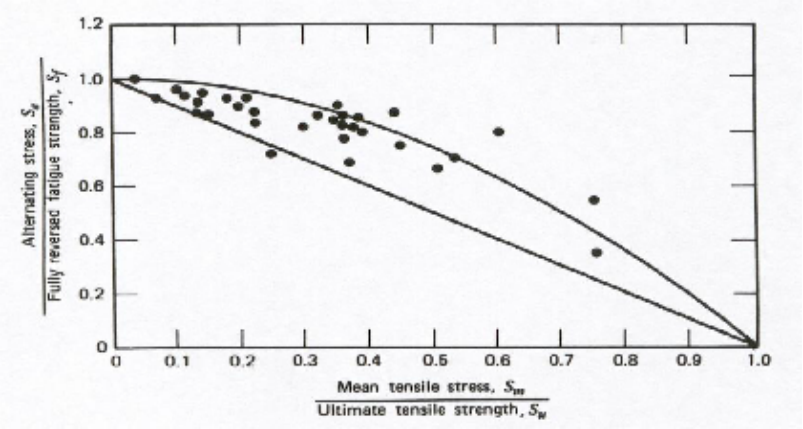

Figure 50: Effect of mean stress on alternating fatigue strength at long life for steels based on ~10^7 cycles

Small tensile mean stresses often have only a small effect. It appears that much of the data fall between the straight and curved lines. The straight line is modified Goodman line, described by Equation 12, and the curve is the Gerber parabola, which can be obtained from Equation 13.

$$\frac{S_a}{S_f} + \frac{S_m}{S_u} = 1$$

Equation 12: Modified Goodman

$$\frac{S_a}{S_f} + \left(\frac{S_m}{S_u}\right)^2 = 1$$

Equation 13: Gerber

Another relationship was formulated (Morrow line) by replacing S_u with the true fracture strength σ_f (***Equation 14***).

$$\frac{S_a}{S_f} + \frac{S_m}{\sigma_f} = 1$$

Equation 14: Morrow

All these three equations can be used in fatigue design after been modified for notches, size, surface finish, environmental effects, and finite life. A yield criterion also can be used with these expressions.

Figure 51 provides information about the effect of the compression mean stresses.

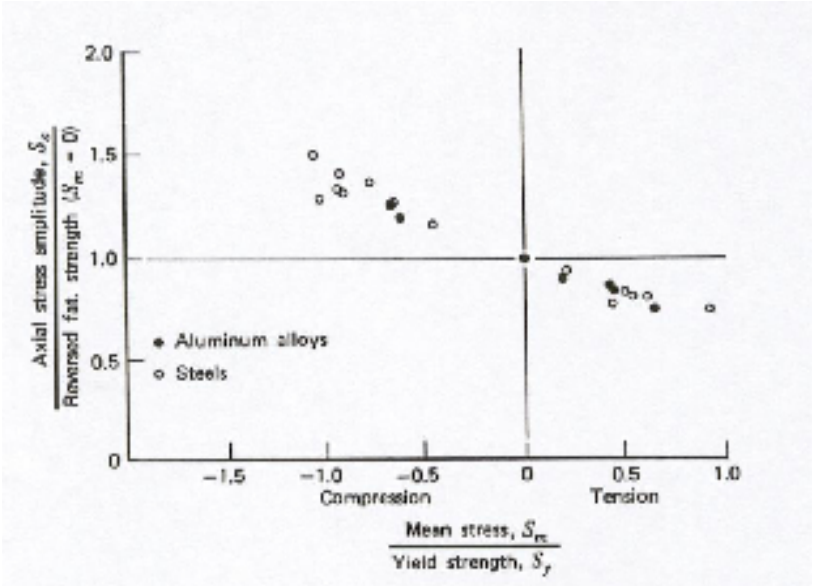

Figure 51: Compressive and tensile mean stress effect. (●) Aluminum alloys, (○) steels.

It can be seen that these compressive mean stresses have beneficial effect on the fatigue strength leading to its increase up to 50 percent. The modified Goodman or Morrow equations can be extrapolated to the compressive mean stress region, but the Gerber expression gives incorrectly a detrimental effect of this stress.

The modified Goodman and Morrow equations are shown for a given long life along with the yield criterion (Equation 15).

$$\frac{S_a}{S_y'} + \frac{S_m}{S_y} = 1$$

Equation 15: Modified Goodman and Morrow equations along with the yield criterion

In Equation 15 S_y is the monotonic tensile yield strength and S_y' is the cyclic yield strength.

Figure 52 shows a graphic representation of Equation 15.

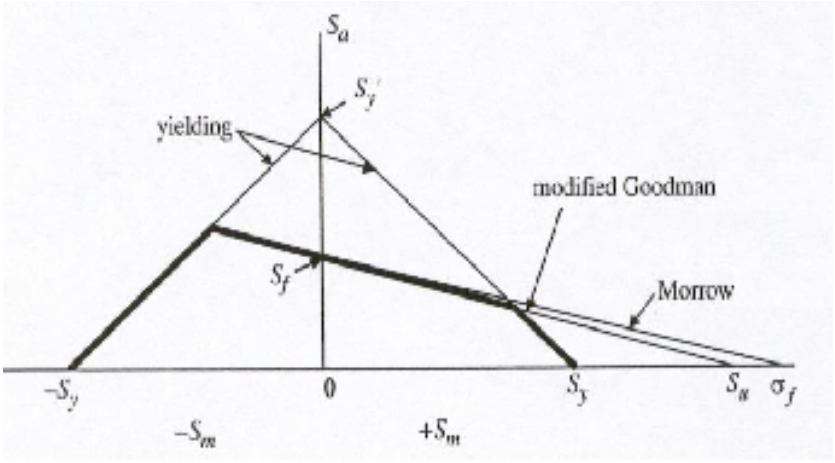

Figure 52: Fatigue and yielding criteria for constant life of unnotched parts

If the coordinates of the applied alternating and mean stresses fall within the modified Goodman or Morrow lines, then fatigue failure should not occur prior to the given life. If yield is not to occur, then the applied and mean stresses must fall within the two yield lines connecting $\pm S_y$ to S_y. If both fatigue and yielding are not to occur, then neither criterion, as indicated by the three bold lines, should be exceeded.

- Microstructure

In solid mechanics the metals are often modeled as homogeneous, isotropic, and linearly elastic, which form a microscopic point of view is not correct and thus the metal fatigue is significantly influenced by the microstructure. Microstructural effects such as chemistry, heat treatment, cold working, grain size, anisotropy, inclusions, voids/porosity, delaminations, and other discontinuity and imperfections should be accounted for is the actual S – N data is not available. If the actual S – N data are present all of these effects are inherently accounted for already. Chemistry, heat treatment, and cold working have a significant influence on the ultimate tensile strength. Due to their enormous number of synergetic variations a generalization of their effect on the fatigue behavior is not practical. However, for the other microstructural effects some generalization can be done. Fine grains usually provide better S – N fatigue resistance than coarse ones except of the cases of elevated temperature because of the creep/fatigue interaction. Fine grains reduce localized strains along slip bands by decreasing the amount of irreversible slip, and provide more grain boundaries to help in transcrystalline crack arrest and deflection and reducing in this way the fatigue crack growth rates. Anisotropy caused by cold working gives increased S –N fatigue resistance when loaded in the direction of the working than when loaded in the transverse direction due to the elongated grain structure in the direction of the original cold working. Inclusions, voids/porosity, and laminations act as stress concentrations and thus are common locations for microcracks to nucleate under cyclic loading, or to form during heat treatment or cold working prior to cyclic loading. Under these conditions, fatigue resistance is reduced. In order to obtain good fatigue resistance a minimization of inclusions, voids/porosity, laminations, and other discontinuities through carefully controlled production and manufacturing procedures should be done.

- Size effects

The S – N fatigue behavior is related to the dimensions of the specimens (diameter or thickness). If the diameter or the thickness is less than 10 mm the fatigue behavior is independent of the dimensions, while for larger sizes there is a decrease in the fatigue resistance. There could be a slight difference in the case of rotating bending in comparison with the nonrotating one. Under unnotched axial conditions, S – N fatigue resistance is lower than the one in the case of bending conditions. These effects are due to several factors. In the case of bending conditions, the stress gradient depends on the specimen's diameter and thickness for a given nominal stress. With increasing the dimensions of the specimen the bending stress gradient decreases which lead to higher average stress in a local region on the surface. These average stresses may be the governing ones for fatigue, not the maximum. For axial loaded unnotched specimens, nominal stresses have the same magnitude, resulting in less size effect than in bending. Axial fatigue resistance is lower than the bending one because of the possible eccentricity or alignment difficulties that cause an influence of the bending stresses on the axial resistance. Also because in the case of axial loading the whole specimen is subjected to uniform stress, hysteresis energy may not dissipate adequately that can cause an increase in the temperature of the specimen and a decrease in the fatigue resistance. For both bending and axial loading, specimens with larger sizes have a higher probability of microstructural discontinuities that contribute to the decrease in the fatigue resistance.

- Surface finish

As mentioned earlier most of the fatigue failures originate at the surface, and hence the surface will have a substantial influence on the fatigue behavior. Several surface effects that can be cause by differences in surface roughness, microstructure, chemical composition, and residual stress have a significant importance. Their influence will be more pronounced in the long lives where a higher number of cycles are involved in the crack nucleation as shown before in Figure 46. The fatigue strengths shown in this figure are referenced to highly polished and smooth specimens, which is not the case for most of the engineering parts. The grinding and machining of the elements, even carefully done, cause degradation in the fatigue resistance. Generalization of these two effects is difficult to be done because of the many variables that affect them. However some data is available for these two operations for steels of varying strength, along with surface effects for hot-rolled and as-forged specimens. Figure 53 shows surface factors, k_s, applied to highly polished fatigue limits as a function of ultimate tensile strength for steels involving grinding, machining, hot-rolling, and as-forged surface conditions.

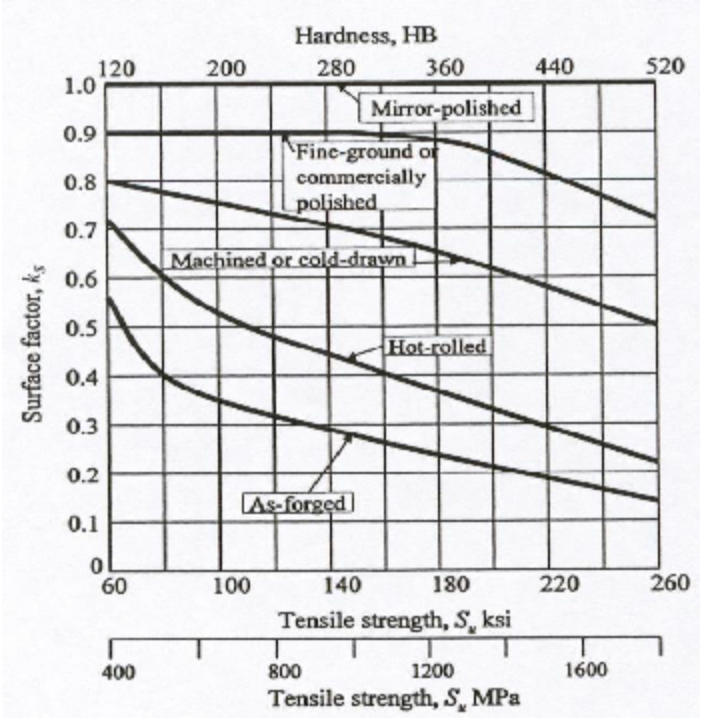

Figure 53: Effects of surface finish on the fatigue limit of steel

From Figure 53 it can be seen that, the higher the ultimate tensile strength and hardness, the greater the degradation of fatigue limits. The decreases caused by grinding and machining are more closely related to surface roughness and residual stresses, while hot-rolled and as-forged behavior include thee two important factors along with significant surface microstructural and chemical composition changes such as decarburization and hence surface hardenability.

- Frequency

The influence of the frequency on S – N behavior of metals is complicated because of the synergistic effects of test temperature, corrosive environment, stress-strain sensitivity to strain rate, and frequency. Both elevated temperature and corrosive environments are usually detrimental to fatigue resistance. Specimen heating at higher test frequency due to internal hysteresis damping can increase the specimen's temperature and thus disguise the true fatigue behavior at ambient temperature. This is important for lower-strength metals. Generation of heat due to cyclic loading is related to the volume of highly stresses material. Thus, axial loading and large specimens will produce more heat than small bending specimens or notched specimens, and therefore frequency effects could be different in these situations. If heating effects are negligible due to various cooling techniques and/or low stress amplitude during testing, along with negligible corrosion effects, then frequency effects can be evaluated. Under these conditions, using axial or bending specimens, frequencies ranging from less than 1 Hz to 200 Hz have had only a small effect on S – N behavior for most structural metals. At higher frequencies (but still<200 Hz), fatigue strengths at 10^6 to 10^8 cycles have shown increases from 0 to 10 percent. At higher stress amplitudes, small increases in fatigue life have also occurred; however, many of these life changes are similar to typical scatter at a given frequencies. Based on the above, with known absence of corrosion and temperature effects and other aggressive environments, frequency effects of up to about 200 Hz have

often been neglected in fatigue design and testing. Other effects may be more important. The key, however, is the absence of corrosion and an increase in temperature.

In the kHz frequency range, greater changes in fatigue resistance have occurred compared to those at less than 200 Hz. The temperature increases at these frequencies (1 to 25 kHz) and are more difficult to control, and specimens have been cooled by air, water, water plus inhibitors, or oil that make contact with the specimen surface. Intermittent testing has also been used to maintain isothermal conditions. Changes in fatigue limits at kHz frequency compared to those obtained below 200 Hz have ranged from a factor of less than 1 to up to 2.6, with the significant majority above 1. This more prevalent increase in fatigue limit has been accompanied by a beneficial shift in the finite life region (>10^5 cycles at these frequencies). In most cases, fatigue crack growth resistance has also increased at the kHz frequencies. However, despite the many trends toward increased fatigue resistance at kHz frequencies, it is still difficult to make this generalization due to the large number of complex test/material variables involved.

3.3.5. S – N curve representation and approximation

The actual fatigue behavior up to the present is unknown. In such a case the information can be generated approximating the S – N behavior. Many models for the fatigue behavior exist, usually applying a median fatigue life. One of these models is the Basquin S – N curve (Figure 54), which is a log-log straight line S – N relationship, described by ***Equation 16***.

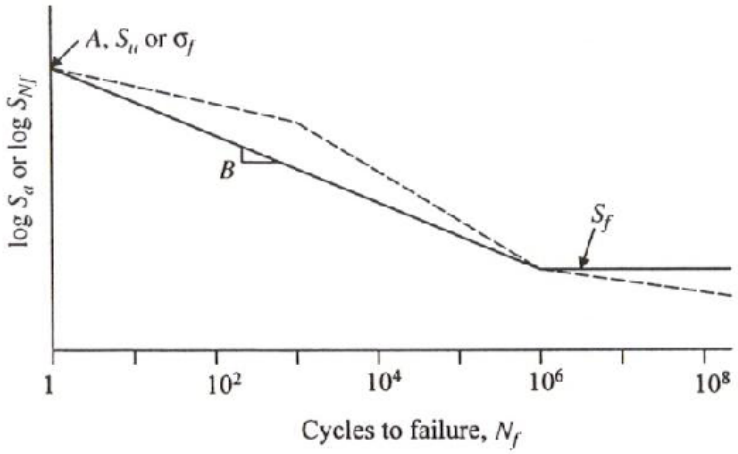

Figure 54: Basquin type S – N curves

$$S_a \text{ or } S_{Nf} = A\left(N_f\right)^B$$ ***Equation 16: Basquin equation***

Where:

S_a is an applied alternating stress and S_{Nf} is the fully reversed, $R = 1$, fatigue strength at N_f cycles, A is the coefficient and represents the value of S_a and S_{Nf} at one cycle, and B is the exponent or slope of the log-log S – N curve.

One possible approximation is the tri-slope model shown with the dashed line on Figure 54. It has one slope between 1 and 10^3 cycles, another between 10^3 and 10^6 or 10^8, and third after 10^6 or 10^8. In this

model a fatigue limit does not exist. Another model assumes one sloping straight line from 1 cycle to 10^6, 10^7, or 10^8 cycles followed by a horizontal line or another sloped line. The intercept, A, at N_f=1 could be chosen as the ultimate tensile strength, S_u, the true fracture strength, σ_f, or an intercept found from regression of the fatigue data.

Constant fatigue life diagrams (Figure 55), relating S_a and S_m are often modeled by using one of the models shown in Figure 54 and the modified Goodman or Morrow equations for mean stress (***Equation 12*** and ***Equation 14***).

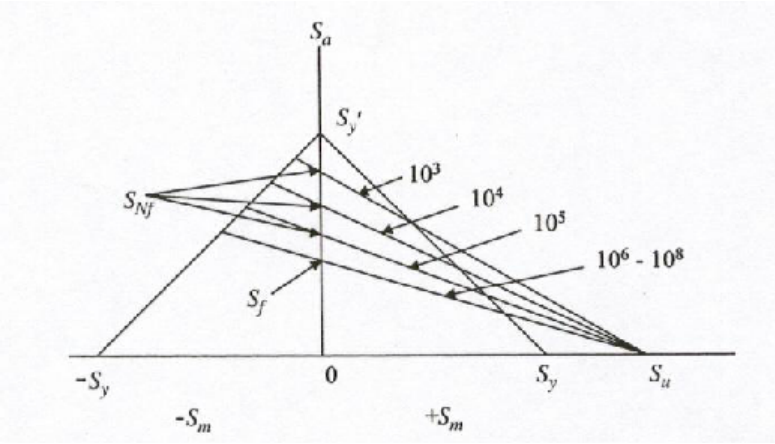

Figure 55: Constant life diagrams with superimposed yield criterion

In Figure 55, the intercept, S_{Nf}, at S_m=0 for a given life are found from the fully reversed, R=-1, modeled S – N curves. Modified Goodman straight lines are shown passing through these intercepts and the ultimate tensile strength, S_u. For these finite fatigue lives, the modified Goodman and Morrow equations should have S_f replaced with S_{Nf}, for a given life. Using the Basquin's equation for the fully reversed, R=-1, finite life region, gives the following equations:

$$S_{Nf} = A\left(N_f\right)^B, \text{ and}$$

$$\frac{S_a}{S_{Nf}} + \frac{S_m}{S_u} = 1 \text{ or } \frac{S_a}{S_{Nf}} + \frac{S_m}{\sigma_f} = 1 \qquad \textit{Equation 17}$$

Either of Equation 17 along with Equation 16provides information to determine S_a and S_m for a given fatigue life of unnotched parts. When these equations are used (Equation 16 and Equation 17) the S – N curve for a given mean stress is parallel to the fully reversed, R=-1, and the slope B remains unchanged. That means that the mean stress is handled in the same manner for short and long lives. In reality this is not exactly true in the case of short lives due to plastic deformations, such as when the mean stress represents a residual stress. In such a case it is more realistic to apply the mean stress correction to the fatigue strength at long life which can be done by means of a straight line to S_u or σ_f at one cycle. This assumes a full effect of mean stress at long life, with gradually decreasing effect, to no effect at 1 cycle.

3.4. Fatigue crack growth

The presence of crack can significantly reduce the life of a component or structure. The fatigue behavior in such case can be modeled using the concept and use of fracture mechanics for fatigue crack growth. Cracks can be present in the element due to some metallurgical discontinuities such as inclusions or they can be a result of the fatigue phenomenon. For the life estimations a several parameters are needed such as the stress intensity factor, K, the fracture toughness, K_c, the applicable fatigue crack growth rate expression, the initial crack size, a_i (or a_0) and the final or critical crack size, a_f (or a_c).

3.4.1. LEFM concepts

One of the methods used to analyze the fatigue crack growth process is the linear elastic fracture mechanics (LEFM). This methods work under the basic assumption that material conditions are predominantly linear elastic during the fatigue process. Before analyzing the crack growth it is necessary to define the basic crack surface displacement modes by which a crack can extend.

- Loading modes

There are three modes by which a crack can extend (Figure 56).

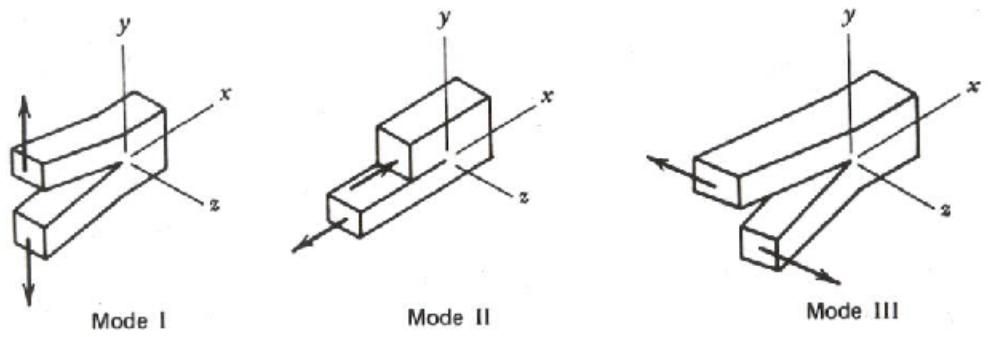

Figure 56: Modes of crack extension

Mode I is the opening mode. It is the most common mode for fatigue process since the cracks tend to grow on the plane of maximum tensile stress. Hence this is typical mode for uniaxial loaded elements. Mode II is the in-plane shearing or sliding mode and Mode III is the tearing or antiplane shear mode and it is associated with s pure shear condition, typical of a round notched bar loaded in torsion. Combination of these three modes is also possible to occur.

- Stress Intensity Factor, K

The foundations for development of the stress intensity factor K were laid by Griffith. Based on the energy balance of a cracked body for ideally brittle behavior (i.e. glass) showed that:

$$S\sqrt{a} = \text{const} \qquad \textit{Equation 18}$$

Using the Griffith's energy approach Irwin applied Griffith's theory to metals with small plastic deformations at the crack tip and used the stress intensity factor K to quantify the crack tip driving force.

$$G = \frac{K^2}{E} \text{ for plane stress and } G = \frac{K^2}{E}\left(1-\nu^2\right) \text{ for plane strain} \qquad \textit{Equation 19}$$

If we consider a through-thickness sharp crack in linear elastic isotropic body subjected to mode I loading, such as the one shown in Figure 57. An arbitrary stress element in the vicinity of the crack tip with coordinates r and θ relative to the crack tip and crack plane are also shown.

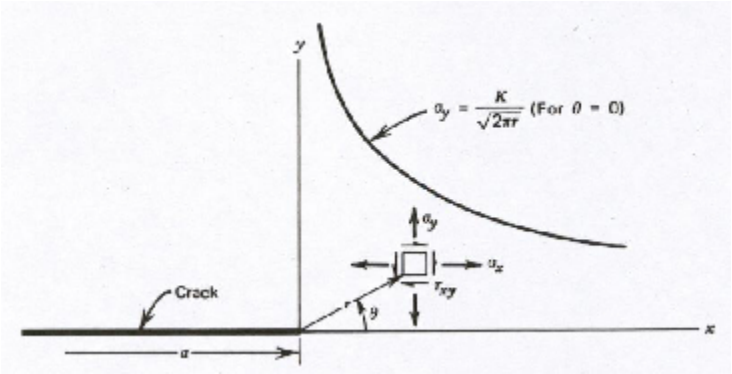

Figure 57: Elastic stress near the crack tip (r/a<<1)

Using the theory of linear elasticity the stress field at any point near the crack tip can be described with Equation 20:

$$\sigma_y = \frac{K}{\sqrt{2\pi r}}\cos\frac{\theta}{2}\left[1+\sin\frac{\theta}{2}\sin 3\frac{\theta}{2}\right]$$

$$\sigma_x = \frac{K}{\sqrt{2\pi r}}\cos\frac{\theta}{2}\left[1-\sin\frac{\theta}{2}\sin 3\frac{\theta}{2}\right]$$

$$\tau_{xy} = \frac{K}{\sqrt{2\pi r}}\cos\frac{\theta}{2}\sin\frac{\theta}{2}\cos 3\frac{\theta}{2}$$

$$\sigma_z = \tau_{xz} = \tau_{yz} = 0 \text{ for plane stress}$$

$$\left.\begin{aligned}\sigma_z &= \mu\left(\sigma_x+\sigma_y\right)\\ \tau_{xz} &= \tau_{yz} = 0\end{aligned}\right\} \text{for plane strain}$$

Equation 20

From Equation 18can be seen that the elastic nominal and elastic shear stresses in the vicinity of the crack tip are dependent on r, θ and K only. The magnitudes of these stresses at a given point are thus

dependent entirely on K and for that reason K is referred as a “stress field parameter” or “stress intensity factor”. The value of the stress intensity factor depends on many factors such as the loading, crack shape, mode of crack displacement, and the configuration of the component, specimen or configuration.

The values of the stress intensity factor can be evaluated by using the theory of elasticity involving analytical and computational calculations or with experimental methods.

3.4.2. Fracture toughness – K_c, K_{Ic}

The fracture toughness is a critical value of K referring to a condition in which a crack extends in a rapid (unstable) manner without an increase of the applied load or energy. It is described with Equation 21.

$$K_c = S_c\sqrt{\pi a_c}\, f\left(\frac{a_c}{w}\right) \qquad \textit{Equation 21}$$

Where S_c is the applied nominal stress at crack instability and a_c is the crack length in instability. The fracture toughness depends on the material, strain rate, environment, thickness, and to the crack length. It typically represents the stress intensity factor at the last cycle of a fatigue fracture.

On Figure 58 is shown the general relationship between fracture toughness and the thickness.

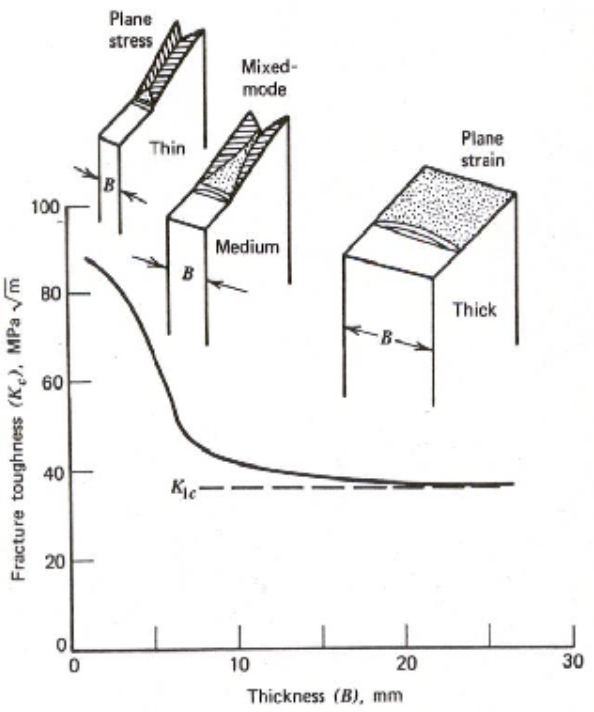

Figure 58: Effect of specimen thickness on fracture toughness

It can be seen that thin parts have a high K_c value along with appreciable “shear lips” or slant fracture. Increasing the thickness the percentage of shear lips decreases as does K_c. this type of fracture is known as a “mixed – mode”, implying both slant and flat fractures. For thick parts the entire fracture is flat and K_c approaches an asymptotic minimum value. Any further increase of the thickness does not lead

to decrease of the fracture toughness, nor does change the appearance of the fracture surface. The minimum value of fracture toughness is called the "plane strain fracture toughness", K_{Ic}. These fractures occur almost entirely by the mode I crack opening. The flat surface fracture of the thick sections best approach a true plane strain constraint throughout most of the crack tip region. For thin sections the crack tip region most closely experiences a plane stress situation. Thus, plastic zone sizes at fracture are much larger in thin parts than in thick parts. Plane strain toughness K_{Ic} is a true material property since it is not affected of the thickness.

Low impurity materials provide better fracture toughness. Fracture toughness K_{Ic} and K_c can be very sensitive to metallurgical conditions such as grain orientation, chemistry, and microstructure. They are also dependent on the temperature, strain rate, and corrosive environment. With decrease of the temperature, K_c usually decreases and yield strength increases. Thus, even though unnotched or uncracked tensile strength increases with decreasing temperature, the flaw or crack resistance can be drastically reduced. This can be seen from Figure 59.

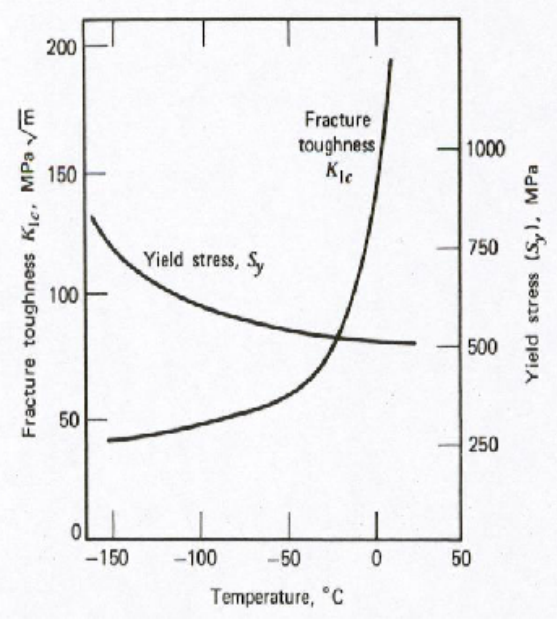

Figure 59: Variation of K_{Ic} with temperature for low alloy nuclear pressure vessel steel A553B

Figure 60, which is a plot of Equation 22, shows how changes in fracture toughness influence the relationship between allowable nominal stress and allowable crack size.

$$S = \frac{K_{Ic}}{\sqrt{\pi a}} \qquad \textit{Equation 22}$$

The allowable stress in the presence of a crack with a given size is proportional to the fracture toughness, while the allowable crack size for a given stress is proportional to the square of the fracture toughness. Hence, an increase of K_{Ic} has a higher influence on allowable crack size than on allowable stress.

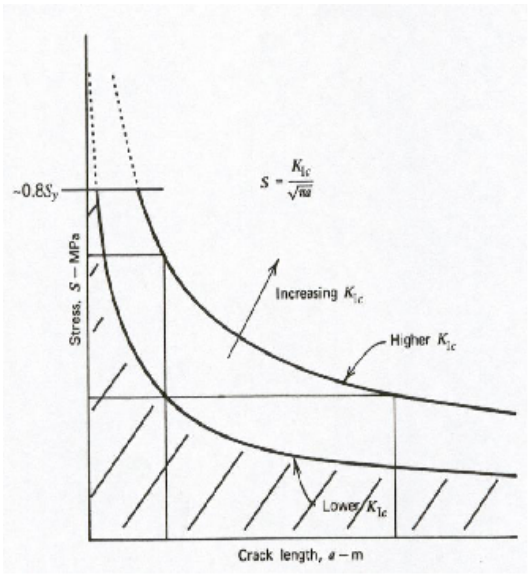

Figure 60: Influence of fracture toughness on allowable stress or crack size

3.4.3. Fatigue crack growth, da/dN – ΔK

The strength of a component or structure can be significantly reduced by the presence of a crack or discontinuity, but in the most cases the initial crack or discontinuity size is not critical to cause catastrophic failure. More commonly, subcritical crack growth occurs from the existing flaw until a critical crack size is reached, causing fracture.

Figure 61 shows three crack lengths versus applied cycles curves for three identical test specimens subjected to different repeated stresses ($S_1>S_2>S_3$). All specimens have the same initial crack length a_0.

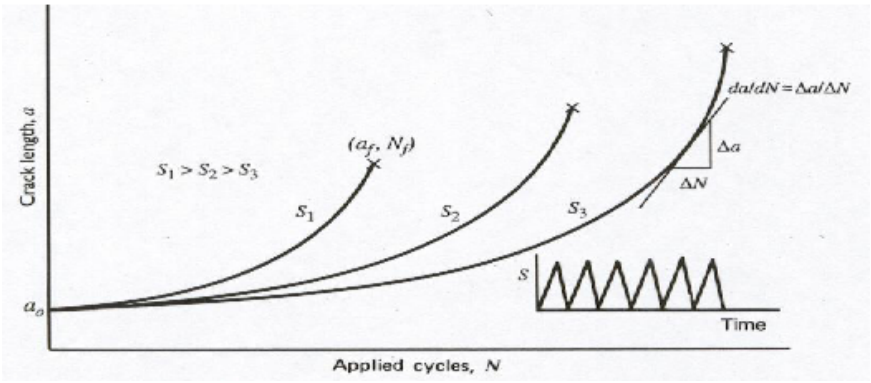

Figure 61: Fatigue crack length versus applied cycles

From Figure 61 can be seen that the higher the stress, the higher the crack growth rate, represented by the slopes of the curves, and the shorter the fatigue crack growth rate (total number of cycles applied, N_f). For a given initial crack size, the life to fracture depends on the magnitude of the applied stress and the fracture resistance of the material.

Applying the LEFM concepts to the data shown in Figure 61 will transform the data to a format useful for the fatigue life prediction. This is done by plotting the obtained fatigue crack growth rate, da/dN, versus the applied stress intensity factor, ΔK, as shown schematically on Figure 62. The fatigue crack growth rates, da/dN, can be obtained at consecutive positions along the curve using graphical or numerical methods. The corresponding applied stress intensity factor range, ΔK, is calculated knowing the crack length, a, the applied stress range, ΔS, and the stress intensity factor solution, K, for the part in question. ΔK can be defined using Equation 23.

$$\Delta K_I = \Delta K = K_{max} - K_{min} = S_{max}\sqrt{\pi a}\alpha - S_{min}\sqrt{\pi a}\alpha = \left(S_{max} - S_{min}\right)\sqrt{\pi a}\alpha = \Delta S\sqrt{\pi a}\alpha$$

Equation 23

Since ΔK is primarily dependent on ΔS, a, and the geometry (α), many models of the form shown in Equation 24 were proposed and developed.

$$\frac{da}{dN} = f\left(\Delta S, a, \alpha\right) = f\left(\Delta K\right) \qquad \textit{Equation 24}$$

The sigmoidal curve, generated from the reduction of a versus N to da/dN versus ΔK data, is independent of the initial crack length.

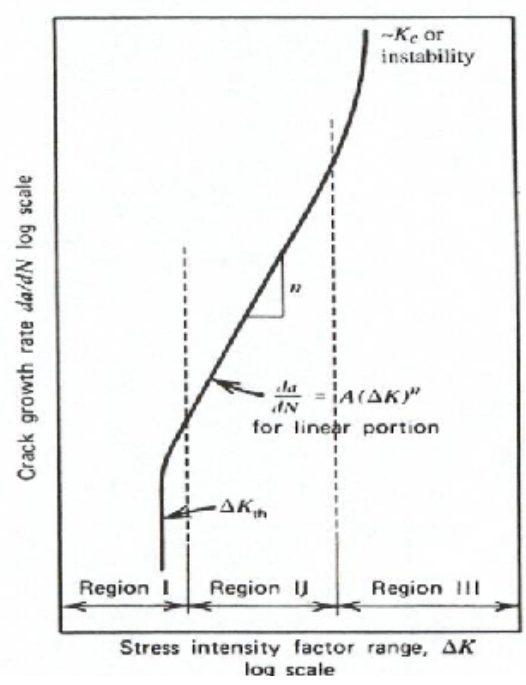

Figure 62: Schematic sigmoidal behavior of fatigue crack growth rate versus ΔK

The typical log – log – plot of da/dN versus ΔK, shown on Figure 62 can be divided into three regions. Region I is the near threshold region and indicates a threshold value, ΔK_{th}, below which there is no observable crack growth. Below ΔK_{th}, fatigue cracks are characterized as nonpropagating cracks. The parameters that mainly control region I are microstructure, mean stress, frequency and environment.

Region II shows essentially linear relationship between log da/dN and log ΔK, which can be described by the Paris's law (Equation 25).

$$\frac{da}{dN} = A\left(\Delta K\right)^n$$ ***Equation 25: Paris law***

Where n is the slope of the line and A is the coefficient found by extending the straight line to ΔK=1 MPa√m.

Region II corresponds to stable macroscopic crack growth that is typically controlled by the environment. In region III the fatigue crack growth rate are very high as they approach instability, and little fatigue crack growth life is involved. This region is controlled mainly by fracture toughness K_c or K_{Ic}, which depend on the microstructure, mean stress, and environment.

If one knows the stress intensity factor expression, K, for a given component and loading, by integrating the sigmoidal curve between the limits of initial crack size and final crack size, the fatigue crack growth life can be obtained.

3.5. Fatigue from variable amplitude load

Most of the cyclic loadings are usually not constant and their amplitude changes in time. When loading occurs in variable manner the cumulative effect of these events may produce fatigue failure. In the literature this is referred as "cumulative damage". The term "spectrum" means a series of fatigue loading events, which are not uniformly repeated cycles.

3.5.1. Damage quantification and the concepts of damage fraction and accumulation

One of the possible approaches for variable load histories uses the concept of "damage", defined as a fraction of life (or also called "cycle damage") used up by an event or a series of events. These fractions are summed together and a failure is expected when this sum becomes equal to 1 or 100%.

Once a crack has been started the damage can be defined as the growth of it. A loading that causes an extend of the crack by $\Delta a = 0.01$ mm for example has damage equal to $D = {\Delta a}/{a_c}$, where a_c is the critical crack length for the highest expected load, and D is the damage fraction. However it worth mentioning that the loading that produces that crack growth may have higher damage at a later stage.

There are of course many more methods to quantify the fatigue damage such as the ones including metallurgical parameters, mechanical parameters, and physical measures. Metallurgical parameters include the size or the number of dislocations and the spacing or intensity of slipbands. Mechanical parameters directly reflect damage through changes in the mechanical response of the material such as hardness, stress, strain, stiffness, and strain energy as the material degrades with fatigue damage accumulation. Pfysical damage indirectly quantify the fatigue damage and consist of mainly nondestructive techniques such as X-radiography, acoustic emission, ultrasonic techniques, magnetic field methods, potential drop, and eddy current techniques.

3.5.2. Cumulative damage theories

- Palmgren – Miner linear damage rule

The damage caused by 1 cycle is $D = {}^{1}/_{N_f}$, where N_f is the number of repetitions of this same cycle that equals the median life to failure. If there are n such cycles the damage is then $D = {}^{n}/_{N_f}$. The linear damage rule proposed by Palmgren and later by Miner is given by Equation 26.

$$\sum \frac{n_i}{N_{fi}} = \frac{n_1}{N_{f1}} + \frac{n_2}{N_{f2}} + \cdots = 1 \qquad \textbf{\textit{Equation 26: Linear damage rule}}$$

The assumption of linear damage is open to many objections. For example the sequence and interaction of events may have major influences on the fatigue life, but also the rate of damage accumulation may be a function of the load amplitude such that at low load levels most of the life is involved in crack nucleation, while a high load levels most of the life is spent in crack growth.

- Nonlinear damage theories

To remedy the differences with the linear damage assumption, many nonlinear cumulative fatigue damage rules have been proposed. These theories account for the nonlinear nature of fatigue damage accumulation by using relations such as

$$D = \sum \left(n_i / N_{fi}\right)^{\alpha_i} \qquad \textbf{\textit{Equation 27}}$$

Where α_i depends on the load level.

Though many nonlinear damage models have been developed, unfortunately none can encompass many of the complicating factors encountered during complex variable amplitude loading. Consequently, the Palmgren-Miner linear damage rule is still dominantly used in fatigue analysis or design in spite of its many shortcomings.

3.5.3. Crack growth and life estimation models

Life estimation associated with fatigue crack growth involves the growth of cracks from an initial length to some intermediate length or to the final length at fracture. It would be straightforward if one can use the crack growth data from tests with a uniform range of load or stress intensity factor. However, fatigue crack growth depends not only on these ranges, but also on the previous load histories, which may have left compressive or tensile residual stress fields. If it is compressive it tends to retard (delay) or arrest crack growth; if tensile to accelerate it.

The fatigue growth life estimation models for variable amplitude loading can be simple and straightforward or complex, requiring extensive computations. In some cases, the actual service load history can be approximated and simplified to give repeated applications of a multiple block loading sequence, where each block represents a given load level. Estimation of the fatigue crack growth life can then be made, evaluating crack growth related to each block (load level) or, in some cases, the entire repeating load history. Another approach is the summation of the crack increments based on each cycle.

These methods of life estimation can be used under the assumption, that crack growth for a given cycle or block is not influenced by the prior history loading (load sequence). This may be a reasonable if the load history is highly irregular (random), where the frequency of overloads in both tension and compression is similar or if the overloads are not too severe. If it is not the case an the overloads may introduce load sequence effects that can significantly affect the overall fatigue crack growth life some models have been developed to provide more accurate life estimations.

- Direct summation

The direct summation method is one of the simplest models for damage accumulation. It consists in the estimation of the crack length after N cycles of load applications (Equation 28).

$$a_N = a_0 + \sum_{i=1}^{N} \Delta a_i = a_0 + \sum_{i=1}^{N} f(\Delta K_i) \qquad \textbf{\textit{Equation 28}}$$

Where a_0 is the initial crack length and Δa_i can be estimated from the constant amplitude fatigue crack growth curve da/dN versus ΔK.

Cycle-by-cycle summation continues until fracture occurs or a predetermined crack length is reached, at which point the number of cycles accumulated is the estimated fatigue crack growth life.

- Equivalent K methods

For repeating histories or block load spectra, where load sequence effects are not expected to be significant, it is often possible to correlate crack growth rates and make life estimations using an equivalent stress intensity factor. Once the equivalent load(s) are developed, the analysis becomes one of constant amplitude loading. This method is usually limited to spectra that exhibit a periodic behavior, i.e., where the repeating load history is relatively short and where crack extension during the repeating load history is small. This method is computationally saving, but it is not as accurate as the direct one.

Ne of the Equivalent K methods is based on the premise that an equivalent R=0 stress intensity factor range, ΔK_{eq}, can be determined that will cause the same amount of fatigue crack growth as in the variable amplitude history, as given by Equation 29.

$$\frac{da}{dN} = f\left(\Delta K_{eq}\right)_{VA\ loading} = f\left(\Delta K_{eq}\right)_{CA\ loading} \qquad \textbf{\textit{Equation 29}}$$

Using the Paris equation (Equation 25) the equivalent stress intensity factor can be written using Equation 30.

$$\Delta K_{eq} = \Delta S_{eq}\sqrt{\pi a}\alpha = \left[\frac{\sum_{i=1}^{N}(\Delta S_i')^n}{N}\right]^{1/n}\sqrt{\pi a}\alpha \qquad \textbf{\textit{Equation 30}}$$

Where ΔS_{eq} is the equivalent R=0 stress range for the repeating load history, $\Delta S_i'$ is the equivalent R=0 stress range in the ith cycle within the variable amplitude history, n is the lope of the Paris equation region II line, and N is the number of cycles contained within the variable amplitude load history. ΔS_i is

obtained for each constant amplitude block within the variable amplitude load history. To account for mean stress effects associated with each constant amplitude block, the Walker approach can be used to calculate the equivalent R=0 stress range where

$$\Delta S' = S_{max}(1-R)^{\gamma}$$

Another equivalent K method used is based on the assumption that the variation of the crack tip stress-strain field can be described in terms of the root-mean-square value of ΔK (ΔK_{rms}) by using Equation 31.

$$\Delta K_{rms} = \Delta S_{rms}\sqrt{\pi a}\alpha = \sqrt{\frac{\sum_{i=1}^{N}\Delta S_i^2}{N}}\sqrt{\pi a}\alpha \qquad \textbf{\textit{Equation 31}}$$

The root-mean-square stress ratio, R_{rms}, can be calculated with Equation 32.

$$R_{rms} = {S_{\min\,(rms)}}\Big/{S_{\max\,(rms)}} \qquad \textbf{\textit{Equation 32: Root-mean-square stress ratio}}$$

Where:

$S_{\max\,(rms)} = \left[\frac{1}{N}\sum_{i=1}^{N}\left(S_{\max\,(i)}\right)^2\right]^{1/2}$ and $S_{\min\,(rms)} = \left[\frac{1}{N}\sum_{i=1}^{N}\left(S_{\min\,(i)}\right)^2\right]^{1/2}$

with $S_{\max\,(i)}$ and $S_{\min\,(i)}$ being the maximum and minimum stresses observed in the ith cycle.

Once obtained ΔK_{rms} and ΔS_{rms} can be then used in the general power law expression (Equation 33).

$$\frac{da}{dN} = f(\Delta K_{rsm}) = \frac{A(\Delta K_{rsm})^n}{(1-R_{rms})^{n(1-A)}} \qquad \textbf{\textit{Equation 33: General power law}}$$

4. Experimental Campaign

4.1. Magnetic particle examination

The original material of the ties of Duomo di Milano has many discontinuities and for further fatigue testing defect free parts must be identified. Two samples of the tie were subjected to magnetic particle examination, which is suitable for locating surface and subsurface cracks. Because of their characteristics ferromagnetic materials are susceptible to an external field and exhibit a strong attraction to an external magnetic field. When the material is free of defects it will transfer lines of magnetic field through itself without any interruption (Figure 63).

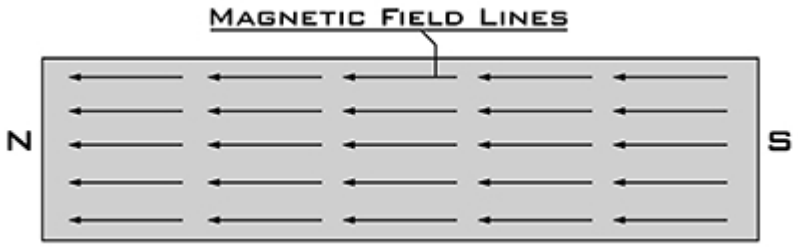

Figure 63: Uninterrupted magnetic field in ferromagnetic material

When a crack or other kind of discontinuity is present, the magnetic field leaks out of the material. If iron particles are sprinkled on the material surface the leakage of the magnetic field will attract and cluster them to the edges of the crack, making it more visible (Figure 64).

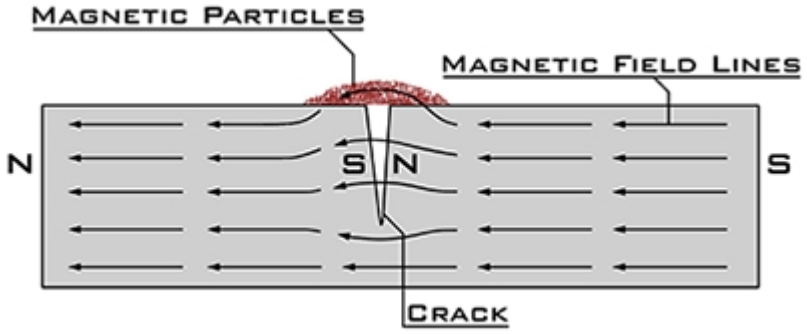

Figure 64: Magnetic particles clustering

However the magnetic field will leak out of the material only in the discontinuity is generally perpendicular to the flow. If the defect is parallel to the lines of magnetic flux it will not cause any leakage and therefore no identification of it will be possible. In order to overcome this problem the surface should be examined twice. The second examination has to be in direction, orthogonal to the first one, to ensure that discontinuities with any orientation are discovered.

Before starting with the experiment the samples' surfaces were cleaned with acetone and then covered with white paint in order to make the clusters of magnetic particles more visible (Figure 65).

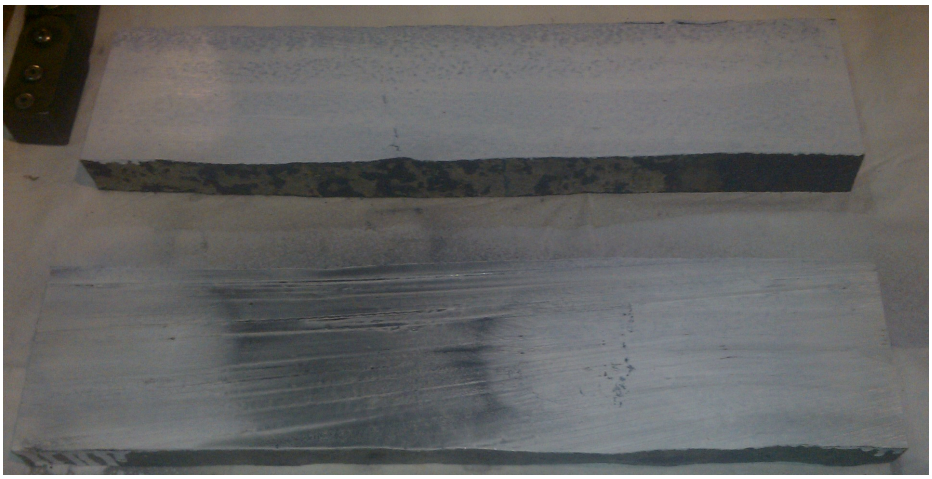

Figure 65: The two samples for magnetic particle testing

Then the magnetic particles were sprinkled over the surface of the samples, magnetic field was applied and surface and subsurface cracks were located. Some pictures, taken during the experiment are given in Figure 66.

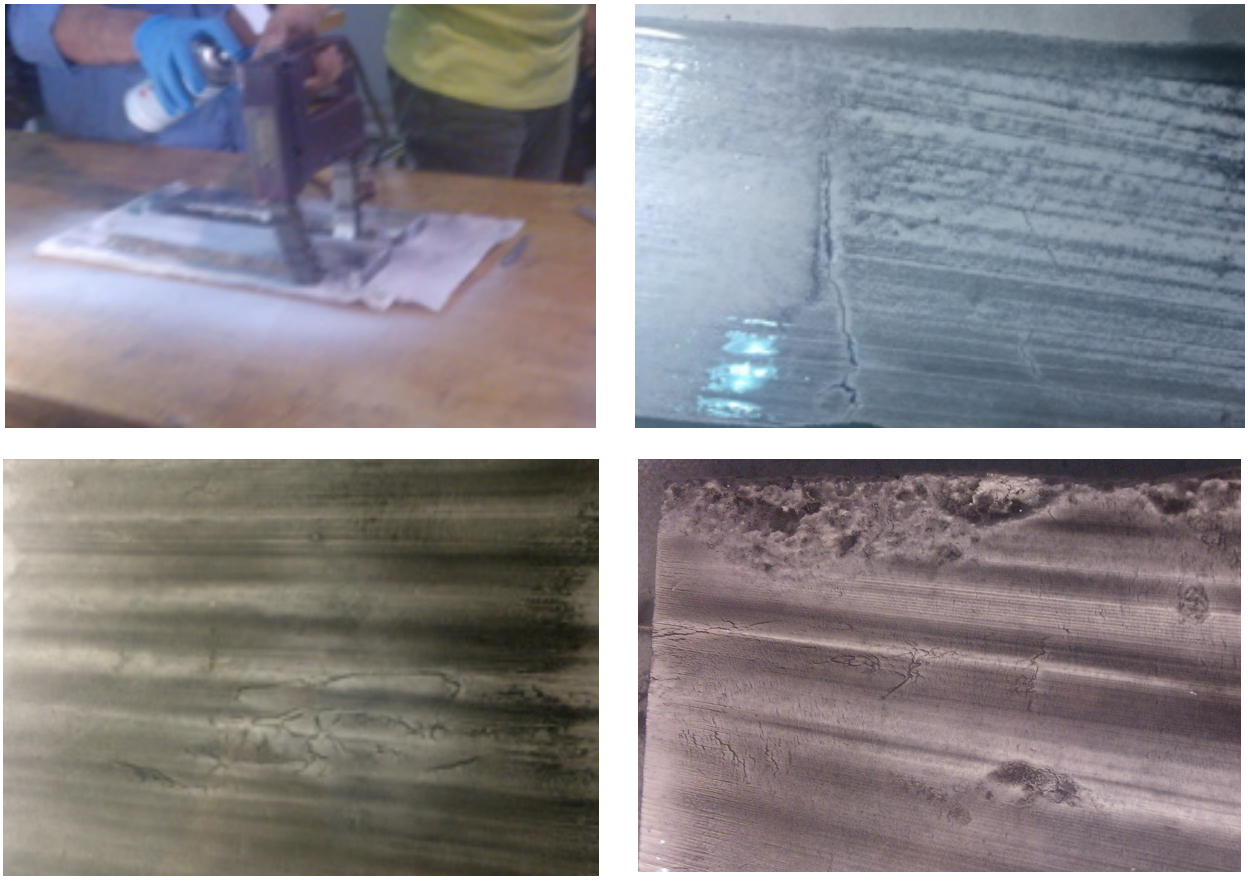

Figure 66: Cracks identified with magnetic particle test

The parts shown in Figure 67 were finally identified as potentially good for the fatigue testing since no dominant surface cracks were present. These parts were later cut and further analyzed for defects by means of ultrasonic testing.

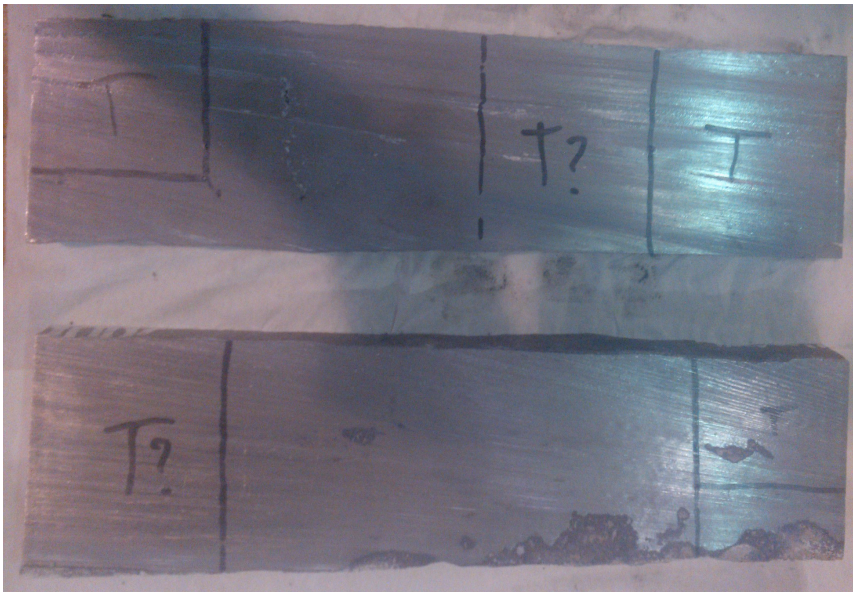

Figure 67: Parts of the tie's samples, free of surface cracks

4.2. Toughness test

The toughness test was performed according to the regulations provided in ASTM E399. The dimensions of the specimen given in the standard are shown in Figure 68.

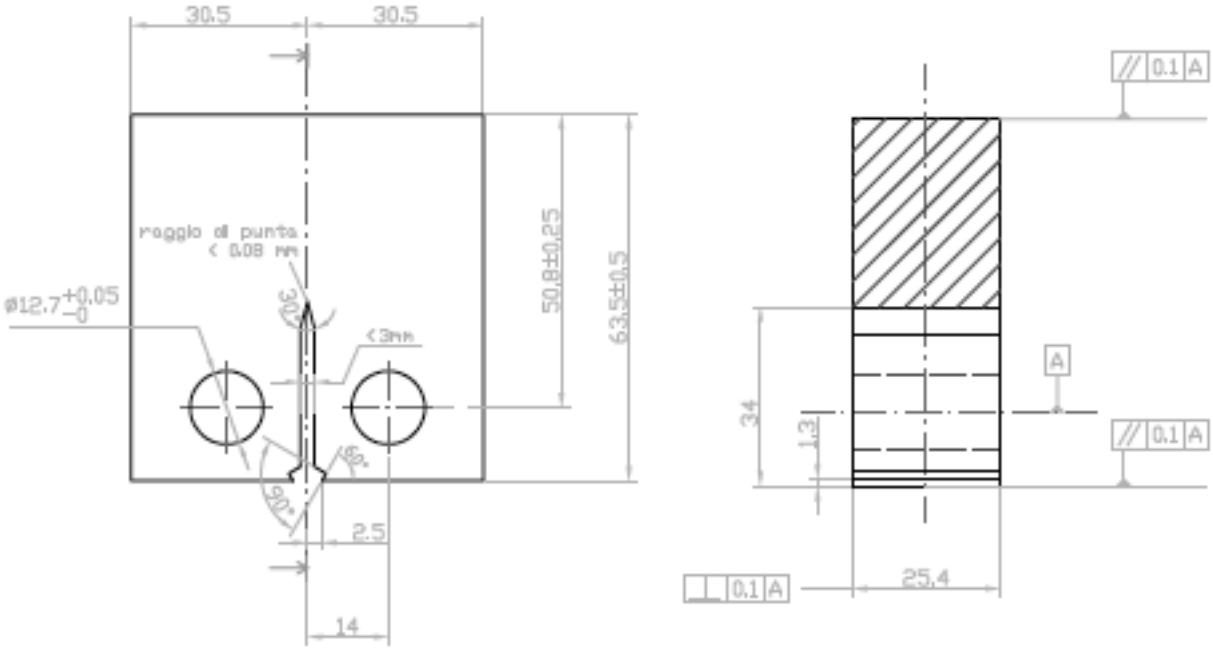

Figure 68: Toughness test specimen given in ASTM E399

Since the two pieces available do not have the thickness shown in Figure 68 all of the dimensions of the specimens were scaled with respect to the available one. That resulted in specimens with the geometry shown in Figure 69.

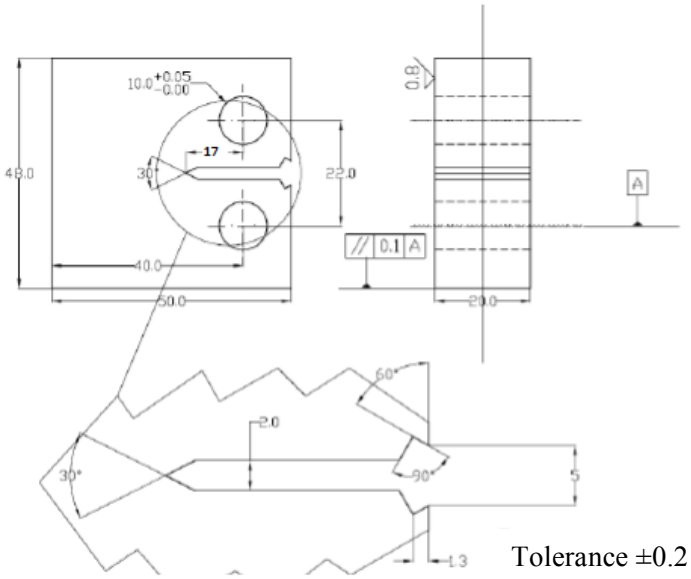

Figure 69: Toughness test specimen

5. Remaining Fatigue Life

5.1. General procedure

Discontinuities are always present in the material, especially when it is an old one as in the case of historical wrought iron. Under cyclic load these discontinuities can grow up to a size that is critical and can cause the failure of the element or even of the whole structure as it has already been explained in Chapter 3. Because of that when a crack is discovered in an element it is very important to understand its influence on the structure and what the remaining fatigue life is. The aim of this chapter is to provide guidelines for the estimation of the critical size of the crack and the remaining fatigue life.

In order to determine the fatigue crack growth life the following steps should be followed:

- The fracture toughness, K_c of the material should be determined. The value used should be taken from the literature or experimentally determined;

- A structural identification of the element have to be done in terms of maximum and minimum stresses, S_{min} and S_{max}, and the stress ratio, R, and the stress range, ΔS, have to be calculated as well according to the following expressions:

$$R = \frac{S_{min}}{S_{max}}; \qquad \Delta S = S_{max} - S_{min} \ \ [\text{MPa}]$$

S_{min} and S_{max} can be measured on site or they can be a result of analysis of the structure under consideration;

- The initial crack length, a_i in the element has to be measured on-site;

- The stress intensity factor range should be calculated using the expression:

$$\Delta K = 1.12 \Delta S \sqrt{a\pi}$$

- The critical crack length can be calculated using the expression:

$$a_f = \frac{1}{\pi}\left(\frac{K_c}{S_{max}\alpha}\right)^2 \ \ [\text{mm}]$$

- The Paris constants, A and n, has to be determined. Their values should be obtained experimentally or from the literature.

- Using the Paris equation

$$\frac{da}{dN} = A\left(\Delta K\right)^n = A\left(\Delta S\sqrt{\pi a}\alpha\right)^n$$

and integrating it over the crack length the number of fatigue cycles can be estimated according to the following:

$$N_f = \frac{a_f^{-\frac{n}{2}+1} - a_i^{-\frac{n}{2}+1}}{\left(-\frac{n}{2}+1\right) A \left(\Delta S\right)^n \left(\pi\right)^{\frac{n}{2}} \alpha^n}$$

The properties of the material needed for the computation of the fatigue crack growth life and the methods they can be obtained are given in Table 11.

a_i	Initial crack opening	Measured directly on the specimen
S_{min}	Minimum stress in the element	Experimentally determined
		Structural analysis
S_{max}	Maximum stress in the element	Experimentally determined
		Structural analysis
K_c	Fracture toughness	Experimentally determined
		Taken from the literature
		Experimental-numerical technique
A and n	Paris constants	Taken from literature
		Determined experimentally

Table 11

5.2. Examples of estimation of the remaining fatigue life

The procedure explained in 5.1 was performed in order to estimate the critical crack length of the tie of Duomo di Milano and its residual fatigue life. Since no experiments for determination of the Paris constants were done the values for these were taken from the available literature. As suggested by Kuhn et al. 2008, for the case of old steel $A=4.10^{-13}$ and n=3 were adopted. Since the fracture toughness of the wrought iron is not known, based on its properties two limit values were taken, corresponding to Steel 4340 and Aluminum. The minimum and maximum stress in the element came from the data of the dynamic testing that was performed on the ties. All properties are given in Table 12.

	Steel 4340	Aluminum
K_c	50 MPa√m	22 MPa√m
S_{min}	54 MPa	54 MPa
S_{max}	78MPa	78 MPa

Table 12: Properties for fatigue life estimation

The results obtained with this analysis are given in Figure 70.

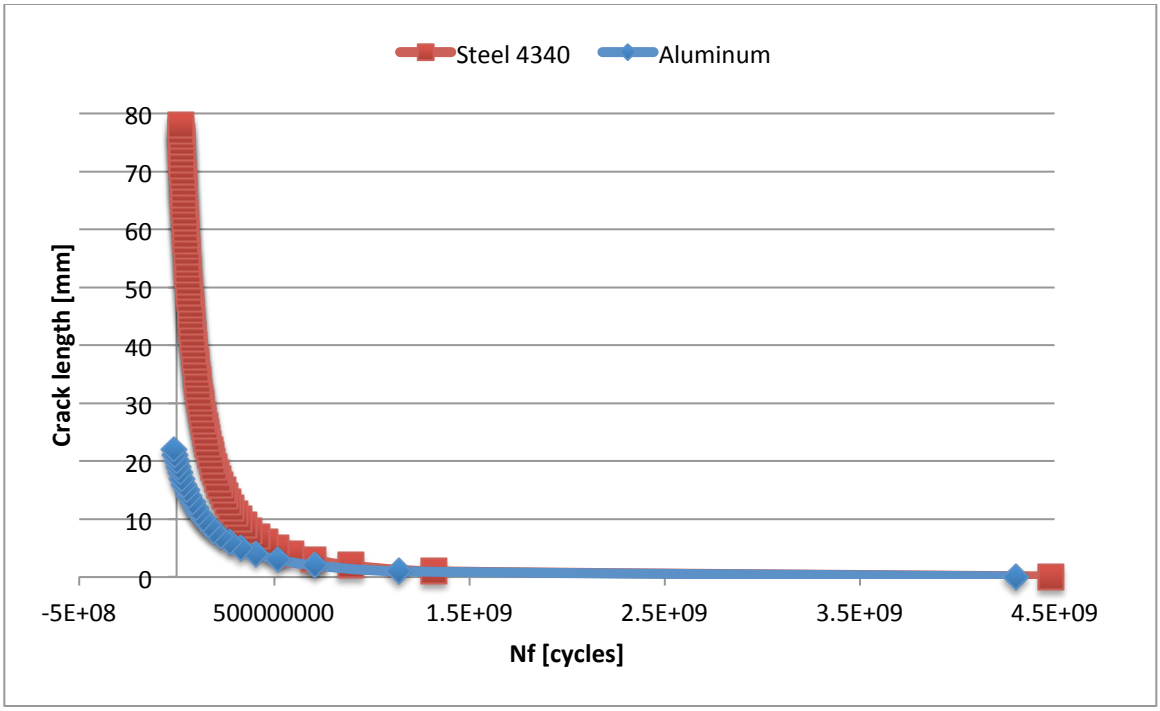

Figure 70: Remaining fatigue life as a function of the crack length

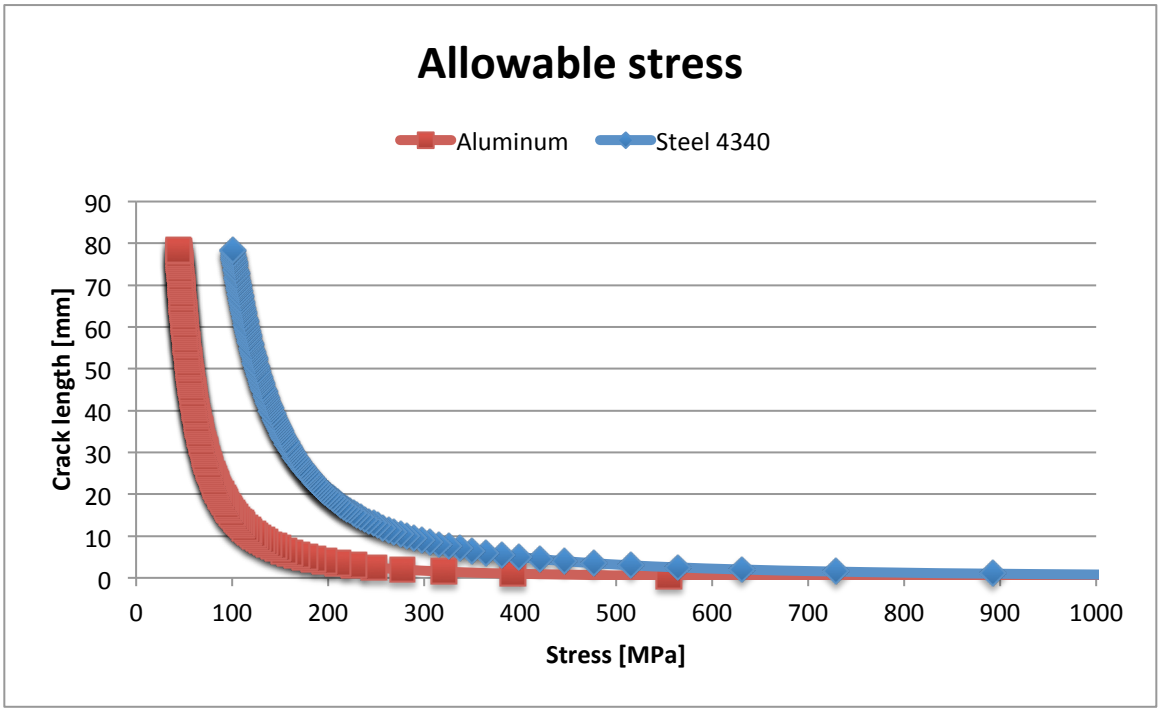

Figure 71: Awollable stress in the section as a function of the crack length

The solution for the case of wrought iron should lie between these two limits.

6. Conclusions

The present thesis presents the assessment of the fatigue behavior due to temperature variation of the iron ties in Duomo di Milano and addresses two main objectives. The first one is related to the review of the available historical investigations, data from monitoring and testing already performed on the Cathedral, information in the literature about the material characteristics and structural behavior. The second regards the experimental campaign performed on samples, taken from an original tie-rod that was replaced within a maintenance campaign. Simplified numerical, modeling of part of the structure along with the principles of the Linear Elastic Fracture Mechanics were functional to define the fatigue behavior and estimate the residual life of the tie-rod.

With regard to the first topic of the thesis the following conclusions can be drawn:

- The review of the literature showed that there is little information about the wrought iron and even when available, the material properties reported vary significantly. The experimental campaign confirmed that observation. The specimens taken from the same tie gave very different results in terms of tensile strength, because of the inclusions and defects present in them. The tensile strength obtained varies in the range 200÷320 MPa. Significant variations in the results for the elastic modulus were also observed.

- The historical investigation of the Cathedral gave evidence for the complex structural system, which despite the experienced perturbations managed to find a new stable condition, by redistribution of the actions. Because of this, a sophisticated model of the structure would be probably able to explain the complex behavior, but it would require great amount of information, which for now is not available.

From the second topic of the thesis it could be concluded:

- The analysis performed by means of simplified numerical model showed that the daily temperature variation is unable to cause alternation of the stress in the ties big enough to lead to fatigue phenomenon. On the other hand the seasonal temperature change could be the reason for the alternation of the stress, observed during the monitoring campaign. This was also confirmed with the performed finite element analysis of the tie-rod. Therefore in the further computations of the crack length propagation and the residual fatigue life only the effect of the seasonal temperature variation was taken into consideration.

- A procedure was developed for estimation of the critical crack length and residual fatigue life of the elements, which could be a powerful tool for their assessment. When a defect is recognized in the tie it will be possible easily to understand if it threatens the stability of the element or not.

Developing a more sophisticated numerical model of the structure would give better understanding of its behavior and more accurate results. However this requires a great number of material properties, which in this moment are unknown and further investigation in that aspect should be done.

References:

Amabili M., Carra S., Collini L., Garziera R., Panno A., 2010, Estimation of tensile force in tie-rods using a frequency-based identification method, Journal of Sound and Vibration 329, 11, 2057-2067.

Brincker R., Kirkegaard P. H., 2010, Special issue on Operational Modal Analysis, Mechanical Systems and Signal Processing 24, 5, 1209-1212.

Cigada A., Comoli L., Giussani A., Roncoroni F., Zenucchi F., Thermal characterization of FBG strain gauges for the monitoring of the cupola of Duomo di Milano, Proc. SPIE 7753, 21st International Conference on Optical Fiber Sensors, May 17, 2011.

Coronelli D., di Prisco C., Pisanó F., 2014a, The tiburio of the Cathedral of Milan: structural analysis of the construction and 20th century foundation settlements.

Coronelli, D., Caggioni, B., Zanella, F. 2014b, The Cathedral of Milan: the structural history of the loadbearing system, International Journal of Architectural Heritage, Accepted for publication.

Ewins D.J., 2001, MODAL ANALYSIS, EXPERIMENTAL | Basic Principles, In Encyclopedia of Vibration, edited by S. Braun, Elsevier, Oxford, Pages 805-813.

Ferrari da Passano, C. 1988. Il Duomo rinato. Diakronia, Vigevano, 136pp.

Ferrari da Passano, C. 2005. Il Nuovo per Salvare l'antico: Il Restauro Statico Conservativo dei Monumenti Vincolati. Milano, Veneranda Fabbrica del Duomo.

Fitchen J. 1961. The construction of gothic cathedrals: a study of medieval vault erection, London, Oxford University Press, 1961.

Gentilini C., Marzani A., Mazzotti M., 2013, Nondestructive characterization of tie-rods by means of dynamic testing, added masses and genetic algorithms, Journal of Sound and Vibration 332, 1, 76-101.

Giussani A., Roncoroni F., Relazione sulle misure eseguite per il controllo delle deformazioni del Duomo di Milano nei anni 2009-2014, Laboratorio IC&T, Politecnico di Milano, Polo Territoriale di Lecco, Italy.

Godfraind S., Pender R., Martin B., 2012, Metals/English Heritage, edited by Godfraind S., Farnham: Ashgate; Burlington.

Guidobaldi M., Vasic M., Gentile C., Poggi C., 2014, Frequency splitting in the tie- rods of the Cathedral of Milan", eds. Cunha A., Caetano E., Ribiero P., Muller G., *Proceedings of the 9th International Conference on Structural Dynamics EURODYN 2014, pp.1477-1483, Porto, 2014.*

Heyman, J. 1995. The stone skeleton, structural engineering of masonry architecture", Cambridge University Press: 159 pp.

Lagomarsino S., Calderini C., 2005, The dynamic identification of the tensile force in ancient tie-rods, Engineering Structures 27, 6, 846-856.

Murakami, Y. 2002, In Metal Fatigue, edited by Murakami Y., Elsevier Science Ltd, Oxford.

Niccolai, C., 1967. Il sottosuolo del territorio di Milano, Rivista Italiana di Geotecnica, n.1: 7-33.

Rebecchi G., Tullini N., Laudiero F., 2013, Estimate of the axial force in slender beams with unknown boundary conditions using one flexural mode shape, Journal of Sound and Vibration 332, 18, 4122-4135.

Stephens R. I., Fatemi A., Stephens R. R., Fuchs H. O., 2001, Metal Fatigue in Engineering, 2nd edition, Wiley New York.

Tulini N., Laudiero F., 2008, Dynamic identification of beam axial loads using one flexural mode shape, Journal of Sound and Vibration 318, 1-2, 131-147.

Tullini N., Rebecchi G., Laudiero F., 2012, Bending tests to estimate the axial force in tie-rods, Mechanics Research Communications 44, 57-64.

Van Overschee P., De Moor B., 1996, Continuous-time frequency domain subspace system identification, Signal Processing 52, 2, 179-194.

Vasic M. 2014, A multidisciplinary approach for the structural assessment of great historical structures, PhD thesis, Politecnico di Milano.

Vasic M., Coronelli D., Poggi C., 2015, A multidisciplinary approach for the assessment of great historical structures: ties of "Duomo di Milano", *Proceedings of International Conference Built Heritage: Monitoring Conservation Management, eds. Toniolo L., Guidi G., Boriani M.,*Springer.

Virgin L.N., Santillan S.T., Holland D.B., 2007, Effect of gravity on the vibration of vertical cantilevers, Mechanics Research Communications 34, 3, 312-317.

Appendix A

Data on several wrought iron samples, taken from an old bridge built in 1910 is Šilutė (Navasaitis et. al 2003):

Parameter	Wrought iron from Šilutė bridge				Wrought iron [2]	Ingot iron (C=0.02 %)[1]	Mild steel St. 15 [12]
	Specimen No.1	Specimen No.2	Specimen No.3	Average meaning			
Yield strength σ_y, MPa	283	286	242	270	232	131	220
Tensile strength σ_U, MPa	378	384	355	372	341	289	370
Elongation δ, %	12	14	19.7	15	28	48	27
Reduction of area ψ, %	12.3	13.6	29.2	18	48	-	55

A 1: Wrought iron properties reported by Navasaitis

Mechanical properties of wrought iron from multiple elements of six late 19th century truss bridges (Kelton et. al 2011):

Specimen	Member thickness		Reduction in area	Average hardness	Hardness standard deviation	Yield stress		Tensile strength	
	[mm]	[in]	[%]			[MPa]	[ksi]	[MPa]	[ksi]
BV-H-1	38.1	1 1/2	48	52	1	154	22.4	273	39.6
BV-H-2	38.1	1 1/2	36	55	4	184	26.7	315	45.7
BV-H-3	38.1	1 1/2	39	55	4	199	28.9	331	48.1
BV-H-4	38.1	1 1/2	46	58	9	206	29.8	334	48.5
BV-H-5	38.1	1 1/2	42	58	7	230	33.3	331	48
BV-H-6	38.1	1 1/2	42	54	5	188	27.3	319	46.2
BV-H-7	38.1	1 1/2	36	52	8	187	27.2	316	45.8
BV-H-8	38.1	1 1/2	42	59	9	212	30.8	329	47.7
RB-H-1	38.1	1 1/2	22	49	3	200	29	316	45.8
RB-H-2	38.1	1 1/2	23	53	8	208	30.1	320	46.4
RB-H-3	38.1	1 1/2	43	55	7	208	30.2	318	46.1
RB-H-4	38.1	1 1/2	41	48	6	187	27.1	305	44.2
RB-H-5	38.1	1 1/2	43	54	3	196	28.5	314	45.5
RB-H-6	38.1	1 1/2	34	59	5	218	31.6	341	49.4
RB-H-7	38.1	1 1/2	43	62	6	223	32.4	335	48.6
GH-H-1	28.6	1 1/8	50	56	5	242	35.1	341	49.4
GH-H-2	28.6	1 1/8	53	56	4	245	35.5	346	50.1
GH-H-3	28.6	1 1/8	47	57	6	228	33	339	49.2
GH-H-4	28.6	1 1/8	47	61	3	239	34.6	345	50

Specimen	Member thickness		Reduction in area	Average hardness	Hardness standard deviation	Yield stress		Tensile strength	
	[mm]	[in]	[%]			[MPa]	[ksi]	[MPa]	[ksi]
GA-H-1	28.6	1 1/8	50	55	6	247	35.9	354	51.4
GA-H-2	28.6	1 1/8	53	55	13	224	32.5	347	50.4
GA-H-3	28.6	1 1/8	47	59	5	253	36.7	356	51.6
GA-H-4	28.6	1 1/8	47	60	4	219	31.7	351	50.9
CB-H-1	44.5	1 3/4	33	62	3	189	27.4	328	47.6
CB-H-2	44.5	1 3/4	41	61	9	185	26.9	330	47.8
CB-H-3	44.5	1 3/4	40	59	6	189	27.4	331	48
CB-H-4	44.5	1 3/4	40	63	5	189	27.4	329	47.7
CB-L-1	6.4	1/4	3	72	4	295	42.8	361	52.3
CB-L-2	6.4	1/4	12	78	3	312	45.2	383	55.5
CB-L-3	6.4	1/4	9	82	2	320	46.5	390	56.5
CB-L-4	6.4	1/4	8	76	2	297	43.1	356	51.6
CB-L-5	6.4	1/4	6	79	4	317	46	365	52.9
SV-H-1	25.4	1	46	59	9	234	33.9	323	46.9
SV-H-2	25.4	1	46	56	12	247	35.8	334	48.4
SV-H-3	25.4	1	43	46	2	204	29.5	300	43.5
SV-H-4	25.4	1	47	47	6	211	30.6	309	44.8
SV-H-5	25.4	1	49	51	3	219	31.7	322	46.7
SV-H-6	25.4	1	53	53	10	221	32.1	322	46.8
SV-H-7	25.4	1	48	46	6	210	30.5	313	45.4
SV-H-8	25.4	1	50	49	5	218	31.6	316	45.9
SV-L-1	6.4	1/4	26	69	3	298	43.3	381	55.3
SV-L-2	6.4	1/4	25	67	2	305	44.3	399	57.9
SV-L-3	6.4	1/4	32	72	4	294	42.6	380	55.1
SV-L-4	6.4	1/4	17	67	1	268	38.9	360	52.1
SV-E-1	22.2	7/8	46	59	5	232	33.7	334	48.4
SV-E-2	22.2	7/8	42	58	6	235	34.1	340	49.3
SV-E-3	22.2	7/8	44	56	7	243	35.3	337	48.9
SV-E-4	22.2	7/8	46	52	6	214	31.1	325	47.2
SV-B-1	22.2	7/8	41	58	4	236	34.3	339	49.2
SV-B-2	22.2	7/8	40	57	5	243	35.3	341	49.4
SV-B-3	22.2	7/8	37	55	6	220	31.9	328	47.6
SV-B-4	22.2	7/8	41	53	2	227	32.9	330	47.8
SV-B-5	22.2	7/8	43	55	6	226	32.8	323	46.8

A 2: Wrought iron properties reported by Kelton

Summary of wrought iron bar tensile strength, elastic limit (yield strength) data of 959 specimens reported by Beardslee:

Size of Bar		Name of Iron	Number of Tests	Strength		Tensile Strength		Elastic limit	
[in]	[mm]			[lbs]	[kN]	[psi]	[MPa]	[psi]	[MPa]
0.25	6.35	F	1	2920	12.99	59885	412.89		
0.38	9.652	F	4	5886	26.19	54090	372.94	40980	282.55
0.5	12.7	C	6	12331	54.87	62700	432.30		
0.5	12.7	C	7	11699	52.06	59000	406.79		
0.5	12.7	C	8	11388	50.68	57700	397.83		
0.5	12.7	C	11	10881	48.42	55400	381.97		
0.5	12.7	F	1	10359	46.10	52275	360.42	39126	269.76
0.63	16.002	F	11	16977	75.55	55450	382.31		
0.63	16.002	F	4	15928	70.88	52050	358.87		
0.63	16.002	F	11	17644	78.52	57660	397.55		
0.75	19.05	F	4	22746	101.22	51546	355.40	35933	247.75
0.88	22.352	F	4	30850	137.28	50630	349.08	33931	233.95
1	25.4	K	13	48456	215.63	61727	425.59		
1	25.4	D	1	47975	213.49	61115	421.37	33486	230.88
1	25.4	O	1	45030	200.38	57363	395.50	37415	257.97
1	25.4	Fx1	5	43778	194.81	55768	384.51	34729	239.45
1	25.4	P	2	45378	201.93	57807	398.57	39230	270.48
1	25.4	A	3	42932	191.05	54690	377.07	34881	240.50
1	25.4	Fx2	3	44580	198.38	56790	391.55	36885	254.31
1	25.4	Fx3	2	42323	188.34	53915	371.73	36336	250.53
1	25.4	F	2	40758	181.37	51921	357.98	31300	215.81
1	25.4	D	8	41527	184.80	52900	364.73		
1	25.4	F	5	41463	184.51	52819	364.17	32267	222.47
1	25.4	F	4	40349	179.55	51400	354.39	34600	238.56
1.13	28.702	K	3	60066	267.29	60458	416.84	37344	257.48
1.13	28.702	D	1	59196	263.42	59582	410.80	33597	231.64
1.13	28.702	C	2	57097	254.08	57470	396.24	31990	220.56
1.13	28.702	Fx1	5	56068	249.50	56434	389.10	34682	239.12
1.13	28.702	P	2	57125	254.21	57498	396.43	41311	284.83
1.13	28.702	N	2	55779	248.22	56143	387.09	32267	222.47
1.13	28.702	Fx2	3	55564	247.26	55927	385.60	37250	256.83
1.13	28.702	E	1	52753	234.75	53097	366.09	33549	231.31
1.13	28.702	Fx3	2	54290	241.59	54644	376.76	34695	239.21
1.13	28.702	D	2	54332	241.78	54687	377.05	28166	194.20
1.13	28.702	A	3	53550	238.30	53900	371.63	26787	184.69
1.13	28.702	F	3	53501	238.08	53850	371.28	33457	230.68
1.13	28.702	O	1	52691	234.47	53035	365.66	32410	223.46
1.13	28.702	F	2	49824	221.72	50149	345.77	35493	244.72
1.13	28.702	F	5	51928	231.08	52267	360.37	32019	220.76

Size of Bar		Name of Iron	Number of Tests	Strength		Tensile Strength		Elastic limit	
[in]	[mm]			[lbs]	[kN]	[psi]	[MPa]	[psi]	[MPa]
1.25	31.75	K	2	59075	262.88	59461	409.97	36501	251.67
1.25	31.75	P	2	56507	251.46	56876	392.15	36868	254.20
1.25	31.75	C	1	57522	255.97	57897	399.19	32469	223.87
1.25	31.75	D	2	57601	256.32	57977	399.74	31996	220.60
1.25	31.75	P	2	55420	246.62	55782	384.60	35596	245.43
1.25	31.75	Px	2	55969	249.06	56334	388.41	33921	233.88
1.25	31.75	N	2	56112	249.70	56478	389.40	33251	229.26
1.25	31.75	Fx1	6	54895	244.28	55253	380.96	34784	239.83
1.25	31.75	D	1	55190	245.60	55550	383.00	28166	194.20
1.25	31.75	E	1	53544	238.27	53893	371.58	32712	225.54
1.25	31.75	Fx2	3	54775	243.75	55132	380.12	38603	266.16
1.25	31.75	Fx3	2	52902	235.41	53247	367.13	32520	224.22
1.25	31.75	A	3	53548	238.29	53897	371.61	27643	190.59
1.25	31.75	M	20	53403	237.64	53752	370.61		
1.25	31.75	M	20	53739	239.14	54090	372.94		
1.25	31.75	F	2	52627	234.19	52970	365.22	32075	221.15
1.25	31.75	F	2	52387	233.12	52729	363.55	39608	273.09
1.25	31.75	M	20	52678	234.42	53022	365.57		
1.25	31.75	F	5	52279	232.64	52620	362.80	33220	229.04
1.25	31.75	O	1	49716	221.24	50040	345.01	30730	211.88
1.31	33.274	P	94	73724	328.07	54518	375.89	35898	247.51
1.38	35.052	M	48	87454	389.17	58926	406.28	37548	258.88
1.38	35.052	M	35	85559	380.74	57649	397.48	38578	265.99
1.38	35.052	D	1	86111	383.19	58921	406.25	32152	221.68
1.67	42.418	K	2	121653	541.36	55790	384.66	31034	213.97
1.67	42.418	C	1	119819	533.19	54949	378.86	31030	213.94
1.67	42.418	M	28	118563	527.61	54373	374.89	35820	246.97
1.67	42.418	N	2	118354	526.68	54277	374.23	33622	231.82
1.67	42.418	Fx1	5	115500	513.98	52968	365.20	33275	229.42
1.67	42.418	Fx3	2	114987	511.69	52733	363.58	34606	238.60
1.67	42.418	E	1	113943	507.05	52254	360.28	25930	178.78
1.67	42.418	A	3	116784	519.69	53557	369.26	33650	232.01
1.67	42.418	P	1	114601	509.97	52556	362.36	30802	212.37
1.67	42.418	F	5	114560	509.79	52537	362.23	34469	237.66
1.67	42.418	F	2	114128	507.87	52339	360.86	39103	269.61
1.67	42.418	M	4	115604	514.44	53016	365.53	35379	243.93
1.67	42.418	Fx2	3	112270	499.60	51487	354.99	35911	247.60
1.67	42.418	F	2	111854	497.75	51296	353.67	31992	220.58
1.67	42.418	O	1	110323	490.94	50594	348.83	34940	240.90
1.44	36.576	P	1	86532	385.07	53345	367.80		
1.44	36.576	E	1	87504	389.39	53944	371.93	32543	224.38
1.44	36.576	G	1	86359	384.30	53238	367.06	32534	224.31

Size of Bar		Name of Iron	Number of Tests	Strength		Tensile Strength		Elastic limit	
[in]	[mm]			[lbs]	[kN]	[psi]	[MPa]	[psi]	[MPa]
1.44	36.576	B	4	84816	377.43	52287	360.51	31411	216.57
1.44	36.576	C	1	83955	373.60	51756	356.85	32655	225.15
1.44	36.576	J	1	81755	363.81	50400	347.50		
1.5	38.1	M	12	100768	448.42	57052	393.36	38417	264.88
1.5	38.1	K	2	101236	450.50	57317	395.19	33412	230.37
1.5	38.1	D	1	99802	444.12	56505	389.59	32496	224.05
1.5	38.1	M	25	97967	435.95	55466	382.42	34780	239.80
1.5	38.1	M	26	97375	433.32	55131	380.11	33771	232.84
1.5	38.1	P	2	95658	425.68	54159	373.41	33140	228.49
1.5	38.1	M	17	96331	428.67	54540	376.04		
1.5	38.1	C	4	97857	435.46	55404	382.00	34770	239.73
1.5	38.1	E	1	97877	435.55	55415	382.07	32869	226.62
1.5	38.1	M	20	96819	430.84	54816	377.94	34716	239.36
1.5	38.1	Px	2	96003	427.21	54354	374.76	34617	238.68
1.5	38.1	M	27	95545	425.18	54095	372.97	35544	245.07
1.5	38.1	E	1	96338	428.70	54544	376.07	33027	227.71
1.5	38.1	P	1	96911	431.25	54868	378.30	29636	204.33
1.5	38.1	M	20	94516	420.60	53512	368.95		
1.5	38.1	M	23	93507	416.11	52941	365.02		
1.5	38.1	Fx3	2	93292	415.15	52819	364.17	34840	240.21
1.5	38.1	Fx1	5	94478	420.43	53491	368.81	34307	236.54
1.5	38.1	M	4	94592	420.93	53555	369.25	34901	240.63
1.5	38.1	N	2	93081	414.21	52700	363.35	34690	239.18
1.5	38.1	C	1	92661	412.34	52462	361.71	35880	247.38
1.5	38.1	H	1	92119	409.93	52155	359.60	29992	206.79
1.5	38.1	D	1	91640	407.80	51884	357.73	27708	191.04
1.5	38.1	A	2	91834	408.66	51994	358.49	28794	198.53
1.5	38.1	F	2	89936	400.22	50919	351.07	32054	221.00
1.5	38.1	O	1	90884	404.43	51456	354.78	32312	222.78
1.5	38.1	F	5	90928	404.63	51481	354.95	34591	238.50
1.5	38.1	Fx2	3	90162	401.22	51047	351.96	34917	240.74
1.5	38.1	J	1	90162	401.22	51047	351.96		
1.5	38.1	M	1	87062	387.43	49292	339.86	32597	224.75
1.63	41.402	N	2	116795	519.74	56344	388.48	35889	247.45
1.63	41.402	K	4	118428	527.00	57132	393.91	35026	241.50
1.63	41.402	M	10	118988	529.50	57402	395.77	35701	246.15
1.63	41.402	P	2	115323	513.19	55634	383.58	33522	231.13
1.63	41.402	C	4	116552	518.66	56227	387.67	33207	228.95
1.63	41.402	Px	2	113364	504.47	54689	377.07	33427	230.47
1.63	41.402	A	2	112628	501.19	54334	374.62	32163	221.76
1.63	41.402	D	1	111304	495.30	53695	370.21	30087	207.44
1.63	41.402	Fx3	2	110566	492.02	53339	367.76	33540	231.25

Size of Bar		Name of Iron	Number of Tests	Strength		Tensile Strength		Elastic limit	
[in]	[mm]			[lbs]	[kN]	[psi]	[MPa]	[psi]	[MPa]
1.63	41.402	T	5	110976	493.84	53537	369.12	34335	236.73
1.63	41.402	D	1	111136	494.56	53614	369.66	30664	211.42
1.63	41.402	J	1	109341	486.57	52748	363.68		
1.63	41.402	E	1	109190	485.90	52675	363.18	33745	232.66
1.63	41.402	Fx2	3	110771	492.93	53438	368.44	35870	247.32
1.63	41.402	H	1	108441	482.56	52314	360.69	29364	202.46
1.63	41.402	E	1	107678	479.17	51946	358.16	27695	190.95
1.63	41.402	O	1	108622	483.37	52401	361.29	34012	234.50
1.63	41.402	F	2	108128	481.17	52163	359.65	33907	233.78
1.63	41.402	G	1	106142	472.33	51205	353.05	33318	229.72
1.63	41.402	F	2	104741	466.10	50529	348.39	35390	244.01
1.63	41.402	F	5	105655	470.16	50970	351.43	33625	231.84
1.63	41.402	C	1	101634	452.27	49030	338.05	31099	214.42
1.69	42.926	K	1	126513	562.98	56595	390.21	38310	264.14
1.69	42.926	B	1	121117	538.97	54181	373.56		
1.69	42.926	J	1	120967	538.30	54114	373.10		
1.69	42.926	B	3	118242	526.18	52895	364.70	33145	228.53
1.69	42.926	E	1	116510	518.47	52120	359.35	35549	245.10
1.69	42.926	G	1	129182	574.86	57789	398.44	34160	235.52
1.69	42.926	C	1	111370	495.60	49821	343.50	33184	228.80
1.75	44.45	K	1	139133	619.14	57874	399.03		
1.75	44.45	P	2	130329	579.96	54212	373.78	33908	233.79
1.75	44.45	C	5	130805	582.08	54410	375.14	31354	216.18
1.75	44.45	P	2	127040	565.33	52844	364.35	33842	233.33
1.75	44.45	F	5	129449	576.05	53846	371.26	36573	252.16
1.75	44.45	J	1	129339	575.56	53800	370.94	27856	192.06
1.75	44.45	M	2	132267	588.59	55018	379.34	34283	236.37
1.75	44.45	D	1	128550	572.05	53472	368.68	31802	219.27
1.75	44.45	K	1	128050	569.82	53264	367.24		
1.75	44.45	D	1	126692	563.78	52699	363.35	27817	191.79
1.75	44.45	F	2	127786	568.65	53154	366.48	35323	243.54
1.75	44.45	E	1	124064	552.08	51606	355.81	26541	182.99
1.75	44.45	A	2	123831	551.05	51509	355.14	29404	202.73
1.75	44.45	F	1	121862	542.29	50690	349.50	32229	222.21
1.75	44.45	G	1	121153	539.13	50395	347.46	36254	249.96
1.75	44.45	C	1	120953	538.24	50312	346.89	30852	212.72
1.75	44.45	F	2	121518	540.76	50547	348.51	35954	247.89
1.75	44.45	F	3	125766	559.66	52314	360.69	35320	243.52
1.75	44.45	E	1	119761	532.94	49816	343.47	31214	215.21
1.75	44.45	F	5	119573	532.10	49738	342.93	28907	199.31
1.75	44.45	O	1	120513	536.28	50129	345.63	32271	222.50
1.81	45.974	K	1	145903	649.27	56577	390.08		

Size of Bar		Name of Iron	Number of Tests	Strength		Tensile Strength		Elastic limit	
[in]	[mm]			[lbs]	[kN]	[psi]	[MPa]	[psi]	[MPa]
1.81	45.974	B	4	138368	615.74	53655	369.94		
1.81	45.974	C	1	131441	584.91	50969	351.42	30814	212.46
1.81	45.974	G	1	129742	577.35	50310	346.88	33565	231.42
1.81	45.974	E	1	129734	577.32	50307	346.85	29767	205.24
1.81	45.974	J	1	126242	561.78	48953	337.52		
1.88	47.752	K	2	148484	660.75	53803	370.96	31031	213.95
1.88	47.752	C	1	150261	668.66	54447	375.40	32334	222.94
1.88	47.752	D	1	146544	652.12	53100	366.11	32074	221.14
1.88	47.752	M	1	149038	663.22	54004	372.34	33610	231.73
1.88	47.752	F	5	145923	649.36	52875	364.56	35641	245.74
1.88	47.752	F	2	147264	655.32	53361	367.91	35032	241.54
1.88	47.752	P	2	144901	644.81	52505	362.01	32312	222.78
1.88	47.752	E	2	140417	624.86	50880	350.81	27100	186.85
1.88	47.752	D	1	142015	631.97	51459	354.80	27816	191.78
1.88	47.752	P	2	142851	635.69	51762	356.89	32261	222.43
1.88	47.752	,	2	138990	618.51	50363	347.24		
1.88	47.752	A	2	139600	621.22	50584	348.76	28713	197.97
1.88	47.752	F	2	140856	626.81	51039	351.90	33067	227.99
1.88	47.752	F	3	141187	628.28	51159	352.73	33970	234.21
1.88	47.752	F	2	137282	610.90	49744	342.97	35615	245.56
1.88	47.752	F	3	136208	606.13	49355	340.29	32855	226.53
1.88	47.752	F	2	134318	597.72	48670	335.57	23250	160.30
1.88	47.752	O	1	131028	583.07	47478	327.35	30842	212.65
1.94	49.276	M	2	151684	674.99	51474	354.90		

A 3: Summary of wrought iron bar tensile strength, Elastic limit (Yield strength) Data of 959 Specimens reported by Beardslee

Test number	Diameter		Length		Percent Elongation (per original length)	Elastic Limit		Tensile Limit	
	[in]	[mm]	[in]	[mm]		[psi]	[MPa]	[psi]	[MPa]
1	0.874	22.20	3.5	88.90	24.9	31,172	214.92	50925	351.12
2	0.875	22.23	3.5	88.90	28	31,598	217.86	51470	354.87
3	0.875	22.23	3.5	88.90	25.7	31,598	217.86	50640	349.15
4	0.872	22.15	3.5	88.90	13.3	39,080	269.45	48141	331.92
5	0.875	22.23	3.5	88.90	11.7	34,256	236.19	50527	348.37
6	0.976	24.79	3.5	88.90	16	34,092	235.06	51139	352.59
7	0.976	24.79	3.9	99.06	26.7	27,466	189.37	48048	331.28
8	0.976	24.79	3.9	99.06	22.3	35,204	242.72	52339	360.86
9	0.976	24.79	3.9	99.06	23.6	32,578	224.62	51958	358.24
10	0.976	24.79	3.92	99.57	25	28,338	195.38	46378	319.77
11	0.976	24.79	3.92	99.57	29.1	34,521	238.01	53762	370.68
12	0.976	24.79	2.88	73.15	22.2	32,181	221.88	51657	356.16
13	0.976	24.79	0.9	22.86	26	31,977	220.47	53796	370.91
14	0.976	24.79	3.9	99.06	16.7	37,423	258.02	54631	376.67
15	0.976	24.79	3.9	99.06	26.4	29,404	202.73	49652	342.34
16	0.976	24.79	3.92	99.57	21.2	33,519	231.11	50788	350.17
17	0.976	24.79	3.92	99.57	28	32,649	225.11	50788	350.17
18	0.976	24.79	3.92	99.57	28	34,621	238.70	52693	363.31
19	0.976	24.79	3.87	98.30		2,864	19.75	49519	341.42
20	0.964	24.49	3.9	99.06	29	30,141	207.81	50075	345.26
21	0.964	24.49	3.9	99.06	3.8	33,646	231.98	50958	351.34
22	0.976	24.79	3.92	99.57	27.6	23,559	162.43	47580	328.05
23	0.976	24.79	3.92	99.57	28.3	27,402	188.93	51924	358.00
24	0.565	14.35	3.92	99.57	31.1	26,467	182.48	51490	355.01
25	0.564	14.33	2.27	57.66	27.3	35,500	244.76	53250	367.15
26	0.56	14.22	2.26	57.40	23.8	33,623	231.82	56145	387.11
27	0.564	14.33	2.26	57.40	3.5	33,008	227.58	52213	360.00
28	0.564	14.33	2.23	56.64	3.9	26,821	184.92	47138	325.01
29	0.564	14.33	2.23	56.64	3.9	37,270	256.97	52922	364.88
30	0.564	14.33	2.28	57.91	32	34,327	236.68	52542	362.26
31	0.565	14.35	2.27	57.66	23.3	33,075	228.04	50059	345.14
32	0.565	14.35	2.26	57.40	27.9	3,893	26.84	58436	402.90
33	0.565	14.35	2.27	57.66	22.5	35,400	244.07	55743	384.33
34	0.565	14.35	2.23	56.64	26.6	29,916	206.26	47168	325.21
35	0.564	14.33	2.23	56.64	16.6	41,484	286.02	53949	371.97
36	0.565	14.35	2.23	56.64	16.6	38431	264.97	49039	338.11
37	0.565	14.35	2.27	57.66	23.3	30115	207.64	49062	338.27
38	0.565	14.35	2.27	57.66	23.3	40128	276.67	55843	385.02
39	0.565	14.35	2.27	57.66	26.8	37295	257.14	53330	367.70
40	0.565	14.35	2.26	57.40	30.5	30514	210.39	51136	352.57
41	0.565	14.35	2.26	57.40	23	39090	269.52	56641	390.53
42	0.565	14.35	2.26	57.40	24.8	39609	273.09	55943	385.71

Size of Bar		Name of Iron	Number of Tests	Strength		Tensile Strength		Elastic limit	
[in]	[mm]			[lbs]	[kN]	[psi]	[MPa]	[psi]	[MPa]
43	0.564	14.33	2.27	57.66	22	34928	240.82	52442	361.57
44	0.564	14.33	2.27	57.66	21.6	39832	274.63	57546	396.77
45	0.564	14.33	2.27	57.66	25.5	38130	262.90	54363	374.82
46	0.565	14.35	2.26	57.40	31.4	30514	210.39	52054	358.90
47	0.565	14.35	2.26	57.40	21.7	39888	275.02	55943	385.71
48	0.565	14.35	2.26	57.40	19.5	37216	256.60	52353	360.96
49	0.564	14.33	2.26	57.40	20.4	25551	176.17	56545	389.86
50	0.564	14.33	2.26	57.40	12.8	47896	330.23	69856	481.64
51	0.564	14.33	2.26	57.40	23.8	32064	221.07	56945	392.62
52	0.564	14.33	2.26	57.40	34.1	35028	241.51	55044	379.52
53	0.564	14.33	2.26	57.40	26.1	36869	254.20	54644	376.76
54	0.564	14.33	2.26	57.40	23.8	39970	275.58	57968	399.68
55	0.517	13.13	1.98	50.29	20.7	NA	NA	58837	405.67
56	0.518	13.16	1.98	50.29	18.9	NA	NA	61700	425.41
57	0.517	13.13	1.98	50.29	22.5	NA	NA	60862	419.63
58	0.402	10.21	1.57	39.88	16.5	NA	NA	59300	408.86
59	0.402	10.21	1.56	39.62	10.9	NA	NA	58700	404.72
60	0.402	10.21	1.5	38.10	15.8	NA	NA	60500	417.13
61	0.402	10.21	1.58	40.13	26.8	NA	NA	60285	415.65
62	0.875	22.23	3.5	88.90	16	34259	236.21	51139	352.59
63	0.875	22.23	3.5	88.90	11.7	34092	235.06	50751	349.92
64	0.789	20.04	3.87	98.30	7.2	32009	220.69	42237	291.21
65	782	19862.80	3.87	98.30	22	33989	234.35	50490	348.12
66	2.02	51.31	6	152.40	29	34199	235.79	51960	358.25
67	2.06	52.32	9	228.60	24	26403	182.04	52500	361.97
68	1.95	49.53	6	152.40	25	22059	152.09	52138	359.48
69	1.95	49.53	10	254.00	25	29000	199.95	54000	372.32
70	1.99	50.55	13.25	336.55	20	27781	191.54	53710	370.32
71	2.02	51.31	10	254.00	20	30600	210.98	53670	370.04
72	2.03	51.56	8.5	215.90	19.4	34939	240.90	53290	367.42
73	2.03	51.56	8.5	215.90	22	35217	242.81	54525	375.94
74	2.02	51.31	8.5	215.90	22.3	35295	243.35	53664	370.00
75	2.02	51.31	8.5	215.90	19.4	35444	244.38	54290	374.32
76	1.84	46.74	12.3	312.42	22	31049	214.08	49823	343.52
77	1.83	46.48	13	330.20	22	30110	207.60	53292	367.44
78	1.61	40.89	7.37	187.20	22	29233	201.55	54695	377.11
79	1.6	40.64	9.65	245.11	16	28165	194.19	55375	381.80
80	1.61	40.89	7.4	187.96	20	27853	192.04	55402	381.98
81	1.6	40.64	7.33	186.18	19	29139	200.91	56807	391.67
82	1.62	41.15	9.44	239.78	24	33071	228.02	52634	362.90
83	1.6	40.64	9.44	239.78	28	34848	240.27	55375	381.80
84	1.63	41.40	20	508.00	21	28850	198.91	56000	386.11

Size of Bar		Name of Iron	Number of Tests	Strength		Tensile Strength		Elastic limit	
[in]	[mm]			[lbs]	[kN]	[psi]	[MPa]	[psi]	[MPa]
85	1.63	41.40	20	508.00	19	29500	203.40	57000	393.00
86	1.61	40.89	9	228.60	21	29000	199.95	51200	353.01
87	1.5	38.10	10	254.00	24	28000	193.05	48100	331.64
88	1.23	31.24	5	127.00	19	25000	172.37	48100	331.64
89	1.14	28.96	4	101.60	29	24480	168.78	54960	378.94
90	1.12	28.45	4	101.60	24	24900	171.68	56387	388.77
91	1.81	45.97	10	254.00	25	33000	227.53	52420	361.42
92	1.851	47.02	7.38	187.45	24	28434	196.05	51217	353.13
93	1.51	38.35	7.4	187.96	23	32764	225.90	54167	373.47
94	1.02	25.91	4	101.60	18	35000	241.32	55800	384.73
95	0.99	25.15	4.06	103.12	31	26027	179.45	48992	337.79
96	0.92	23.37	3.9	99.06	33.3	25617	176.62	47483	327.38
97	0.987	25.07	3.93	99.82	27.8	34374	237.00	51365	354.15
98	0.974	24.74	3.89	98.81	2.72	32210	222.08	50066	345.19
99	0.974	24.74	3.89	98.81	2.8	30197	208.20	51805	357.18
100	0.565	14.35	2.26	57.40	23.5	33805	233.08	50618	349.00
101	0.565	14.35	2.26	57.40	11	36896	254.39	52333	360.82
102	0.565	14.35	2.28	57.91	26.3	34623	238.72	51655	356.15
103	0.565	14.35	2.28	57.91		33306	229.64	49162	338.96
104	0.56	14.22	2.28	57.91	30	34943	240.92	51854	357.52
105	0.565	14.35	2.28	57.91	30	35600	245.45	52353	360.96
106	0.566	14.38	2.29	58.17	26.6	39546	272.66	51271	353.50
107	0.567	14.40	2.29	58.17	27	39306	271.01	51980	358.39
108	0.567	14.40	2.22	56.39	27	31683	218.45	49505	341.33
109	0.567	14.40	2.3	58.42	23.8	32871	226.64	50396	347.47
110	0.567	14.40	2.25	57.15	27.8	36831	253.94	51485	354.98
111	0.562	14.27	2.25	57.15	20.9	38291	264.01	50181	345.99
112	2	50.80	7	177.80	23	31786	219.16	55014	379.31
113	2	50.80	8	203.20	21	27507	189.65	49662	342.41
114	2	50.80	8	203.20	21	17627	121.53	51193	352.96
115	2	50.80	9	228.60	28	28118	193.87	49360	340.33
116	2	50.80	11	279.40	24	28729	198.08	50796	350.23
117	2	50.80	11	279.40	15	27507	189.65	48748	336.11
118	2	50.80	11	279.40	8	30869	212.83	45998	317.15
119	2	50.80	11	279.40	24	29353	202.38	51805	357.18
120	0.978	24.84	11	279.40	24	NA	NA	48962	337.58
121	0.978	24.84	3.91	99.31	27.1	28620	197.33	51502	355.09
122	0.998	25.35	3.91	99.31	33	27954	192.74	48587	335.00
123	0.999	25.37	4	101.60	26	31958	220.34	51901	357.84
124	1	25.40	4	101.60	18	33177	228.75	50217	346.23
125	1	25.40	4	101.60	32.8	32597	224.75	51225	353.18
126	1	25.40	4	101.60	29.5	30812	212.44	50064	345.18

Size of Bar		Name of Iron	Number of Tests	Strength		Tensile Strength		Elastic limit	
[in]	[mm]			[lbs]	[kN]	[psi]	[MPa]	[psi]	[MPa]
127	1	25.40	4	101.60	30.7	26738	184.35	49424	340.77
128	1	25.40	4.01	101.85	28.6	46738	322.25	49436	340.85
129	1	25.40	4.02	102.11	23.9	30557	210.68	49898	344.03
130	1	25.40	3.99	101.35	30	29603	204.11	48701	335.78
131	1	25.40	3.99	101.35	31.1	30049	207.18	49816	343.47
132	1	25.40	3.99	101.35	31	29539	203.66	50191	346.05
133	1	25.40	3.99	101.35	29.1	31691	218.50	49465	341.05
134	1	25.40	3.99	101.35	34.4	25464	175.57	46486	320.51
135	1	25.40	3.99	101.35	33.8	25460	175.54	46728	322.18
136	0.975	24.77	3.9	99.06	27.2	3352	23.11	51405	354.43
137	0.975	24.77	3.9	99.06	17.9	25448	175.46	45779	315.64
138	0.975	24.77	3.9	99.06	36.4	26204	180.67	49289	339.84
139	1	25.40	6	152.40	21	35124	242.17	55218	380.71
140	1	25.40	6	152.40	25	34071	234.91	55683	383.92
141	1	25.40	5.5	139.70	22	35448	244.41	53170	366.59
142	1.125	28.58	7	177.80	21	25789	177.81	54050	372.66
143	1.125	28.58	7	177.80	24.4	26249	180.98	53860	371.35
144	1.125	28.58	5.5	139.70	25	28324	195.29	53790	370.87
145	1.25	31.75	7	177.80	25	25036	172.62	53670	370.04
146	1.25	31.75	7	177.80	24.7	26118	180.08	54451	375.43
147	1.25	31.75	5.5	139.70	29	31295	215.77	53515	368.97
148	1.375	34.93	7	177.80	24.3	33215	229.01	53210	366.87
149	1.375	34.93	7	177.80	25	33867	233.50	53340	367.77
150	1.375	34.93	7	177.80	25.4	33800	233.04	54122	373.16
151	1.5	38.10	7	177.80	24.4	28794	198.53	51286	353.60
152	1.5	38.10	7	177.80	26.4	28800	198.57	52482	361.85
154	1.625	41.28	11	279.40	29	32605	224.80	54218	373.82
155	1.625	41.28	9	228.60	29	31722	218.72	54451	375.43
156	1.75	44.45	11	279.40	20.7	29718	204.90	52058	358.93
157	1.75	44.45	9	228.60	23.6	29210	201.40	50960	351.36
158	1.875	47.63	12	304.80	21	29741	205.06	51200	353.01
159	1.875	47.63	12	304.80	23.5	27765	191.43	50508	348.24
160	2	50.80	12	304.80	19.7	30709	211.73	51402	354.40
161	2	50.80	12	304.80	23.5	30225	208.39	50828	350.45
162	2.125	53.98	12	304.80	17	30459	210.01	48382	333.58
163	1.4375	36.51	27	685.80	15.9	NA	NA	54892	378.47
164	1.4375	36.51	27	685.80	NA	NA	NA	54773	377.65
165	1.4375	36.51	27	685.80	NA	NA	NA	54773	377.65
166	1.4375	36.51	27	685.80	NA	NA	NA	54773	377.65
167	1.6875	42.86	27	685.80	15	NA	NA	54181	373.56
168	1.6875	42.86	27	685.80	NA	NA	NA	53183	366.68
169	1.6875	42.86	27	685.80	NA	NA	NA	53183	366.68

Size of Bar		Name of Iron	Number of Tests	Strength		Tensile Strength		Elastic limit	
[in]	[mm]			[lbs]	[kN]	[psi]	[MPa]	[psi]	[MPa]
170	1.6875	42.86	27	685.80	NA	NA	NA	53183	366.68
171	1.8125	46.04	27	685.80	16.6	NA	NA	55294	381.24
172	1.8125	46.04	27	685.80	NA	NA	NA	52217	360.02
173	1.8125	46.04	27	685.80	NA	NA	NA	52217	360.02
174	1.8125	46.04	27	685.80	NA	NA	NA	52217	360.02
175	1.4375	36.51	27	685.80	16.2	32655	225.15	51756	356.85
176	1.5	38.10	27	685.80	13	35880	247.38	52700	363.35
177	1.625	41.28	27	685.80	15.7	31099	214.42	49030	338.05
178	1.6875	42.86	27	685.80	15.7	30852	212.72	50312	346.89
179	1.75	44.45	27	685.80	15	33184	228.80	49821	343.50
180	1.8125	46.04	27	685.80	13.9	30814	212.46	50969	351.42
181	1.4375	36.51	27	685.80	13.9	32542	224.37	53994	372.28
182	1.4375	36.51	27	685.80	NA	NA	NA	51936	358.09
183	1.4375	36.51	27	685.80	NA	NA	NA	51936	358.09
184	1.4375	36.51	27	685.80	NA	NA	NA	51936	358.09
185	1.5	38.10	27	685.80	14.4	33027	227.71	54544	376.07
186	1.5	38.10	27	685.80	NA	NA	NA	51200	353.01
187	1.5	38.10	27	685.80	NA	NA	NA	51200	353.01
188	1.5	38.10	27	685.80	NA	NA	NA	51200	353.01
189	1.675	42.55	27	685.80	13	33745	232.66	52675	363.18
190	1.675	42.55	27	685.80	NA	NA	NA	52800	364.04
191	1.675	42.55	27	685.80	NA	NA	NA	52800	364.04
192	1.675	42.55	27	685.80	NA	NA	NA	52800	364.04
193	1.6875	42.86	27	685.80	11.1	33549	231.31	52120	359.35
194	1.6875	42.86	27	685.80	NA	NA	NA	53000	365.42
195	1.6875	42.86	27	685.80	NA	NA	NA	53000	365.42
196	1.6875	42.86	27	685.80	NA	NA	NA	53000	365.42
237	1.75	44.45	27	685.80	11.1	27856	192.06	53800	370.94
238	1.75	44.45	27	685.80	NA	NA	NA	51217	353.13
239	1.75	44.45	27	685.80	NA	NA	NA	51217	353.13
240	1.75	44.45	27	685.80	NA	NA	NA	51217	353.13
241	1.5	38.10	27	685.80	NA	NA	NA	44500	306.82
256	1.4375	36.51	27	685.80	12	NA	NA	50400	347.50
257	1.4375	36.51	27	685.80	NA	NA	NA	47067	324.52
258	1.4375	36.51	27	685.80	NA	NA	NA	47067	324.52
259	1.4375	36.51	27	685.80	NA	NA	NA	47067	324.52
260	1.5	38.10	27	685.80	14	NA	NA	51047	351.96
261	1.5	38.10	27	685.80	NA	NA	NA	51867	357.61
262	1.5	38.10	27	685.80	NA	NA	NA	51867	357.61
263	1.5	38.10	27	685.80	NA	NA	NA	51867	357.61
264	1.625	41.28	27	685.80	9.3	NA	NA	52748	363.68
265	1.625	41.28	27	685.80	NA	NA	NA	50367	347.27

Size of Bar		Name of Iron	Number of Tests	Strength		Tensile Strength		Elastic limit	
[in]	[mm]			[lbs]	[kN]	[psi]	[MPa]	[psi]	[MPa]
266	1.625	41.28	27	685.80	NA	NA	NA	50367	347.27
267	1.625	41.28	27	685.80	NA	NA	NA	50367	347.27
268	1.6875	42.86	27	685.80	14.8	NA	NA	54114	373.10
269	1.6875	42.86	27	685.80	NA	NA	NA	51783	357.03
270	1.6875	42.86	27	685.80	NA	NA	NA	51783	357.03
271	1.6875	42.86	27	685.80	NA	NA	NA	51783	357.03
272	1.75	44.45	27	685.80	11.6	NA	NA	53264	367.24
273	1.75	44.45	27	685.80	NA	NA	NA	51750	356.80
274	1.75	44.45	27	685.80	NA	NA	NA	51750	356.80
275	1.75	44.45	27	685.80	NA	NA	NA	51750	356.80
276	1.75	44.45	27	685.80	NA	NA	NA	51750	356.80
277	1.8125	46.04	27	685.80	14	NA	NA	48953	337.52
278	1.8125	46.04	27	685.80	NA	NA	NA	48800	336.46
279	1.8125	46.04	27	685.80	NA	NA	NA	48800	336.46
280	1.8125	46.04	27	685.80	NA	NA	NA	48800	336.46
281	1.8125	46.04	27	685.80	NA	NA	NA	48800	336.46
282	1.4375	36.51	NA	NA	NA	32162	221.75	69205	477.15
283	1.4375	36.51	NA	NA	NA	NA	NA	66167	456.21
284	1.4375	36.51	NA	NA	NA	NA	NA	66167	456.21
285	1.4375	36.51	NA	NA	NA	NA	NA	66167	456.21
286	1.5	38.10	NA	NA	NA	28579	197.05	69779	481.11
287	1.5	38.10	NA	NA	NA	NA	NA	75167	518.26
288	1.5	38.10	NA	NA	NA	NA	NA	75167	518.26
289	1.5	38.10	NA	NA	NA	NA	NA	75167	518.26
290	1.625	41.28	NA	NA	NA	44792	308.83	46116	317.96
350	1.8125	46.04	1.3	33.02	38.1	NA	NA	49200	339.22
352	1.8125	46.04	1.3	33.02	36.1	NA	NA	50162	345.85
353	1.5	38.10	17	431.80	22	29881	206.02	55956	385.80
354	1.5	38.10	15.5	393.70	19.3	NA	NA	53726	370.43
355	1.5	38.10	NA	NA	NA	35857	247.23	55419	382.10
356	1.5	38.10	NA	NA	NA	57487	396.36	57045	393.31
357	1.5	38.10	NA	NA	NA	35857	247.23	54872	378.33
358	1.625	41.28	19.5	495.30	18.5	33309	229.66	56010	386.18
359	1.625	41.28	19.5	495.30	20.5	32402	223.40	56473	389.37
360	1.625	41.28	NA	NA	NA	319.9	NA	54158	373.41
361	1.625	41.28	NA	NA	NA	35180	242.56	56878	392.16
362	1.75	44.45	20	508.00	18.7	31531	217.40	53883	371.51
363	1.75	44.45	12	304.80	16.7	32329	222.90	54285	374.28
364	1.75	44.45	12	304.80	16.7	31930	220.15	55873	385.23
365	1.75	44.45	10	254.00	18.7	31057	214.13	54290	374.32
366	1.75	44.45	20	508.00	16.1	29935	206.39	53723	370.41
367	1.125	28.58	11	279.40	20.4	30000	206.84	56992	392.95

Size of Bar		Name of Iron	Number of Tests	Strength		Tensile Strength		Elastic limit	
[in]	[mm]			[lbs]	[kN]	[psi]	[MPa]	[psi]	[MPa]
368	1.125	28.58	11	279.40	17	33802	233.06	57948	399.54
369	1.25	31.75	14	355.60	19.6	32469	223.87	57897	399.19
370	1.375	34.93	18	457.20	11.7	31034	213.97	54940	378.80
371	1.625	41.28	21	533.40	17	32334	222.94	54447	375.40
372	2	50.80	21	533.40	14.3	29335	202.26	51153	352.69
373	1.125	28.58	5.07	128.78	36.9	NA	NA	53387	368.09
374	1.125	28.58	4.65	118.11	22.6	NA	NA	53073	365.93
375	1.125	28.58	4.15	105.41	33.1	NA	NA	52899	364.73
376	1.125	28.58	4.18	106.17	26.5	NA	NA	52436	361.53
377	1.125	28.58	3.67	93.22	27.2	NA	NA	52228	360.10
378	1.125	28.58	4.15	105.41	27.1	NA	NA	52805	364.08
379	1.125	28.58	3.45	87.63	25.3	NA	NA	53354	367.86
380	1	25.40	3.8	96.52	22.63	NA	NA	53454	368.55
381	1	25.40	3.7	93.98	24.3	NA	NA	54644	376.76
382	1	25.40	3.4	86.36	23.3	NA	NA	54159	373.41
383	1	25.40	3.97	100.84	30.8	NA	NA	53120	366.25
384	1	25.40	4	101.60	21.2	NA	NA	53582	369.43
385	1	25.40	4.07	103.38	30.6	NA	NA	53171	366.60
386	1	25.40	4.07	103.38	30.6	NA	NA	52640	362.94
387	0.5	12.70	2.72	69.09	53	NA	NA	59066	407.25
388	0.5	12.70	2.87	72.90	53	NA	NA	57216	394.49
389	0.5	12.70	2.9	73.66	35	NA	NA	60739	418.78
390	0.5	12.70	2.9	73.66	57	NA	NA	76032	524.22
391	0.5	12.70	2.92	74.17	45	NA	NA	55428	382.16
392	0.5	12.70	2	50.80		64837	447.04		
393	0.5	12.70	2.15	54.61	52	NA	NA	52649	363.00
394	0.5	12.70	2.15	54.61	55	NA	NA	64431	444.23
395	0.5	12.70	2.15	54.61	57	NA	NA	60461	416.86
396	0.5	12.70	2.15	54.61	45	NA	NA	63246	436.06
397	0.5	12.70	2.15	54.61	47	NA	NA	51257	353.40
398	0.5	12.70	2.15	54.61	50	NA	NA	55400	381.96
399	0.5	12.70	2.1	53.34	18.7	NA	NA	56540	389.82
400	0.5	12.70	2	50.80	21.2	NA	NA	55555	383.03
401	0.5	12.70	2.65	67.31	16	NA	NA	55791	384.66
402	0.5	12.70	2.47	62.74	20.2	NA	NA	54849	378.17
403	0.5	12.70	2.45	62.23	16.3	NA	NA	56216	387.59
404	0.5	12.70	2.45	62.23	21.2	NA	NA	49920	344.18
405	0.5	12.70	1.99	50.55	24.6	NA	NA	58333	402.19
406	0.5	12.70	2.25	57.15	25.3	NA	NA	52705	363.38
407	0.5	12.70	2	50.80	21.2	NA	NA	56467	389.32
408	0.5	12.70	1.98	50.29	21.8	NA	NA	59132	407.70
409	0.5	12.70	1.85	46.99	17.6	NA	NA	55311	381.35

Size of Bar		Name of Iron	Number of Tests	Strength		Tensile Strength		Elastic limit	
[in]	[mm]			[lbs]	[kN]	[psi]	[MPa]	[psi]	[MPa]
410	2	50.80	22	558.80	18.2	28567	196.96	51146	352.64
411	1.625	41.28	22	558.80	20	27816	191.78	51459	354.80
412	1.75	44.45	20	508.00	21.2	27817	191.79	52699	363.35
413	1.625	41.28	19	482.60	19.7	30087	207.44	53695	370.21
414	1.5	38.10	18	457.20	18.9	27708	191.04	52155	359.60
415	1.423	36.14	16	406.40	18.7	31676	218.40	54949	378.86
416	1.25	31.75	14	355.60	14.2	28166	194.20	55550	383.00
417	1.125	28.58	10	254.00	19.8	29476	203.23	54687	377.05
418	2	50.80	9	228.60	NA	NA	NA	46151	318.20
419	1.625	41.28	9.25	234.95	23.2	32074	221.14	53100	366.11
420	1.75	44.45	9	228.60	17.2	31892	219.89	53472	368.68
421	1.625	41.28	9	228.60	16.2	30664	211.42	53614	369.66
422	1.5	38.10	8.5	215.90	22.7	32496	224.05	56505	389.59
423	1.425	36.20	7.55	191.77	24	62152	428.52	58021	400.04
424	1.25	31.75	7	177.80	17.6	31996	220.60	57979	399.75
425	1.125	28.58	6.5	165.10	20.5	33597	231.64	59582	410.80
426	1	25.40	6	152.40	26.1	33486	230.88	61115	421.37
428	2	50.80	10.75	273.05	7.5	33068	228.00	49146	338.85
429	2	50.80	3.2	81.28	18.8	32071	221.12	48585	334.98
430	2	50.80	3.2	81.28	13.4	30066	207.30	46624	321.46
431	1.825	46.36	3.2	81.28	28.1	29866	205.92	47850	329.91
432	1.825	46.36	3.18	80.77	16.7	33464	230.73	46624	321.46
433	1.75	44.45	3.2	81.28	29.7	30060	207.26	48300	333.02
434	1.75	44.45	3.18	80.77	28.6	32071	221.12	47850	329.91
435	1.625	41.28	2.25	57.15	22.2	38862	267.94	52030	358.73
436	1.625	41.28	2.27	57.66	21.1	34823	240.10	51435	354.63
437	1.5	38.10	2.28	57.91	25.2	33322	229.75	49209	339.28
438	1.5	38.10	2.28	57.91	25.63	31910	220.01	49758	343.07
439	1.25	31.75	2.25	57.15	32.4	36821	253.87	51635	356.01
440	1.25	31.75	2.25	57.15	28	36845	254.04	51034	351.87
441	1.125	28.58	2.25	57.15	33.3	32022	220.78	49734	342.90
442	1.125	28.58	2.25	57.15	30.2	30020	206.98	50334	347.04
443	1	25.40	4.4	111.76	28.4	36129	249.10	52701	363.36
444	1	25.40	4.43	112.52	24.1	35495	244.73	52715	363.46
445	1	25.40	4.03	102.36	31.5	37330	257.38	55377	381.81
446	1	25.40	3.9	99.06	28.9	32544	224.38	52769	363.83
447	1	25.40	3.75	95.25	26.4	33830	233.25	51625	355.94
448	1	25.40	3.65	92.71	31.2	33838	233.30	51848	357.48
449	1	25.40	3.63	92.20	31.7	34913	240.72	53453	368.55
450	2	50.80	6	152.40	26.5	24050	165.82	49768	343.14
451	2	50.80	6	152.40	41.3	23574	162.54	49735	342.91
452	1.9375	49.21	10	254.00	19.7	27087	186.76	49095	338.50

Size of Bar		Name of Iron	Number of Tests	Strength		Tensile Strength		Elastic limit	
[in]	[mm]			[lbs]	[kN]	[psi]	[MPa]	[psi]	[MPa]
453	1.9375	49.21	8	203.20	28	27010	186.23	48726	335.95
454	1.825	46.36	11	279.40	18	33183	228.79	49512	341.37
455	1.825	46.36	7.5	190.50	26	29934	206.39	51367	354.16
456	1.8125	46.04	10	254.00	25.4	27700	190.98	51499	355.07
457	1.8125	46.04	5	127.00	33.2	32990	227.46	51895	357.80
458	1.75	44.45	11	279.40	18.1	29748	205.11	51233	353.24
459	1.75	44.45	7	177.80	16.1	30222	208.37	49419	340.73
460	1.625	41.28	10	254.00	16.7	27268	188.01	51127	352.51
461	1.625	41.28	5.5	139.70	30	32279	222.56	50385	347.39
462	1.5	38.10	6	152.40	27	32472	223.89	52156	359.60
463	1.5	38.10	5	127.00	31.2	33681	232.22	53347	367.81
464	1.375	34.93	6.5	165.10	25.2	33422	230.44	58296	401.94
465	1.25	31.75	5.75	146.05	1.4	34188	235.72	43040	296.75
466	1.125	28.58	5.25	133.35	0.7	37088	255.71	50045	345.05
467	1	25.40	6	152.40	56.7	36960	254.83	56541	389.84
468	1.375	34.93	6.5	165.10	9.7	35026	241.50	57486	396.35
469	1.25	31.75	5.5	139.70	9.8	33740	232.63	53952	371.99
470	1.125	28.58	7	177.80	17	33495	230.94	54000	372.32
471	1	25.40	5.74	145.80	6	37694	259.89	60947	420.21
472	1.375	34.93	2.98	75.69	32.1	26526	182.89	50267	346.58
473	1	25.40	2.45	62.23	35.4	30799	212.35	54608	376.51
474	1.735	44.07	3.02	76.71	36.3	26526	182.89	49515	341.39
475	1	25.40	2.55	64.77	30.2	30431	209.81	51949	358.18
476	1.15	29.21	5	127.00	29.2	33549	231.31	53097	366.09
477	1.09	27.69	6	152.40	26.3	28086	193.65	53497	368.85
478	1.26	32.00	4	101.60	29.2	22712	156.59	53836	371.19
479	1.17	29.72	6	152.40	27	23306	160.69	52254	360.28
480	1.39	35.31	6	152.40	29.3	25930	178.78	51843	357.44
481	1.35	34.29	6	152.40	27	30181	208.09	55415	382.07
482	1.5	38.10	4	101.60	32.7	32869	226.62	55409	382.03
483	1.44	36.58	6	152.40	35	29591	204.02	51940	358.11
484	1.63	41.40	5	127.00	30.4	27695	190.95	50844	350.56
485	1.54	39.12	6	152.40	24	27110	186.92	51606	355.81
486	1.75	44.45	8	203.20	24.5	26541	182.99	51740	356.73
487	1.64	41.66	8	203.20	28.7	27722	191.14	50880	350.81
488	1.89	48.01	9	228.60	27.4	27156	187.23	49044	338.15
489	1.87	47.50	10	254.00	23.5	25445	175.44	49088	338.45
490	0.976	24.79	3.9	99.06	31.3	27667	190.76	50458	347.90
491	0.976	24.79	3.9	99.06	26.9	28071	193.54	49054	338.22
492	0.976	24.79	3.9	99.06	33.3	27147	187.17	49225	339.39
493	0.976	24.79	3.9	99.06	28.2	27077	186.69	48199	332.32
494	0.976	24.79	3.9	99.06	26.9	25395	175.09	48399	333.70

Size of Bar		Name of Iron	Number of Tests	Strength		Tensile Strength		Elastic limit	
[in]	[mm]			[lbs]	[kN]	[psi]	[MPa]	[psi]	[MPa]
495	0.976	24.79	3.9	99.06	30	25997	179.24	49709	342.73
496	0.976	24.79	3.9	99.06	28.4	26732	184.31	48152	332.00
497	0.976	24.79	3.9	99.06	30	26231	180.86	51818	357.27
498	2.03	51.56	6	152.40	29.4	27318	188.35	51818	357.27
499	1.12	28.45	13.5	342.90	25.3	32640	225.04	53800	370.94
500	1.12	28.45	13.5	342.90	22.2	34180	235.66	53978	372.17
501	1.25	31.75	15.5	393.70	20.2	32469	223.87	53211	366.88
502	1.25	31.75	15.5	393.70	22	31687	218.47	21730	149.82
503	1.38	35.05	16.5	419.10	22.5	32346	223.02	51347	354.03
504	1.38	35.05	16.5	419.10	20.7	31639	218.14	51245	353.32
505	1.5	38.10	17.5	444.50	14.7	31511	217.26	51612	355.85
506	1.5	38.10	17.5	444.50	8.6	32597	224.75	52375	361.11
507	1.62	41.15	19	482.60	14.3	33766	232.81	51698	356.45
508	1.62	41.15	19	482.60	17.4	34048	234.75	52629	362.86
509	1.75	44.45	18	457.20	20.4	32329	222.90	50291	346.74
510	1.75	44.45	18	457.20	22.5	32130	221.53	51089	352.25
511	1.88	47.75	20	508.00	20.1	32508	224.13	50902	350.96
512	1.78	45.21	20	508.00	21.6	33625	231.84	51176	352.85
513	1.99	50.55	20	508.00	17.5	27779	191.53	49385	340.50
514	1.99	50.55	20	508.00	20.8	27490	189.54	48522	334.55
515	1.015	25.78	3.8	96.52	17.8	NA	NA	52539	362.24
516	1.014	25.76	4	101.60	23.7	NA	NA	52370	361.08
517	1.017	25.83	4	101.60	24	NA	NA	53025	365.59
518	0.897	22.78	3.52	89.41	21.6	NA	NA	51946	358.16
519	0.896	22.76	3.47	88.14	24.4	NA	NA	52975	365.25
520	0.895	22.73	3.57	90.68	24.7	NA	NA	52575	362.49
521	1.018	25.86	3.95	100.33	25.9	NA	NA	51800	357.15
522	1.017	25.83	3.72	94.49	28.1	NA	NA	52175	359.73
523	1.018	25.86	3.9	99.06	24.3	NA	NA	52660	363.08
524	1.016	25.81	3.9	99.06	24.3	NA	NA	51987	358.44
525	0.872	22.15	3.6	91.44	29.8	NA	NA	51657	356.16
526	0.897	22.78	3.54	89.92	27.5	NA	NA	51076	352.16
527	0.892	22.66	0.57	14.48	29.1	NA	NA	51888	357.76
528	0.892	22.66	0.57	14.48	29.1	NA	NA	51564	355.52
529	0.632	16.05	2.46	62.48	24	NA	NA	56022	386.26
530	0.643	16.33	2.48	62.99	19.3	NA	NA	58900	406.10
531	64	1625.60	2.48	62.99	22.9	NA	NA	55950	385.76
532	0.641	16.28	2.48	62.99	18.9	NA	NA	56864	392.06
533	0.646	16.41	2.5	63.50	32.8	NA	NA	55210	380.66
534	0.643	16.33	2.47	62.74	18.6	NA	NA	60594	417.78
535	0.526	13.36	2	50.80	20.5	NA	NA	58670	404.52
536	0.525	13.34	2	50.80	28.5	NA	NA	56460	389.28

Size of Bar		Name of Iron	Number of Tests	Strength		Tensile Strength		Elastic limit	
[in]	[mm]			[lbs]	[kN]	[psi]	[MPa]	[psi]	[MPa]
537	0.526	13.36	2	50.80	26	NA	NA	56775	391.45
538	0.526	13.36	2	50.80	16.5	NA	NA	59130	407.69
539	0.526	13.36	2	50.80	25.5	NA	NA	57295	395.04
540	0.632	16.05	2.55	64.77	25.1	NA	NA	56585	390.14
541	0.642	16.31	2.47	62.74	25.5	NA	NA	54825	378.01
542	0.637	16.18	2.5	63.50	22.9	NA	NA	55140	380.18
543	0.631	16.03	2.5	63.50	26	NA	NA	56610	390.31
544	0.636	16.15	2.5	63.50	25.6	NA	NA	55630	383.56
545	0.637	16.18	2.47	62.74	25.5	NA	NA	55090	379.83
546	0.525	13.34	2.1	53.34	30	NA	NA	55195	380.56
547	0.525	13.34	2.05	52.07	32.5	NA	NA	55085	379.80
548	0.525	13.34	2.05	52.07	26.8	NA	NA	54733	377.37
549	0.525	13.34	2.06	52.32	31	NA	NA	54735	377.38
550	0.525	13.34	2.05	52.07	33.1	NA	NA	55080	379.76
551	0.572	14.53	3.6	91.44	30	25164	173.50	51658	356.17
552	0.897	22.78	3.54	89.92	27.7	33389	230.21	51073	352.14
553	0.892	22.66	3.58	90.93	29.36	34245	236.11	51887	357.75
554	0.892	22.66	3.58	90.93	28.5	35205	242.73	51667	356.23
555	0.564	14.33	2.25	57.15	0.7	36725	253.21	53530	369.08
556	0.564	14.33	2.25	57.15	1.1	37625	259.42	53036	365.67
557	0.564	14.33	2.19	55.63	32.4	32022	220.78	51036	351.88
558	0.566	14.38	2.26	57.40	30	33684	232.24	51470	354.87
559	0.564	14.33	2.25	57.15	31.1	37625	259.42	53036	365.67
560	0.564	14.33	2.27	57.66	30	34075	234.94	50840	350.53
561	0.565	14.35	2.27	57.66	30.4	34501	237.88	50275	346.63
562	0.567	14.40	2.26	57.40	26.5	35645	245.76	49705	342.70
563	0.565	14.35	2.2	55.88	31.4	33205	228.94	51454	354.76
564	0.565	14.35	2.27	57.66	31.7	35890	247.45	51154	352.69
565	0.566	14.38	2.18	55.37	34.4	34739	239.52	51371	354.19
566	0.564	14.33	2.23	56.64	30.9	34023	234.58	51235	353.25
567	0.804	20.42	3.19	81.03	31.3	35454	244.45	50717	349.68
568	0.79	20.07	3.19	81.03	28.8	34683	239.13	50342	347.10
569	0.799	20.29	3.13	79.50	30.9	35899	247.51	20171	139.07
570	0.803	20.40	3.13	79.50	32.9	35543	245.06	51734	356.69
571	0.798	20.27	3.14	79.76	30.2	31991	220.57	49586	341.88
572	0.8	20.32	3.06	77.72	33	27852	192.03	49786	343.26
573	0.99	25.15	5	127.00	22.8	31826	219.43	51963	358.27
574	0.99	25.15	5	127.00	26.4	32216	222.12	51312	353.78
575	0.99	25.15	5	127.00	24.8	32475	223.91	53260	367.21
576	0.99	25.15	5	127.00	21.6	32475	223.91	54299	374.38
577	0.99	25.15	6	152.40	20.3	32346	223.02	53260	367.21
578	1.1	27.94	7	177.80	25.3	31579	217.73	52631	362.88

Size of Bar		Name of Iron	Number of Tests	Strength		Tensile Strength		Elastic limit	
[in]	[mm]			[lbs]	[kN]	[psi]	[MPa]	[psi]	[MPa]
579	1.1	27.94	7	177.80	25.4	31368	216.27	51579	355.62
580	1.1	27.94	6.75	171.45	24.4	32831	226.36	52720	363.49
581	1.1	27.94	6.75	171.45	24.9	32421	223.53	51773	356.96
582	1.1	27.94	7.5	190.50	20.6	31894	219.90	52631	362.88
583	1.23	31.24	7	177.80	19.5	31986	220.54	51346	354.02
584	1.23	31.24	7	177.80	15.5	33670	232.15	52609	362.73
585	1.23	31.24	7	177.80	14	34511	237.95	55134	380.14
586	1.23	31.24	5.5	139.70	31.6	32823	226.31	31346	216.12
587	1.24	31.50	6	152.40	17	33123	228.38	52666	363.12
588	1.38	35.05	8	203.20	21	35427	244.26	52550	362.32
589	1.38	35.05	8	203.20	16.8	36764	253.48	52489	361.90
590	1.38	35.05	8.25	209.55	24.2	33763	232.79	51347	354.03
591	1.38	35.05	7	177.80	21.8	32092	221.27	53286	367.39
592	1.38	35.05	7	177.80	20.9	34298	236.48	51013	351.72
593	1.5	38.10	9	228.60	22	35993	248.16	50993	351.58
594	1.5	38.10	9	228.60	27	35936	247.77	51499	355.07
595	1.5	38.10	7.5	190.50	24.6	33105	228.25	50820	350.39
596	1.5	38.10	9	228.60	35.6	33331	229.81	52572	362.47
597	1.625	41.28	6	152.40	22.6	34978	241.16	21590	148.86
598	1.625	41.28	6	152.40	27.3	36499	251.65	51109	352.38
599	1.625	41.28	9.75	247.65	23.9	32635	225.01	50782	350.13
600	1.625	41.28	9	228.60	24.4	32779	226.00	50830	350.46
601	1.625	41.28	10	254.00	25.9	33236	229.15	50538	348.45
602	1.73	43.94	8	203.20	24	29987	206.75	49553	341.66
603	1.73	43.94	8	203.20	25.2	29561	203.82	49553	341.66
604	1.74	44.20	7	177.80	25.7	29859	205.87	49831	343.57
605	1.74	44.20	7.2	182.88	26.4	24852	171.35	49287	339.82
606	1.74	44.20	10	254.00	30.5	30278	208.76	50464	347.94
607	1.86	47.24	11	279.40	20.9	23408	161.39	48943	337.45
608	1.86	47.24	11	279.40	23.6	23187	159.87	48398	333.69
609	1.87	47.50	10	254.00	26.3	33711	232.43	48948	337.48
610	1.87	47.50	9	228.60	21.4	33861	233.46	49517	341.41
611	1.86	47.24	9	228.60	23.5	31593	217.83	49499	341.28
612	2	50.80	12	304.80	23	27021	186.30	47581	328.06
613	2	50.80	12	304.80	23.5	27371	188.72	48058	331.35
614	2	50.80	12	304.80	23.5	27307	188.28	47099	324.74
615	2	50.80	10	254.00	24.5	30844	212.66	47428	327.00
616	2	50.80	10	254.00	22.5	31417	216.61	47682	328.76
617	0.95	24.13	5	127.00	28	32798	226.13	52810	364.11
618	0.99	25.15	6.75	171.45	23.7	33762	232.78	51675	356.29
619	1.13	28.70	5.5	139.70	22.2	33300	229.60	51949	358.18
620	1.3	33.02	7	177.80	21.1	30212	208.30	50403	347.52

Size of Bar		Name of Iron	Number of Tests	Strength		Tensile Strength		Elastic limit	
[in]	[mm]			[lbs]	[kN]	[psi]	[MPa]	[psi]	[MPa]
621	1.4	35.56	7.5	190.50	25.3	32675	225.29	50709	349.63
622	1.55	39.37	9	228.60	23.9	31400	216.50	49605	342.01
623	1.61	40.89	7.2	182.88	26.5	34482	237.75	50201	346.12
624	1.71	43.43	8.6	218.44	24	33972	234.23	49682	342.55
625	1.87	47.50	8.65	219.71	23.9	31166	214.88	48170	332.12
626	0.502	12.75	2.5	63.50	25.2	41940	289.17	51823	357.31
627	0.504	12.80	2.58	65.53	NA	37844	260.93	50877	350.78
628	0.503	12.78	2.35	59.69	30.1	36739	253.31	51205	353.05
629	0.503	12.78	2.25	57.15	30.8	37493	258.51	51708	356.51
630	0.503	12.78	2.32	58.93	NA	33866	233.50	51675	356.29
631	0.5	12.70	2.55	64.77	NA	32742	225.75	50165	345.88
632	0.5	12.70	2.5	63.50	28	33725	232.53	50728	349.76
633	0.552	14.02	2.72	69.09	28.6	36982	254.98	49726	342.85
634	0.554	14.07	2.77	70.36	29.6	32054	221.00	50197	346.10
635	0.601	15.27	2.97	75.44	31.6	37102	255.81	49087	338.44
636	0.601	15.27	2.99	75.95	20	38646	266.45	49351	340.26
637	0.654	16.61	3.25	82.55	31.1	28575	197.02	49118	338.66
638	0.653	16.59	3.21	81.53	29.8	38818	267.64	49641	342.26
639	0.653	16.59	3.2	81.28	29.6	38444	265.06	46865	323.12
640	0.725	18.42	3.63	92.20	28.1	34934	240.86	49539	341.56
641	0.728	18.49	3.63	92.20	31.2	38437	265.01	46250	318.88
642	0.726	18.44	3.55	90.17		49676	342.50		
643	0.8	20.32	4	101.60	30.2	37996	261.97	49437	340.86
644	0.801	20.35	3.97	100.84	29.7	39687	273.63	49314	340.01
645	0.805	20.45	4.04	102.62	30.4	35790	246.76	49710	342.74
646	0.8	20.32	4.1	104.14	30.5	33819	233.17	49736	342.92
647	0.875	22.23	4.3	109.22	29.5	NA	NA	48559	334.80
648	0.875	22.23	4.3	109.22	29.5	26110	180.02	48560	334.81
649	0.875	22.23	3.85	97.79	32.5	25364	174.88	49225	339.39
650	0.874	22.20	4.37	111.00	29.4	320505	2209.80	48922	337.31
651	1.01	25.65	5	127.00	29	32676	225.29	48308	333.07
652	1.19	30.23	5.88	149.35	30.8	35790	246.76	48473	334.21
653	1	25.40	4.93	125.22	31	35790	246.76	46982	323.93
654	1	25.40	4.89	124.21	31.2	29284	201.91	47301	326.13
657	0.5	12.70	2.46	62.48	26	32340	222.98	50178	345.97
658	0.5	12.70	2.4	60.96	29.1	32300	222.70	50178	345.97
659	0.5	12.70	2.41	61.21	28.2	31991	220.57	50165	345.88
660	0.552	14.02	2.73	69.34	31.1	37401	257.87	49935	344.29
661	0.55	13.97	2.73	69.34	29.6	26826	184.96	49877	343.89
662	0.53	13.46	2.72	69.09	31.3	31224	215.28	49962	344.48
663	0.55	13.97	2.68	68.07	25.5	32302	222.71	50825	350.43
664	0.601	15.27	2.93	74.42	32.4	41067	283.15	49175	339.05

Size of Bar		Name of Iron	Number of Tests	Strength		Tensile Strength		Elastic limit	
[in]	[mm]			[lbs]	[kN]	[psi]	[MPa]	[psi]	[MPa]
665	0.603	15.32	3	76.20	32.1	NA	NA	49024	338.01
666	0.602	15.29	2.99	75.95	32.1	38386	264.66	48853	336.83
667	0.654	16.61	3.26	82.80	27.6	37806	260.66	49267	339.68
668	-0.653	-16.59	3.22	81.79	28.4	32323	222.86	49865	343.81
669	0.653	16.59	3.25	82.55	28.2	29859	205.87	50015	344.84
670	0.725	18.42	3.62	91.95	29	36350	250.62	50143	345.72
671	0.726	18.44	3.6	91.44	26.9	32466	223.85	49676	342.50
672	0.727	18.47	3.6	91.44	28.5	31588	217.79	49867	343.82
673	0.801	20.35	4.01	101.85	30.2	37497	258.53	49266	339.68
674	0.8	20.32	4.05	102.87	29.9	34615	238.66	49438	340.86
675	0.876	22.25	4.36	110.74	28.2	39741	274.00	48531	334.61
676	0.875	22.23	4.31	109.47	29.4	36587	252.26	48809	336.53
677	0.802	20.37	4.01	101.85	27.5	29693	204.73	48597	335.06
678	1.004	25.50	4.96	125.98	31.2	34408	237.23	46862	323.10
679	1.01	25.65	5	127.00	29.2	38192	263.32	51422	354.54
680	1.01	25.65	5	127.00	27	39940	275.38	52420	361.42
681	1.13	28.70	8	203.20	24.5	35493	244.72	49850	343.70
682	1.13	28.70	8	203.20	23.7	35493	244.72	50448	347.83
683	1.25	31.75	9	228.60	13.6	39608	273.09	52485	361.87
684	1.25	31.75	9	228.60	21.7	39608	273.09	52974	365.24
685	1.38	35.05	10	254.00	20.8	39037	269.15	52406	361.33
686	1.38	35.05	10	254.00	17.5	39170	270.07	52272	360.40
687	1.5	38.10	13	330.20	23.9	34522	238.02	50367	347.27
688	1.5	38.10	13	330.20	25	35653	245.82	51273	353.51
689	1.62	41.15	13	330.20	23	34934	240.86	49684	342.56
690	1.61	40.89	13	330.20	25.5	35854	247.20	51375	354.22
691	1.74	44.20	13	330.20	27	35996	248.18	50464	347.94
692	1.74	44.20	13	330.20	25.5	35912	247.60	50630	349.08
693	1.87	47.50	13	330.20	19.1	36416	251.08	49380	340.46
694	1.87	47.50	13	330.20	25.5	34818	240.06	50109	345.49
695	2.01	51.05	13	330.20	NA	35297	243.36	47777	329.41
696	2.01	51.05	13	330.20	NA	36432	251.19	47967	330.72
697	2.24	56.90	37.5	952.50	20	31059	214.14	48112	331.72
698	2.24	56.90	37.5	952.50	20.4	31415	216.60	48898	337.14
699	2.09	53.09	11	279.40	26.7	32002	220.65	48965	337.60
700	2.1	53.34	12	304.80	27	31931	220.16	49364	340.35
701	2.5	63.50	37.5	952.50	20.5	30456	209.99	47507	327.55
702	2.5	63.50	37.5	952.50	20.6	29060	200.36	47181	325.30
703	2.34	59.44	14	355.60	17.9	28644	197.49	48407	333.75
704	2.38	60.45	14	355.60	16	29220	201.46	48550	334.74
705	0.504	12.80	2.57	65.28	22.5	38596	266.11	51128	352.52
706	0.502	12.75	2.43	61.72	22.8	0.7771	NA	50530	348.39

Size of Bar		Name of Iron	Number of Tests	Strength		Tensile Strength		Elastic limit	
[in]	[mm]			[lbs]	[kN]	[psi]	[MPa]	[psi]	[MPa]
916	1.51	38.35	10	254.00	27.3	32312	222.78	50919	351.07
917	1.62	41.15	8	203.20	22.1	34012	234.50	52401	361.29
918	1.72	43.69	10	254.00	23.8	32271	222.50	50120	345.57
919	1.86	47.24	10	254.00	24	30842	212.65	47478	327.35
920	2	50.80	11	279.40	25.6	31413	216.59	48249	332.67
921	1.27	32.26	6.7	170.18	31.5	35596	245.43	55782	384.60
922	1.38	35.05	7	177.80	29.6	30802	212.37	52550	362.32
923	1.46	37.08	NA	NA	NA	NA	NA	53345	367.80
924	1.52	38.61	8	203.20	28	29630	204.29	52865	364.49
925	2.02	51.31	10	254.00	24	29959	206.56	49872	343.86
926	0.99	25.15	4.25	107.95	0.9	38971	268.70	55858	385.13
927	0.99	25.15	4.25	107.95	18.8	39489	272.27	59755	412.00
928	1.12	28.45	6	152.40	20	41006	282.73	56840	391.90
929	1.12	28.45	6	152.40	17.7	41615	286.93	57739	398.10
930	1.28	32.51	7	177.80	25.4	37218	256.61	56721	391.08
931	1.28	32.51	7	177.80	23.9	36519	251.79	57031	393.22
932	1.4	35.56	8	203.20	25.6	33788	232.96	55230	380.80
933	1.4	35.56	8	203.20	23.7	37737	260.19	55230	380.80
934	1.52	38.61	10	254.00	22.2	33057	227.92	53664	370.00
935	1.52	38.61	10	254.00	24	33233	229.13	54655	376.83
936	1.64	41.66	8	203.20	1	33522	231.13	53799	370.93
937	1.77	44.96	9	228.60	24.7	33238	229.17	51889	357.76
938	1.77	44.96	9	228.60	22	33726	232.53	51801	357.16
939	1.88	47.75	10	254.00	23.8	32420	223.53	52806	364.08
940	1.88	47.75	10	254.00	25.6	32204	222.04	50866	350.71
941	2.01	51.05	11	279.40	23	31673	218.38	50803	350.27
942	2.01	51.05	11	279.40	29.1	32083	221.20	56535	389.80
943	1.26	32.00	7.5	190.50	29.3	34482	237.75	56134	387.03
944	1.26	32.00	7.5	190.50	21	33360	230.01	54606	376.50
945	1.51	38.35	7.5	190.50	22.3	34617	238.68	54103	373.03
946	1.51	38.35	9	228.60	23	NA	NA	54455	375.45
947	1.64	41.66	7	177.80	26.4	33143	228.51	54924	378.69
948	1.64	41.66	7	177.80	25.4	33712	232.44	54089	372.93
949	1.76	44.70	9	228.60	22.8	33703	232.37	54336	374.63
950	1.76	44.70	9	228.60	24.7	34112	235.19	51860	357.56
951	1.87	47.50	10	254.00	28.4	32046	220.95	51665	356.22
952	1.87	47.50	10	254.00	27.1	32477	223.92	53172	366.61

A 4: Detailed investigation of the strength of wrought iron bars, reported by Beardlee